THE EFFECT OF TIP CLEARANCE AND TIP GAP GEOMETRY ON THE PERFORMANCE OF A ONE AND A HALF STAGE AXIAL GAS TURBINE

By
Ivan Kaiser

Thesis submitted in fulfilment of the academic requirements for the degree of Doctor of Philosophy in the Department of Mechanical Engineering

University of Natal
Durban

1996

ABSTRACT

In a previous work of a similar nature, the performance of a low speed axial turbine with a second stage nozzle was examined with respect to the effect of the variation of tip clearance for various tip shapes. Present findings suggest some interesting phenomena, including the effect of tip clearance on the flow within the rotor and show that poor resolution from a transducer and insufficient data points in the critical tip region, where a high velocity peak was found, were responsible for a number of incorrect conclusions in the original study.

In terms of blade tip geometry, a standard flat tip shape was found to deliver only a marginally better performance when compared to a double squealer tip and the two streamlined shapes previously investigated. Although contemporary opinion suggests that a streamlined tip should increase the leakage flow and hence cause greater mixing losses, the machine efficiency was not significantly reduced. This is an exciting result since it suggests that a streamlined tip shape can be used to alleviate the problem of blade tip burnout without significantly reducing machine efficiency .

When the single stage performance in the absence of a second nozzle was examined, slightly different trends were obtained. The low entropy tips produced slightly lower mixing loss, suggesting that the internal gap loss is an important parameter in determining the rate at which the leakage jet mixes downstream of the rotor.

The flow behind the rotor (ie time averaged) was found to be in remarkable agreement with linear cascade data when time averaged even though the latter did not include any effects of relative motion. An increase in clearance was seen to reduce the Euler work and also to cause a deficit of mass flow across the remainder of the blade right down to the hub. The

leakage flow was also seen to induce a flow blockage which resulted in a higher driving pressure across the rotor for the same mass flow rate.

As in the previous study, the second stage nozzle efficiency was seen to be independent of tip clearance or tip shape and was moderately better than that of the first nozzle. However, the improvement was not found to be as large, due to a previously undetected very thin ring of high energy leakage fluid. When this is taken into account, the efficiency of the second stage nozzle is comparable to the first.

The second nozzle was seen to have a flow straightening effect on the poorly deflected, high energy leakage flow, causing a rapid mixing process within these downstream blade passages. The growth of secondary flow was reduced at both the hub and the tip and this is believed to result in a slight decrease in loss. The outlet flow was closer to design conditions than that of the first stage nozzle.

PREFACE

The author hereby states that this entire thesis, unless specifically indicated to the contrary in the text, is his own original work, and has not been submitted in part, or in whole to any other University. This dissertation was carried out by the author at the Department of Mechanical Engineering, University of Natal from May 1993 to July 1996. The work is a continuation of a number of years of study to understand the phenomenon of tip clearance and was supervised by Prof J P Bindon.

Dedicated to my daughter Shannon whom hopefully I can inspire one day to have as much pleasure as I have had during the past few years of postgraduate study.

ACKNOWLEDGEMENTS

Although many people have contributed financially and morally to the success of this thesis, the author wishes to express his sincere thanks to the following people in particular

The workshop staff for their assistance with modifications to the rig.

George Morphis for his assistance and enthusiasm.

His parents Lionel and Daphne and his other parents Graham and Barbara for their continual support and encouragement.

Graham Smith for his support and general insight.

Candace for her unfailing help, encouragement and moral support.

The FRD for helping with financial support.

And finally, a special thanks to Prof J P Bindon for his dedicated supervision, original thinking and lengthy discussions of the results. It would not have been possible without him.

TABLE OF CONTENTS

NOMENCLATURE

Variables

A	Area (m^2)
C	Dimensionless coefficient
h	Specific enthalpy (kJ/kg)
i	Incidence (°)
$\dot{m}$	Mass flow rate (kg/s)
q	Dynamic pressure (Pa)
R	Radius (m)
s	Pitch (m), specific entropy (kJ/kg·K)
T	Temperature (K)
U	Blade speed (m/s)
V	Absolute velocity (m/s)
W	Relative velocity (m/s)
Y	Any coefficient
α	Absolute angle (°)
β	Relative angle (°)
η	Efficiency
ρ	Density (kg/m^3)
w	Specific work (kJ/kg)
ω	Angular velocity (s^{-1})
θ	Swirl angle (°)

Coefficients

C_m	Mass flow coefficient
$C_{P_{0\,ref} - P_S}$	Static pressure coefficient

$C_{P_{0ref}-P_0}$	Total pressure coefficient
$C_{P_{0a}-P_{Sb}}$	Driving pressure coefficient
$C_{P_{0a}-P_{0b}}$	Total pressure loss coefficient
C_V	Velocity coefficient
C_W	Work coefficient
V_x / U	Axial Velocity to Blade Speed ratio (Based on tip speed)

Subscripts

0	Total
1	First nozzle inlet
1.5	One and a half stage
2	Rotor inlet (first nozzle outlet)
3	Rotor outlet (second nozzle inlet)
4	Second nozzle outlet
a	Upstream
aero	Aerodynamic quantity
b	Downstream
i,j,m,n	Grid summation variables (also represents a time of measurement at i,j)
is	Isentropic
N1	First nozzle
N2	Second nozzle
o	Total
P	Pressure
R	Rotor
ref	reference (at inlet to turbine)
s	Static
ts	Total-to-static (single stage)

tt	Total-to-total (single stage)
V	Velocity
X	Axial
θ	Swirl component

CHAPTER 1

INTRODUCTION

1.1 Scope

Turbines offer a very high mass flow throughput and thus power for their size compared to other heat engines. Because of this they are the first choice thermal power unit when weight is an important parameter such as in an aircraft. In such an application, gas turbines are commonly used. In the generation of electrical power large steam turbines are also utilised. Small improvements in efficiency of a turbine can therefore have a significant impact on the utilization of natural resources and can for example reduce fuel consumption and increase a payload.

The sources of inefficiency in a turbine are due to a number of unavoidable processes. These are generally categorised as profile loss and endwall loss due to viscous friction, secondary flow losses and tip leakage loss. Each of these processes generates entropy, however, the loss associated with tip clearance is a slightly more complicated process. Entropy is generated by viscous shearing on the tip surfaces, mixing of separated flow within the gap as well as by the subsequent mixing of the leakage flow into the passage flow between the rotor blades and also downstream of the rotor. The tip gap is an unavoidable clearance between an unshrouded rotor blade tip and the stationary outer casing or endwall and is necessary to avoid contact between the surfaces. This clearance is also dependent on the operating conditions and varies during take-off in an aircraft gas turbine for example. Research has shown that to avoid rubbing, the minimum clearance

generally lies in the range of 1-3.5% of the blade chord if the turbine is designed according to optimum conditions.

In a reaction turbine, the pressure differential across the blade pressure and suction surfaces causes fluid to leak through the gap with the creation of entropy. This fluid then enters the blade passage flow at a highly sheared angle and forms a vortex structure in the blade suction corner near the tip as shown in Figure 1.1. This vortex then mixes out with the passage flow, generating further losses downstream of the rotor. In addition to the generation of entropy, the leakage flow tends to have a reduced deflection. This further reduces the work output from the rotor, but not necessarily lowering the overall efficiency.

In quantifying the loss generated by tip clearance, it has been found that the internal gap loss contributes about 40% of the tip clearance loss with the remainder caused by the mixing process of the leakage flow into the passage flow. An assumption of most researchers is that the leakage flow has completely mixed out with the passage fluid before the subsequent stage and is not recoverable. Accordingly most work has concentrated on minimising the leakage flow rate with the intention of reducing the mixing loss.

Because the size of the tip clearance gap is fixed by the initial turbine design, the reduction of the leakage flow rate can only be achieved by using various tip geometries that effectively block the leakage flow by increasing the boundary layer velocity deficit and hence generating entropy. This is generally achieved by creating additional flow separation zones within the gap. Such tip geometries may take the form of winglets or squealer tips. However, it should be realised that the process of entropy generation within the tip gap is a non recoverable one.

If the leakage flow is allowed to exit the tip gap isentropically, the resulting magnitude, as seen in Figure 1.2, is similar to that expected of the fully turned velocity at the outlet from the rotor. However, significant underturning occurs and this gives rise to a leakage fluid at the gap exit with relatively large kinetic energy as indicated in Figure 1.2. This high velocity leakage flow then proceeds to wrap up into the suction corner vortex and mixes out with the passage flow.

It is possible that the nozzle downstream of a rotor may recover a part of the kinetic energy of the leakage flow. The literature shows that a low entropy tip may indeed reduce the internal gap loss but this is at the expense of a higher leakage flow rate and hence creates higher mixing losses in the fully mixed out condition.

A previous study in a linear cascade suggested that a low entropy tip may have a slight advantage over the flat tip. This was believed possible because of the reduced entropy within the tip gap as well as the leakage flow rate having a higher kinetic energy than that of the flat tip which had the potential of being recovered by the subsequent nozzle.

Most of the experimental research conducted so far has also been with the aid of linear turbine cascades. However, a number of important differences to a real machine exist which include the radial pressure gradient, the effect of relative motion at the rotor tip and boundary layer skewing that the rotor experiences in the relative frame and the similar effect on a subsequent stage in the absolute frame. Because of the limitations in the smallest size of measuring device used, the test blades are generally much larger than that in a real machine and while this has resulted in the identification of a number of important phenomena, considerable

doubt exists over the validity of applying linear cascade data to a working machine.

The experimental turbine used in the present study was a single stage turbine followed by a second stage nozzle. The turbine was based on a free vortex design with fully twisted blades. A number of axial positions were used to measure the time averaged flow data by means of pneumatic probes in an attempt to discern the mechanism of the leakage flow mixing process as well as to investigate the possible effects of the second nozzle on the leakage flow. The power developed by the rotor was measured mechanically using a high accuracy transducer and the results were non-dimensionalised to obtain a repeatable indication of the effect of each tip shape. Various other flow quantities were also rendered independent of inlet conditions and were used as indicators of the tip leakage flow and the mixing process.

A previous study investigated the overall effect of two low entropy tips, namely a radiused pressure corner tip and a contoured suction squealer tip as illustrated in Figure 1.3. These were referenced to a flat tip shape in an attempt to correlate the outcome for each case. The effect of tip clearance in each case was also examined by changing the clearance from 1-3% of the blade tip chord. Some interesting trends were seen but poor resolution from a transducer and insufficient data points in the critical tip region were found to be responsible for some incorrect conclusions. This necessitated a re-evaluation of the uncertainty in the results which was considerably improved.

The present study re-examines the effect of varying tip shape clearance and includes a leakage flow rate reducing tip, namely a double squealer tip as shown

in Figure 1.3. The simulated time averaged flow from a linear cascade was used to isolate the influence of the tip leakage fluid on the flow behind the rotor. The influence of the second stage nozzle on the rotor outlet flow was also considered by removing the nozzle and measuring the flow and subsequent mixing of the leakage fluid with the main passage flow.

The experimental results showed that the performances for the various tip shapes were similar in magnitude. Even though the measurements were taken at low speed and the flow was incompressible, the trends were found to be sufficiently interesting to warrant a full scale evaluation of the various tip shapes and are believed to be reliable.

1.2 Objectives

The overall objectives of this thesis are to examine the effect of tip clearance and tip geometry on the performance of a rotor and a subsequent stator. The objectives for the research program are discussed in further detail at the end of the literature review in Chapter 2. This is necessary since a deeper understanding of current work and various models of tip clearance is required in order to formulate a hypothesis for tip clearance effects in a 3-D rotating machine.

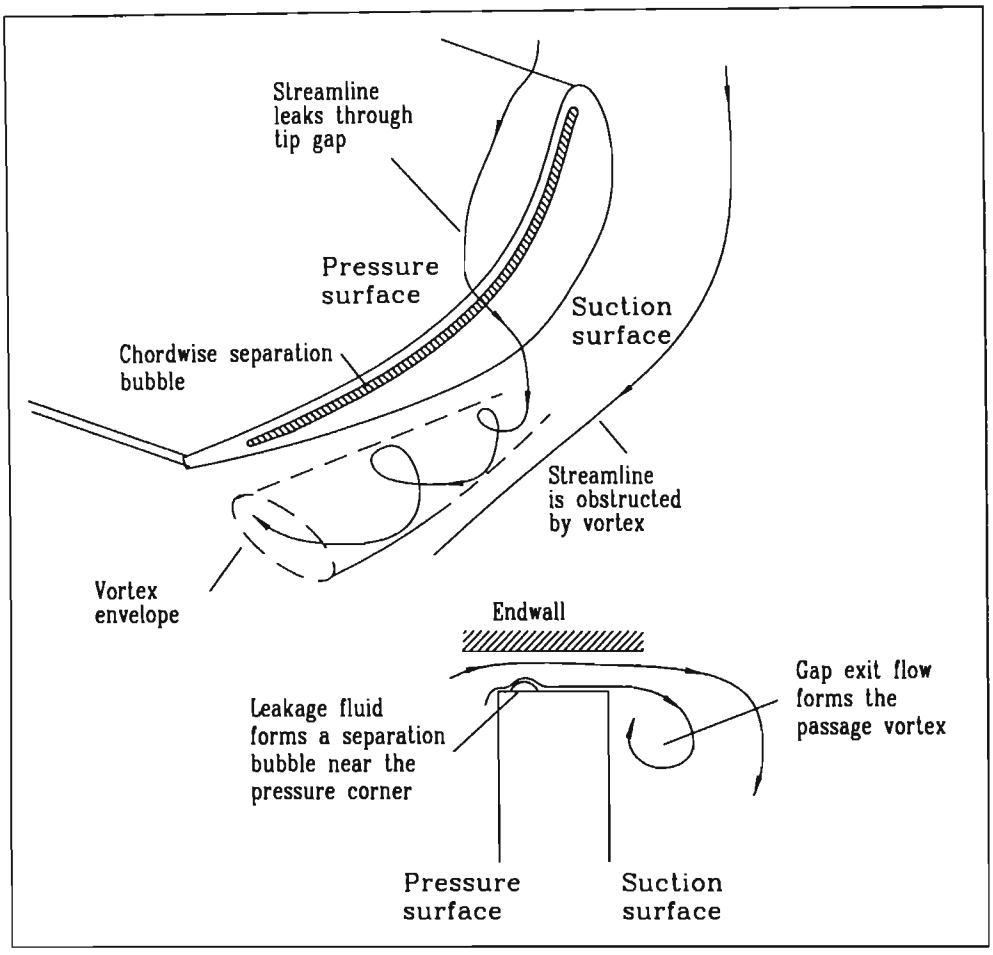

Figure 1.1 The pressure differential causes flow to leak though the tip gap and forms the passage vortex in the suction corner.

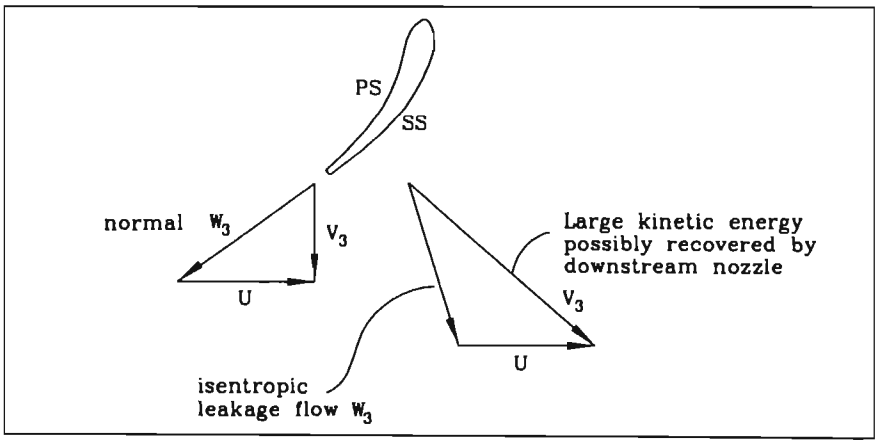

Figure 1.2 The isentropic leakage flow expands to the same velocity as that expected at the outlet from the rotor but is poorly deflected.

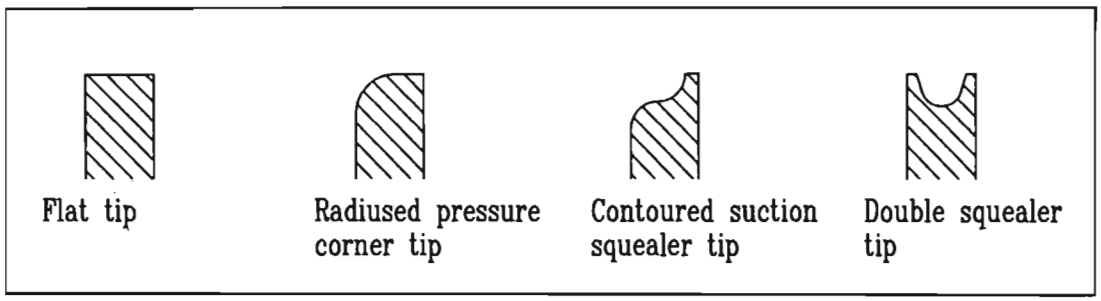

Figure 1.3 The various tip treatments investigated in this study

CHAPTER 2

LITERATURE REVIEW AND OBJECTIVES

1. Introduction

To illustrate the importance of tip clearance, Booth (1985) showed in a lecture series that approximately 25% of the total stage loss or about a third of the overall rotor loss can be attributed to tip clearance phenomena. However, the overall estimation of tip clearance loss tended to be a generalised quantity and it was realised that a meaningful understanding of tip clearance phenomena was essential to predicting and designing effective rotor blade geometries to minimise this loss formation.

Originally work was performed to quantify tip clearance effects and simple models were used to understand the mechanism of tip clearance. Ainley & Mathieson (1951) presented an empirical formulation that related the stator and rotor efficiency reduction due to radial tip clearance. Experimental data was not generally available and very few other models existed for the prediction and improvement of tip clearance pressure loss.

A more detailed understanding was necessary to minimise tip clearance effects and pioneering work was initiated by Rains (1954) in order to understand the mechanism of tip clearance. In this innovative study, coloured oil droplets were injected into the flow of an axial water pump which simulated a compressor. Two simple tip clearance models were developed, the first being a basic mixing model based on Bernoulli's equation at the gap entrance and the second which included

viscous effects and a separation zone with reattachment. He also described the separation bubble on the tip surface near the pressure corner

From this and other preliminary studies, the subject of tip clearance in turbine and compressor rotors has been investigated to reveal the complexity of the phenomenon. Primarily, use was made of linear cascades because of the low cost and simplicity of construction and the ease of obtaining detailed measurements. Important results were delivered and much of the qualitative understanding has been obtained from cascades.

A distinction is made between the phenomenon of tip clearance within a compressor and a turbine. The main differences between the two situations are the direction of rotation of the rotor relative to the leakage flow and the blade thickness. Although compressor and turbine tip leakage flows have much in common, this review concentrates on turbine tip clearance.

2. The mechanism of the tip clearance leakage flow

2.1. The leakage flow within the gap

Rains (1954) noted that tip clearance caused cavitation in a water pump. Additionally, in gas turbines, tip clearance has been linked to the problem of blade tip burnout where high temperatures from the combustion chamber cause enhanced oxidation of the blade tip surface with a degradation of the machine performance and ultimately failure. This has prompted a number of researchers, in particular Bindon (1986a, 1986b, 1987a, 1987b & 1987c) to investigate the flow details within the tip gap.

The study of Bindon was conducted with a linear cascade which was fitted with standard flat tip blades. The pressure and flow field within the tip gap were investigated by means of micro-pressure tappings on the tip surface and endwall, micro total pressure probes and by smoke trace flow visualisation. The results presented in Figure 2.1 revealed that the flow entering the gap remained attached around the pressure corner and only separates when the sharply accelerated flow begins to diffuse. This was a surprising result since it was previously believed that the flow would separate immediately at the pressure corner. At the point of separation a chordwise bubble was seen to form along the pressure corner on the blade tip surface. This bubble was observed to form a 'vena contracta' or flow blockage near the pressure corner at which point the main leakage flow experienced a maximum velocity. Strong chordwise pressure gradients were also measured in the gap which explained the strong corkscrew cross flows seen inside the bubble via smoke traces.

The flow was seen to reattach behind the separation bubble and the pressure again rose to that of the suction surface at the gap exit. This pressure recovery was seen to cause an endwall separation as noted by Sjolander & Amrud (1987) and Kaiser (1992) in an annular cascade. Highly sheared flow was observed along the tip surface and this was suggested as the origin of high convective heat transfer coefficients which precipitated tip burnout.

Figure 2.2 shows that within the bubble itself, a minimum pressure was obtained near mid chord which suggested a helical, chordwise flow of separated fluid from the leading and trailing edges towards mid chord. The accumulation of separated fluid was thought to occur at mid chord where it was forced to mix with the leakage flow as a high loss core, as illustrated in Figure 2.3.

2.2. The structure of the leakage flow and overall effects

The leakage jet essentially enters the gap isentropically up to the vena contracta. Beyond this point, the manner in which the leakage flow reattaches to the tip surface behind the separation bubble and the subsequent mixing of the leakage jet and the high loss fluid from the separation bubble has been represented in a number of ways by various researchers.

Heyes et al (1991) presented a general model of the leakage flow inside the clearance gap. This model is presented in Figure 2.4 and compares well with the results of Bindon (1988), Dishart & Moore (1989) and Moore & Tilton (1987). Essentially, the leakage jet was speculated to emerge from the clearance gap as a combination of an isentropic jet next to the endwall and a low momentum layer close to the tip surface. Depending on the length of the gap path, complete mixing could occur at the gap exit. It was found that with complete mixing at the gap exit, the local discharge coefficient increased hence increasing the leakage mass flow rate. A further implication of this model is that with complete mixing, a larger leakage flow rate occurs with greater entropy hence the amount of mixing by the gap exit is critical to accurately predict the performance of a rotor.

When the leakage jet emerges from the gap it enters as a highly directionally sheared flow into the main passage flow between the rotor blades. An orderly roll up of the leakage flow into a vortex then takes place in the suction corner of the blade. This was observed by a number of researchers including Bindon (1987b), Sjolander & Amrud (1986) and by Rains (1954) who found the low pressure in the vortex to be responsible for additional cavitation in a water pump. Besides the

single leakage vortex pattern observed by most researchers, Sjolander & Amrud (1986) noted the formation of multiple leakage vortices at the gap exit.

The effect of this suction corner vortex is manifested in a number of ways. Firstly, the suction corner vortex is known to deflect the main passage flow and causes a blockage. This also gives rise to a lower pressure on the suction surface, however, Sjolander & Amrud (1986) presented evidence that this increase in the pressure differential did not increase the net blade loading. The lower suction surface pressure was actually caused by the leakage flow suction corner vortex which then generates further mixing loss and reduces the passage flow deflection.

Another consequence of the relative unloading at the tip is the increase of the pressure differential driving the leakage flow rate that sustains the leakage vortex. The pressure differential has been linked to the discharge coefficient of the tip which will be seen later to be an important parameter in determining the loss due to tip clearance. Heyes et al (1991) found that the discharge coefficient was considerably lower than that predicted by the fully mixed out model for larger clearances indicating that the relationship between the discharge coefficient and tip clearance was complex.

The roll up of the leakage flow into a vortex introduces an additional complexity to the passage flow. This is caused by the fact that the leakage flow enters the passage as a highly sheared flow and contains low energy fluid in the core of the vortex as reported by Bindon (1988) and illustrated in Figure 2.3. The passage vortex proceeds to mix with the main passage flow and is responsible for further mixing losses downstream of the rotor. However, in an investigation of the effects of the tip leakage flow on secondary flows within a turbine cascade, Chan et al

(1994) observed a significant reduction of secondary flow with increasing tip clearance. This reduction of secondary flow could have the advantage of reducing secondary flow loss within the rotor.

Another phenomenon of tip clearance is the effect that the leakage mass flow has on the main passage flow. Heyes & Hodson (1992) mentioned that the underturned leakage flow expands to the same back pressure as the passage flow. As seen in Figure 1.2, this creates a leakage flow with a velocity similar in magnitude to that expected at the outlet from the rotor blade but is largely underturned. This gives rise to an increased axial velocity in the tip region with an accompanying reduction of mass flow over the rest of the blade span. This would reduce the blade loading, further contributing to the loss of work from the blade and is a separate mechanism to the work lost due to a reduction in blade height. In his review, Peacock (1982) noted that the expansion of this high energy jet caused a flow blockage within the blade passages which resulted in further underturning of the passage flow.

3. Quantifying the tip clearance loss

A variety of researchers have investigated the overall effects of tip clearance on the loss generated within and downstream of the gap.

Bindon (1988) separated the loss in a linear cascade into various components and attributed 13% of the overall loss to secondary and endwall loss, 39% to internal gap loss and 48% to mixing loss as seen in Figure 2.5. He found that mixing loss was only significant towards 80% of axial chord and found that the mixing process

was far from complete by the trailing edge, suggesting that a considerable amount of kinetic energy remained in the leakage flow in the exit plane of the cascade.

In contrast to this finding, Yaras & Sjolander (1989) found that the internal gap loss was relatively unimportant in terms of the overall losses associated with tip clearance. A possible explanation here could be the large blade chord used by them with a radically different blade geometry representing the tip section of a real turbine. Yaras & Sjolander (1989) also showed that a considerable amount of the leakage flow kinetic energy at the gap exit had recovered by the trailing edge.

In evaluating the loss due to tip clearance, Heyes & Hodson (1992) used the concept of the conservation of mass and momentum to derive a loss model. The total loss generated was linked to the gap discharge coefficient by Heyes et al (1991) and it was suggested that the reduction of the leakage flow rate was more important then reducing the internal gap loss. Other researchers such as Yaras & Sjolander (1989) and Dishart & Moore (1989) linked the total loss generation to the kinetic energy of the leakage flow at the gap exit on the presumption that the kinetic energy of the flow would dissipate to form entropy.

4. Attempts to modify the tip leakage flow and the subsequent loss

In a study of cavitation in radial impellers, Gearhart (1964) used three types of tips in an attempt to minimise cavitation in the tip region of the blades. He found that a diverging gap resulted in the lowest leakage mass flow but did not eliminate cavitation within the gap. He achieved this by radiusing the inlet corner of the gap and suggested that a combination of these two geometries be used to minimise overall cavitation in the pump.

Booth et al (1982) made use of three water flow rigs to investigate the discharge coefficients of 17 varieties of tip shape including grooved tips and a partially shrouded blade tip or winglet. The winglet shape was seen to deliver a moderately improved performance over the other shapes, the reasons offered being a combination of a reduced discharge coefficient and a reduced pressure loading across the extended tip surface. Wadia & Booth (1982) used a water flow rig and a numerical approach to focus on controlling the tip leakage flow by reducing the discharge coefficient using viscous effects. Five geometries were tested including a flat tip, pressure, suction and double squealer tips and a winglet tip. Again the winglet tip was found to perform better than the other shapes for the reasons given above.

From an investigation of tip clearance flows in a compressor cascade and using a simple numerical approach based on the model of Rains (1954), Storer & Cumpsty (1990) found that the leakage flow in the gap was primarily inviscid and essentially was found to be independent of the tip geometry. The overall loss was found to be a function of the discharge coefficient and mostly independent of the internal gap loss.

Heyes et al (1991) reduced the tip discharge coefficient to minimise the overall leakage loss. They compared a flat tip shape to a pressure and suction side squealer using two linear turbine cascades (Figure 2.6). The internal gap losses were not considered to be significant in the analysis of each tip shape. The first cascade was also used by Bindon (1988) and similar results were obtained in that both squealer tips demonstrated a lower discharge coefficient compared to the flat tip. The opposite trend was measured in the second cascade, however. The reason offered for the discrepancy was that in the first cascade, the measuring plane was

closer to the trailing edge of the blades and it was suggested that further downstream, significantly more mixing would have occurred. Also no flow deflection was measured in the results of Bindon (1988) and this was felt to be important in determining the merit of each tip geometry.

In a follow up paper, Chen et al (1993) investigated the tip gap flow numerically and experimentally. They proposed that the losses due to tip leakage were directly related to the discharge coefficient and obtained very good agreement with numerical and experimental results. It was found that a double squealer and suction squealer as illustrated in Figure 2.6 could potentially reduce the discharge coefficient if designed correctly.

Metzger & Bunker (1985) also showed that a cavity tip or double squealer tip reduced the leakage flow. A shallow cavity was desirable in terms of minimising the local heat transfer coefficient in the cavity because if a deeper cavity was used the increased surface area of the cavity caused an increase in the actual heat transfer at the tip.

Offenburg et al (1987) investigated the effects of 12 configurations of casing treatment on the performance of an axial turbine, some of which are shown schematically in Figure 2.6. The only benefit of trenching the rotor was obtained when the clearance was significantly higher than the nominal value otherwise a smooth shroud was preferred. The presence of a step either before or after the rotor was seen to be detrimental with the backward step being the worst case. A similar study was conducted by Grant et al (1983) where it was also found that a step was the cause of a reduction in the efficiency of a single stage turbine.

Using the results of Bindon (1988) in which the tip clearance loss was quantified into various categories as reviewed earlier, Morphis & Bindon (1988) investigated the effects of radiusing the pressure corner of a flat tip blade in an annular cascade. They found that for a pressure corner radius of 2.5 times the gap width, the separation bubble was visually observed to disappear and this was confirmed by microscopic pressure tappings. The elimination of the separation bubble, however, was seen to allow a greater mass flow and hence a higher discharge coefficient.

In a follow up study, Bindon & Morphis (1990) investigated the possibility of minimising the overall loss by reducing the internal gap loss. Two streamlined, low entropy tips were designed as shown in Figure 2.6. and tested in a linear cascade. The first shape was a radiused pressure corner to eliminate the separation bubble on the tip surface. For the radiused pressure corner tip, it was found that the internal gap loss was reduced but a higher mixing loss penalty was incurred in line with previous observations. Interestingly, the high loss core in the leakage vortex observed for the flat tip was significantly reduced for the streamlined tips, but no relation between gap loss and mixing loss was found. A contoured suction squealer tip was seen to have a slightly lower discharge coefficient than the radiused tip and produced lower loss at the gap exit than the flat tip.

The results were converted to a simulated rotor flow by vectorially adding a hypothetical blade velocity to each vector measured. Although real effects such as a radial pressure gradient and relative motion were not modelled, the computed results indicated that the contoured squealer tip potentially delivered a significant improvement in efficiency over the flat tip despite having a similar measured overall loss coefficient to the flat tip. It is of interest to note that the discharge

coefficient for the contoured squealer and the radiused tip were 0.92 and 0.926 respectively compared to the flat tip value of 0.824, an increase of approximately 12%. The authors did not find a good correlation between discharge coefficient and the cascade overall total pressure loss with the measured values of loss for the flat, radiused and contoured squealer tip were 0.874, 0.964 and 0.843 respectively.

In a similar study of the gap leakage flow, Kaiser (1992) compared a flat tip shape to a double squealer tip and a suction squealer tip in an annular cascade. Although the suction squealer was found to have the lowest loss at the gap exit, it generated the highest leakage mass flow rate. The differing results suggest that the radial pressure gradient among others may be responsible for the differing trend.

Due to the uncertainty in the accuracy of translating linear cascade data to a rotating frame, Morphis (1993) developed a one and a half stage axial turbine using a free vortex design to investigate a variety of tip shapes, namely a flat tip, radiused tip and contoured squealer tip. Unfortunately, follow up work has shown that a faulty reading was responsible for a number of incorrect conclusions in the original study, however, a number of trends were noted which have been found to be valid.

The radiused tip and contour squealer were shown to deliver a comparable performance to the flat tip in contrast with the belief that the overall loss is independent of internal gap loss and a function only of the discharge coefficient. It is important to reiterate that Morphis & Bindon (1990) found a 12% increase of the discharge coefficient for the streamlined tips over the flat tip. Clearly the mechanism of tip clearance loss is highly complex and the extrapolation of linear cascade data may not be reliable enough to compare various tip treatments in a

working turbine. Other factors such as the deflection of the leakage flow are important in comparing the various tip treatments, as noted by Heyes et al (1991).

5. Potential gains using low entropy tip shapes

Whilst a reduction in leakage mass flow has the potential to increase work due to an increased fluid deflection and a lower mixing losses downstream of the rotor, one other benefit has largely been ignored in recent years, namely the minimisation of heat transfer at the tip. This thesis does not investigate the issue of heat transfer directly but considers the work of various researchers as an indication of the merits of a particular tip treatment.

The formation of the separation bubble and subsequent reattachment of the leakage flow behind the bubble has been the subject of an investigation by Bindon (1987a) who related the zone of attached flow around the pressure corner and the reattachment zone behind the bubble to high shearing and hence high local heat transfer coefficients.

Work in a water table analogy of supersonic flow by Moore & Elwood (1992) showed that after accelerating into the gap, the leakage flow reattached to the surface, followed by an oblique shock wave which was associated with increased heat transfer coefficients on the tip surface. Moore et al (1989) found that a peak heat transfer coefficient in the gap was about 1.85 times the fully developed value in the gap.

Metzger & Rued (1988) investigated blade tip burnout near the tip on the pressure surface of a simulated turbine blade. Near the pressure corner, the local heat transfer coefficient increased up to 200% of the normal heat transfer coefficient. The results are very much in line with the high velocities and high shearing measured by Bindon (1987a). Metzger & Bunker (1985) showed earlier that a shallow cavity or double squealer tip could reduce the leakage mass flow rate but the slight reduction of the local heat transfer coefficient was offset by the increased area exposed along the tip surface with a higher overall heat transfer at the tip.

Chen et al (1993) showed that if a secondary jet from blade cooling passages were exhausted at right angles to the main flow in the cavity of a double squealer tip, effective shrouding of the tip surface by the cooling flow was possible, suggesting that the tip heat transfer could be minimised by the secondary jet.

Sjolander & Cao (1994) found that the heat transfer on the tip surface was increased by a previously unnoticed mechanism, namely that the separated flow on the tip surface induced a counter-rotating vortex near the pressure corner which was responsible for high shear and hence high heat transfer coefficients. The author disputes this particular model since it ignores the detailed findings of Bindon (1986a) who showed that the leakage flow enters the gap and remains attached for a short distance up to a point where the surface pressure recovers, forcing the flow to separate. This highly accelerated, attached flow is expected to generate a chordwise zone of high shearing on the tip surface with corresponding elevated heat transfer coefficients.

Considering the flow around a cylinder for which the velocity and pressure distribution is well known, an interesting observation can be made from the distribution of the local heat transfer coefficient as illustrated in Figure 2.7 from Özişik (1985). Taking the case of $Re=1.4x10^5$, two minima can be seen. The first appears at about 80° which is the angle at which the boundary layer changes from laminar to turbulent and the second occurs where separation takes place at about 130°.

Essentially, the boundary layer shields the surface from high heat transfer until it is disturbed by some phenomenon which in the case of the cylinder corresponds to the transition from laminar to turbulent flow and the start of separation. The peak heat transfer coefficient is associated with a high level of turbulence and does not occur at 90° where the maximum velocity is known to occur. It seems likely then that the high heat transfer experienced on the pressure corner of a flat tip blade is due primarily to the highly accelerated flow remaining attached around the pressure corner as well as the separation bubble which contains a highly sheared vortical flow on the tip surface. Near the point of reattachment, the boundary layer on the tip surface can also be expected to be turbulent with an increased convective heat transfer coefficient.

Bindon & Morphis (1990) used two low entropy tip shapes to investigate the effects of tip clearance in a linear cascade. While it was seen that both low entropy tips minimised the entropy within the gap, the leakage flow was slightly larger for the radiused tip as well as the overall mixing loss. The suction squealer showed a potential advantage by reducing the leakage flow compared to the flat tip and this could possibly lower the heat transfer coefficient on the tip surface. Also of interest to tip heat transfer is that the radiused tip effectively eliminated the

separation bubble near the pressure corner. The implication of this is that the highly sheared flow on the tip surface near the pressure corner is minimised, effectively lowering the local heat transfer coefficient. The absence of the separation bubble can therefore be associated with a lowering of the heat transfer coefficient and hence the possibility exists that heat transfer in that region will be lowered.

6. The effects of relative motion

In a turbine, the relative motion of the endwall opposes the direction of the leakage flow. In addition to this the inlet boundary layer is skewed in the relative frame and this has proven difficult to simulate in a linear cascade. Relative motion is seen to be a complex occurrence and a number of interesting findings have been reported.

In an early study, Gearhart (1964) used a moving belt to simulate relative motion at the tip of a compressor cascade. The leakage mass flow was observed to increase as expected in a compressor situation.

In a survey of the heat transfer coefficients in the tip region, Mayle & Metzger (1982) reported no significant changes in the tip region due to relative motion. The leakage flow was seen to be primarily inviscid with no interaction between the endwall and tip surface boundary layers.

Graham (1986), however, observed a reduction in the strength of the leakage vortex with relative motion in a turbine water cascade. This led to a weakening of

the leakage vortex and a rise in pressure on the suction surface near the tip of the blade.

Using an annular cascade with a rotating endwall, Morphis & Bindon (1988) reported that the pressure distribution on the tip surface was not significantly affected by relative motion. The width of the separation bubble and the low pressure within it were also independent of relative motion but the pressure in the reattached zone behind the bubble was moderately higher. The reasons for this were attributed to a slightly lower leakage flow rate, indicating the added complexity of relative motion and the effect on the gap discharge coefficient.

Kaiser (1992) conducted similar work in the same annular cascade and reported that there was little influence on the nature of the leakage mass flow rate with relative motion. The leakage jet appeared to be mainly inviscid and a boundary layer near the endwall was very small and did not interact with the boundary layer on the tip surface. There was a moderate reduction in the chordwise discharge coefficient over the last half of the blade chord with the overall reduction being about 4%.

In contrast to these findings, Yaras & Sjolander (1991) measured a reduction of 50% of the leakage flow with a moving belt in a linear cascade, however, they also mentioned that the leakage flow appeared to be largely inviscid within the tip gap. They advanced the reason for the reduction of the leakage flow rate as an increase in the blade tip loading due to the higher belt speeds. It seems more logical, however, to regard the increase in the pressure-suction differential pressure as the result of a reduced leakage flow rate that generates a weaker passage vortex in the suction corner. Possible reasons for the differing outcome from Kaiser (1992)

could be the length that the moving belt extended above the blade row and differing blade geometries as well as radial effects present in the annular cascade used by Kaiser.

Kingcombe et al (1990) measured a moderate reduction of the leakage flow rate with an increase in blade speed of a rotating cold flow turbine. This was ascribed to two possible reasons, the first being a reduction in the tip clearance due to increased centrifugal forces and the second being a reduced leakage flow rate caused by a shearing action which altered the effective area of the gap or vena contracta. This was seen to reduce the differential pressure across the blade tip by increasing the suction surface pressure. However, as noted previously by Sjolander & Amrud (1986), the reduction was due to the reduced strength of the leakage vortex and an increased blade tip loading was expected to occur.

7. The effects of the clearance gap size

Researchers using compressors and compressor cascades have observed similar tip clearance phenomena to turbines, however, two important differences occur. The first is the opposing effect of relative motion and the second is the diffusing boundary layers present in a compressor blade row compared to an accelerating boundary layer in a turbine blade row. The diffusing boundary layer tends to separate from the walls giving rise to the condition of rotating stall which is the onset of stall in the blade row. Storer (1989) found that an optimum tip clearance did seem to exist for a compressor and attributed this to the leakage flow minimising separation within the blade passage by energising the boundary layer.

Turbine results indicate, however, that there is no optimum clearance size and instead a minimum should be maintained at all times. Booth (1985) suggested in a lecture series that the percentage degradation of turbine performance was a linear function of the percentage increase of tip clearance and the proportional coefficient was found to lie in the range of 1.5-2. In his review, Peacock (1983) also mentioned a number of researchers who measured a linear degradation of turbine performance with increasing tip clearance. Storer (1989) found a linear relationship between clearance and the leakage flow rate or discharge coefficient but observed a non linear increase in the mixing loss, suggesting again that the loss cannot simply be attributed to the loss of the kinetic energy of the leakage flow.

Yaras et al (1988) obtained an approximately linear relationship with tip clearance and the gap discharge coefficient for a range of clearance from 2-3.2% chord. The separation bubble was also seen to fill a larger portion of the gap. In his study using micro pressure tappings, Bindon (1986a) also showed that the pressure distribution on the suction corner decreased with increasing tip clearance, indicating that the increased strength of the leakage vortex was responsible for the reduced pressure on the suction surface. Morphis & Bindon (1988) also showed that the separation bubble width was dependent on the gap size.

8. The endwall boundary layer

In a turbine blade row with no clearance, the loss mechanism is mainly due to profile loss and the secondary flow loss at the hub and tip which further adds to the problem by producing underturning in the mid span region as reported by Moustapha et al (1986) and Gregory-Smith (1982). The formation of the horse

shoe vortex at the inlet to the cascade also influences loss formation, however, it has been seen that at increasing tip clearances, the endwall boundary layer is simply swept away and wrapped up by the leakage vortex (Bindon 1986a).

This was also verified by Yaras et al (1988) who found no evidence of an endwall boundary layer except near the leading edge and Chan et al (1994) who found that secondary flow and tip clearance loss was essentially independent of the thickness of the inlet boundary layer. An added complexity of the hub and endwall boundary layers in a rotating frame is the skewing of the boundary layer relative to the rotor blades. This has been investigated by Bindon (1979) who found significant variations between cascade loss coefficients for various skewed boundary layers. In particular, positive skew was found to reduce the cascade loss which raised concerns over the validity of linear cascade data. Walsh & Gregory-Smith (1989) also found a similar trend with the effects of skewing.

However, in the real tip clearance situation, a rotor does not experience an "endwall" boundary layer, skewed or unskewed. In reality, the nozzle presents the rotor with boundary fluid that as been wrapped up into corner vortices. They are in turn highly periodic due to the motion of the rotor past the nozzle.

In general, though, it should also be remembered that skewing a boundary layer in linear or annular cascade amounts to an addition of energy to the boundary layer by viscous work. An accounting method of this must be used in analysing the effects of artificial skewing. To this effect, Boletis & Sieverding (1991) concluded that the overall results in a 1.5 stage turbine due to hub and endwall skewing did not resemble linear cascade results. Sieverding et al (1984) had previously concluded that due to the complexity of the secondary flow structures in annular

cascades, a numerical method was the only manner in which the details of the flow could be quantified.

9. Work in rotating turbines

Due to the uncertainty of the accuracy of extrapolating linear cascade data to a fully rotating rig, a number of researchers have opted to investigate tip clearance phenomena in rotating machines. The flow is vastly more complicated due to radial pressure gradients and time varying flow due to the interaction of the stator-rotor flows.

Hunter (1982) showed that the results for the first stage nozzle of a single stage turbine were similar to linear cascade results but due to the radial pressure gradient there was a significant tip-to-hub migration of low momentum fluid via the blade wakes and also along the blade suction surfaces. Instantaneous measurements behind the rotor revealed strong secondary flows near the hub. There was little evidence of a secondary flow structure at the tip though. The author also linked a region of underturning with a maximum axial velocity.

In his review, Peacock (1983) noted that the presence of tip clearance caused a higher axial velocity in the tip region. This reduced the axial velocity over the rest of the blade span with the resulting reduction in blade loading and is also mentioned in Heyes & Hodson (1992). Also of interest, Peacock (1983) presented data indicating that the rotor exit pressure in the tip region was significantly higher than that over the rest of the blade span. This corresponded to the region of high axial velocity at the tip with an increased absolute outlet angle.

Sharma et al (1988) investigated the effects of unsteadiness in the rotor-stator interaction of 1.5 stage turbine. They identified the rotor secondary flow structures and observed that these tended to persist through the second stator, reducing the normal secondary flow. These flows were seen to give rise to underturning in the endwall regions and overturning in the midspan region. The overall effect of tip clearance, however, was not shown.

An investigation of three dimensional flow in a 1.5 stage axial turbine was conducted by Joslyn & Dring (1990). The study concluded that hub and tip secondary flows as well as radial flows in the blade wakes were primarily responsible for radial transport in the flow. In the rotor, it was seen that the tip leakage flow also contributed to the radial transport of fluid. There appeared to be a total pressure gain at the exit of the second stator in the tip region. This was attributed to the radial transport of fluid between the inlet and outlet of the stator and the fact that the total pressure loss was determined by the difference between the inlet and outlet conditions at the same radius. The authors also linked various regions of over and underturning to corresponding regions of low and high axial velocities at the rotor exit.

Boletis & Sieverding (1991) presented data from a 1.5 stage turbine to show the flow field at the rotor outlet and behind a second nozzle. In the relative frame, the tip clearance flow caused underturning but close to the endwall, the relative angle increased due to the effect of relative motion. The leakage flow was shown to cause a loss in the relative total pressure at the rotor exit. In the absolute frame, however, the total pressure near the tip at the outlet from the second stator was also seen as a gain . The authors showed that the significant loss in the relative total pressure in the hub region of the rotor outlet was not seen in the absolute

flow. There was a strong radial migration of low momentum fluid from tip to hub within the blade wakes and along the suction surfaces of the blades which culminated in a loss core at approximately 35% of the span from the tip. The authors again concluded that artificially created boundary layer skew is not representative of real conditions.

Morphis & Bindon (1994a) and (1994b) also produced similar findings in terms of the flow at outlet from the rotor and behind the second stator. In particular, at outlet from the second stator, a concentrated loss formation was seen on the suction side of the blade wake. The second stator was found to be more efficient than the preceding one, however, after an initial investigation, a faulty transducer was found to have influenced a number of conclusions. This has led to a re-evaluation of the results and this thesis attempts to explain the recent findings by some of the above mentioned researchers in the field.

As a possible explanation for the reduction in loss of the second nozzle, a number of interesting studies have been conducted to examine the effects of inlet incidence on the formation of secondary loss within a linear cascade. While these results may be tempered by the reality of the radial pressure gradient within a real machine, the conclusions are nonetheless of importance. A study by Tremblay et al (1991) showed that the off-design performance of a turbine cascade was considerably different at large negative and positive incidence angles. At a positive incidence of 25°, the loss showed a large increase, similar to the profile loss at various incidences predicted by Ainley & Mathieson (1951). However, the authors measured only a very slight increase in loss for -25° inlet incidence to the cascade. The deviation of the cascade outlet flow showed a similar trend with a slightly higher deviation at -25° than the design condition.

In a more recent study, Dossena et al (1993) showed that an incidence angle of +30° caused loss of a similar magnitude to that seen by Tremblay et al (1991), however, at -30° incidence there was a slight reduction in the cascade total pressure loss as well as a reduction in the deviation at the cascade exit. The secondary flow vortices were weaker and the loss formation associated with these was found to be concentrated on the suction side of the blade wakes near the endwall.

In a slightly different study, Biesinger & Gregory-Smith (1993) investigated the effect of tangential blowing on the loss associated with secondary flows in a turbine cascade. They found that the strength of the secondary flow vortices could be reduced by blowing which reduced the overall cascade loss, however, there was no net gain when the energy associated with the blowing jet was accounted for. Chan et al (1994) also observed that with increased tip clearance, a reduction of up to 50% of the secondary flow loss occurred in the tip region of a linear cascade thus associating the reduction with the leakage flow rate.

Tip clearance gives rise to a leakage flow that essentially is underturned. Regardless of whether or not the leakage jet exists as a high velocity jet near the wall or has completely rolled up into the suction corner vortex, the flow close to the endwall will enter a downstream stator with negative incidence. This could then reduce the strength of the secondary flows in the downstream stator, effectively lowering the secondary flow loss development, even though additional mixing losses of the leakage jet would occur.

10. Predictive techniques

Although tip clearance is qualitatively understood, accurate predictions of the strength of the leakage flow and the associated mixing losses in a real working machine have not been published. A number of researchers have developed numerical models of the tip clearance flow based on the model of viscous flow presented by Rains (1954).

Moore & Tilton (1987) developed a combined potential flow and mixing model to predict the pressure distributions in the tip region and the gap discharge coefficient. Their calculations agreed very well with experimental results.

Yaras et al (1988) presented a simple tip clearance model based on a number of conditions. The fluid entering the gap was presumed to be undisturbed. The gap driving pressure was assumed to be the undisturbed mid span pressure-suction differential at the local chordwise position and no chordwise pressure gradient was accounted for, a phenomenon shown to be significant by Bindon (1987a). Results were similar to the experimental measurements in a large scale linear turbine cascade, however, an artificial numerical reduction of the gap area was needed to account for the measured flow rate which essentially suggests that a mid span pressure differential is not a valid assumption in determining the discharge coefficient.

Heyes et al (1991) extended the model of Moore & Tilton (1987) and numerically computed the leakage flow over a flat, pressure and suction squealer tip. The models indicated that the leakage flow rate was the critical parameter in determining the loss and that it should be minimised. The results tended to over-

predict the leakage loss due to the fact that curvature over the separation bubble reduced the discharge coefficient as well as the fact that the leakage flow had not mixed completely by the gap exit.

Heyes & Hodson (1992) presented an improved model of the leakage flow using a time-marching scheme and obtained good agreement with measured results. This was used for a variety of tip geometries and flow conditions and included the effect of the chordwise pressure gradients which had been ignored by most other researchers.

Chen et al (1993) used an advanced numerical technique with a 2-D Navier-Stokes solver to investigate the gap flow for a variety of tip geometries. The numerical results showed excellent agreement with experimental measurements and it was concluded that suction squealers could have an overall advantage if designed correctly.

The overall 3-dimensional effect of tip clearance in an axial turbomachine has been investigated by Basson (1993). The author compared the calculated results to the measurements of Bindon (1987a) and Bindon & Morphis (1992) and obtained very good estimates of the actual flow in an axial turbine with tip clearance. Some of the results of the flow at a radius of 50% of the tip gap from the endwall are presented in Figure 2.8. It can be clearly seen that there is a significant axial component to the leakage flow even at the rotor outlet.

A numerical solution obtained by Bindon (1994) was compared to the experimental results of Morphis (1993) for a 1.5 stage turbine. Figure 2.9 illustrates the relationship between clearance size and the strength and position of the leakage

vortex in the relative frame close to the rotor exit. At 1% clearance, there is a suggestion of a classical secondary flow vortex structure near the tip at about mid pitch, but which may also be an induced vortex structure caused by the suction corner vortex. At higher clearances, the leakage vortex dominates and no indication of secondary flow can be observed. It is also apparent at the larger clearances that the leakage flow has a large swirl component that has not completely wrapped up into the suction corner vortex. It is also interesting that the position of the leakage vortex moves away from the suction surface towards the pressure surface on the adjacent blade, a similar result to linear cascade results.

Bindon (1994) also compared the predicted rotor absolute outlet angle for varying tip clearance to the measured results of Morphis (1993) as illustrated in Figure 2.10. Interestingly, both results show relatively good agreement from about 25% span up to the hub, however, at 1% clearance, the angle at the tip is over-predicted. The depth of penetration of the outlet angle variation was also under-predicted.

11. Concluding remarks and statement of objectives

Translating linear cascade data to a rotating machine, while qualitatively correct, may not be sufficiently accurate to predict the loss generation or to optimise the tip gap geometry during the design process.

Measuring and identifying tip clearance micro flow structures even in large experimental turbines will be extremely difficult and it is the opinion of the author that the relatively small details may not be sufficiently resolved to reveal the details of the flow within the rotating blade rows. Instead, it is felt that a

numerical approach holds more promise in establishing the nature and formation of tip clearance effects in a rotating machine. This has also been voiced by Sieverding et al (1984). Modern codes such as Denton (1996) now include micro grid points in the tip region and with an advanced numerical technique, are able to identify micro flow details.

However, based on the linear and annular cascade findings, it is believed that a fully rotating test rig can offer some valuable insights into the overall performance of various tip shapes at varying clearance, since a direct comparison of turbine efficiency is available. Also, time averaged pressure readings to a large extent are able to reveal the total pressure loss and the structure of the flow field behind the rotor as well as the development of that flow field either in the presence or absence of a second stator. A realistic overall effect of tip clearance with various tip shapes can be fully investigated in a representative machine where the aerodynamic performance is correlated with the measured shaft power.

The objectives of this thesis can be summarised below

a) Investigate and confirm the performance of a 1.5 stage axial turbine with differing tip shape rotors for a range of clearances.

b) Re-evaluate the comparison between the flat tip shape rotor and two low entropy tips, namely a radiused pressure corner and a contoured suction squealer tip and additionally investigate a leakage flow rate reducing tip, namely a double squealer tip.

c) Examine the performance of the second stator to determine the nature of the clearance effects on the second stator and possibly to resolve the high efficiency seen in the previous work.

d) Develop a qualitative model of the tip clearance leakage flow behind the rotor of a three dimensional machine and the subsequent interaction of that leakage flow with the downstream stator.

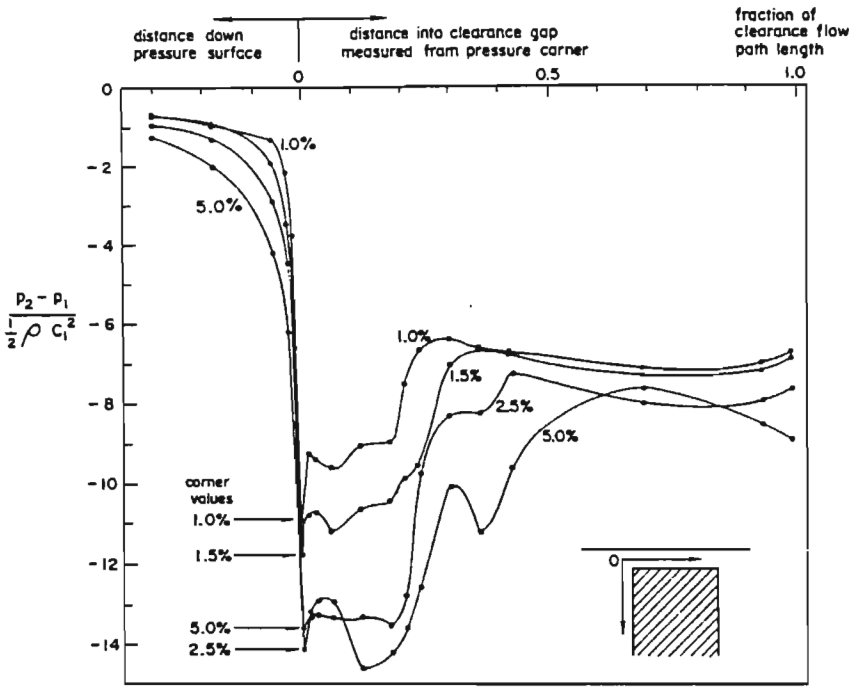

Figure 2.1 The distribution of the blade surface pressure for various clearances at 60% chord showing the attached flow on the tip surface adjacent to the pressure corner (Bindon (1986a)).

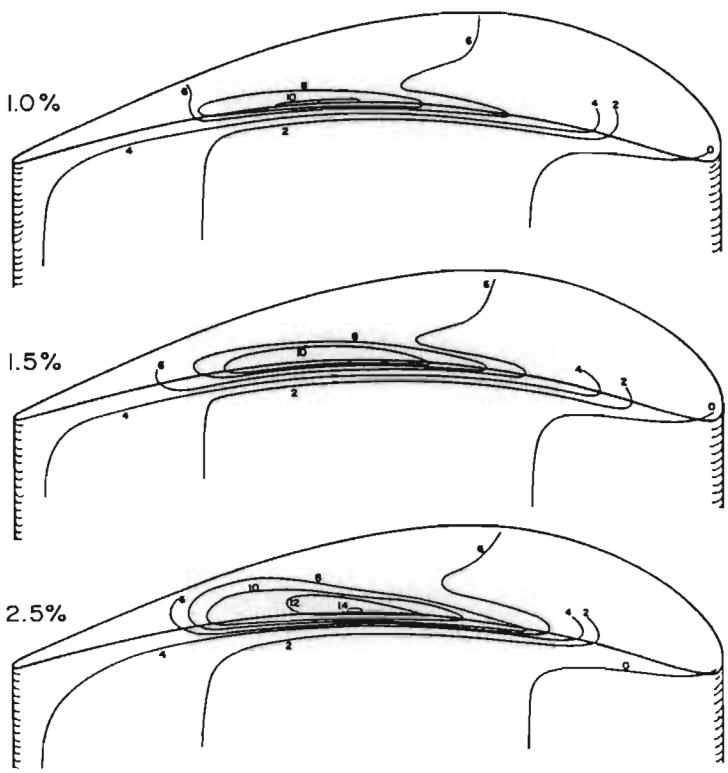

Figure 2.2 Static pressure contours on the blade surface in the clearance gap showing the minimum pressure near mid chord for various clearances (Bindon (1986a)).

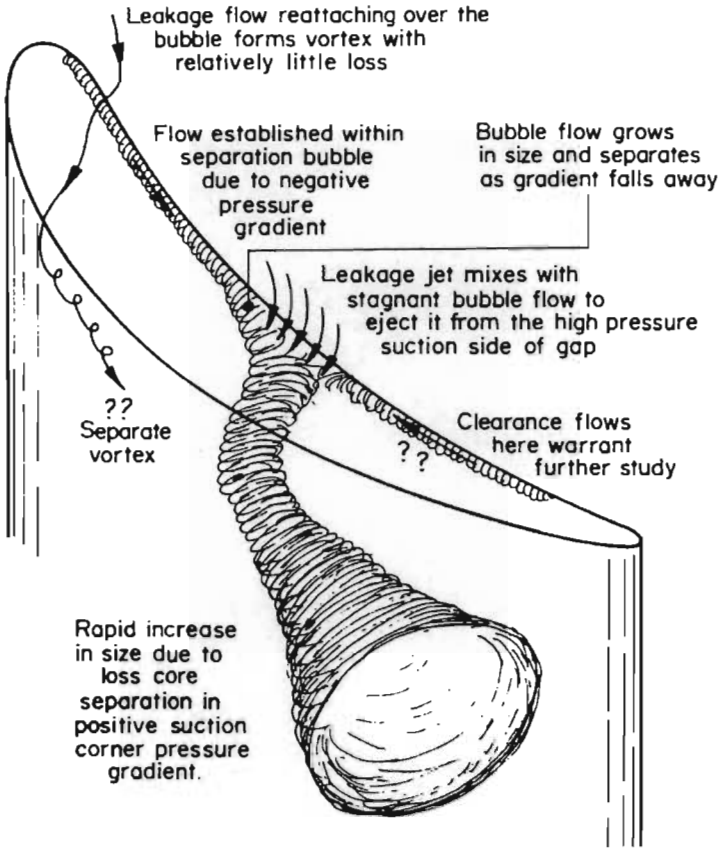

Figure 2.3 The suggested mechanism of the emergence of low momentum fluid from the separation bubble and the subsequent mixing with the passage flow (Bindon (1988)).

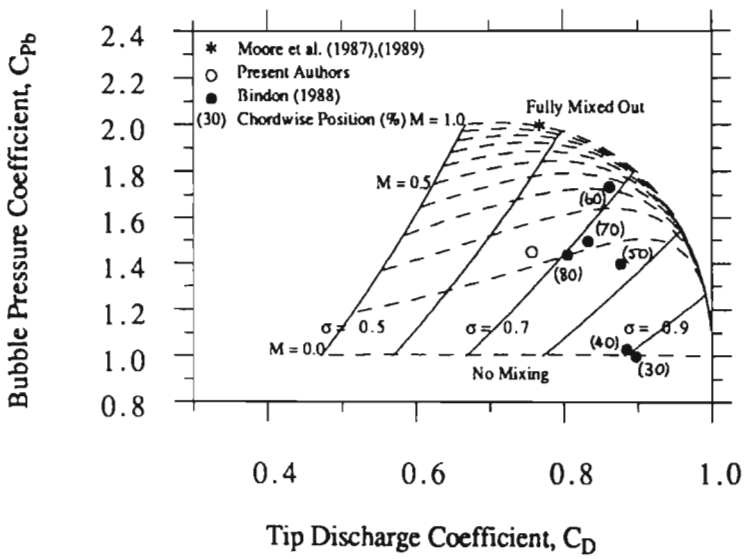

Figure 2.4 The mixing model of Heyes et al (1991) indicating the discharge coefficient as a function of the bubble coefficient and the amount of mixing at the gap exit.

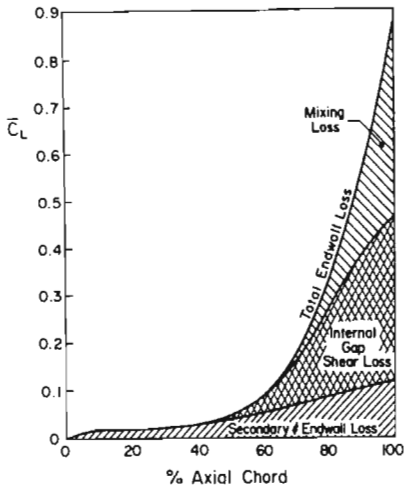

Figure 2.5 The total endwall loss development showing the contributions due to internal gap shear, secondary/endwall loss and leakage jet mixing loss (Bindon (1988)).

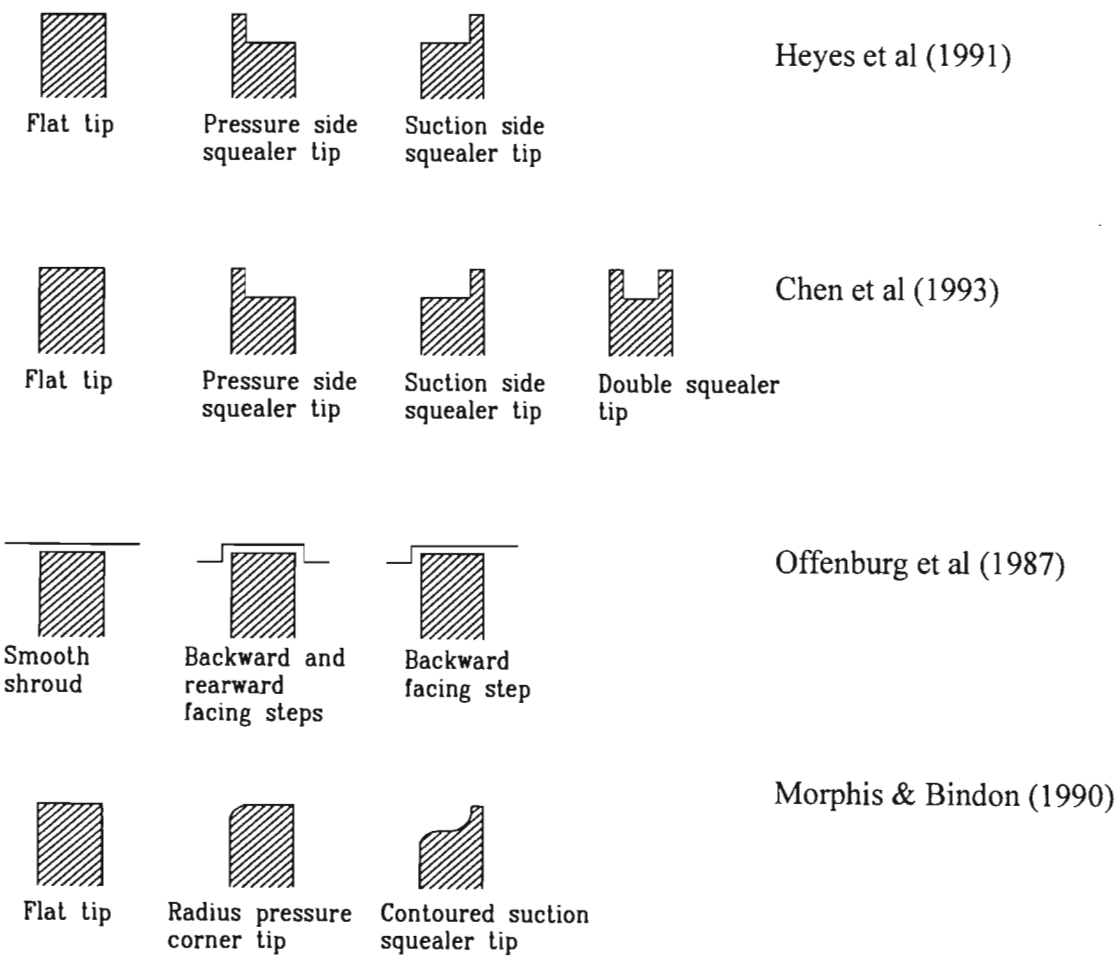

Figure 2.6 A selection of tip treatments by various researchers

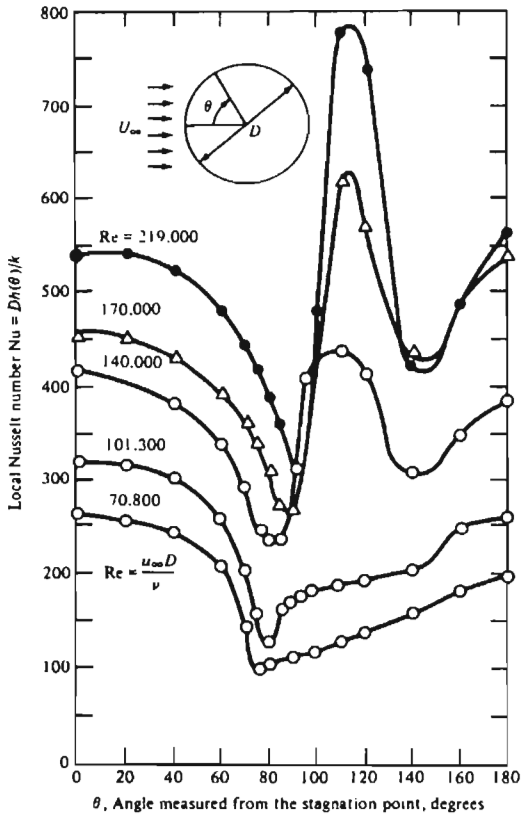

Figure 2.7 The distribution of the heat transfer coefficient around a cylinder (Özişik (1985))

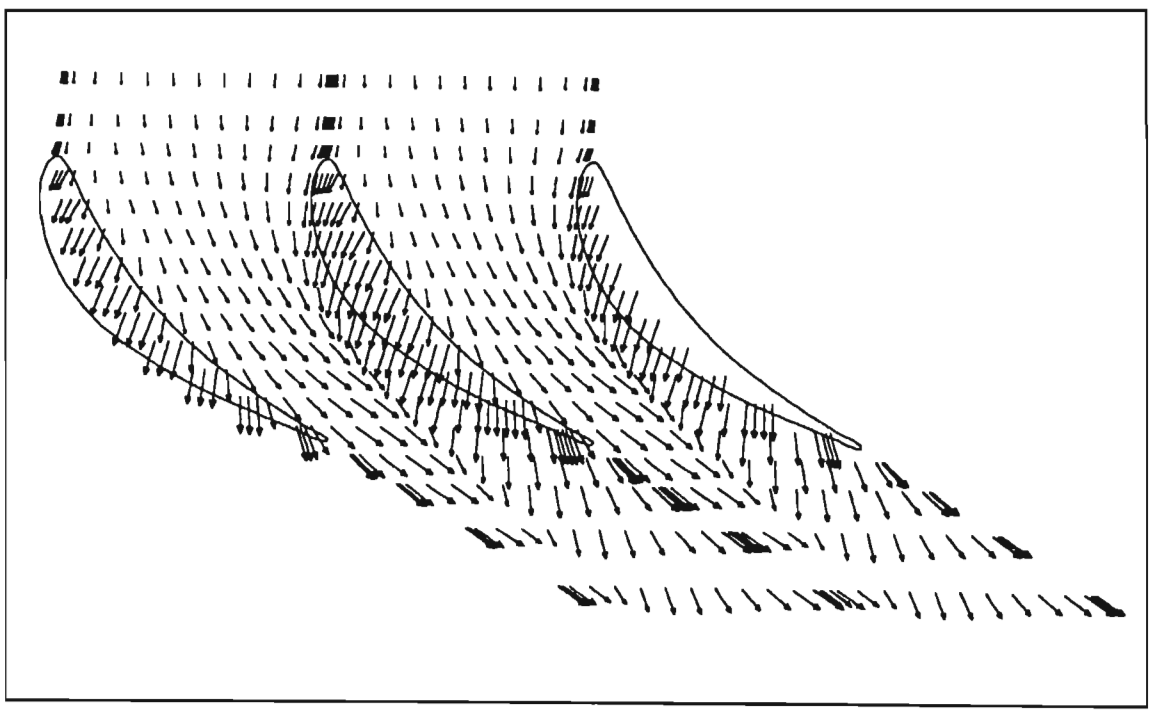

50% of Tip Gap from Endwall

Figure 2.8 The predicted flow of Basson (1993) showing the leakage flow close to the endwall as a poorly deflected wall jet

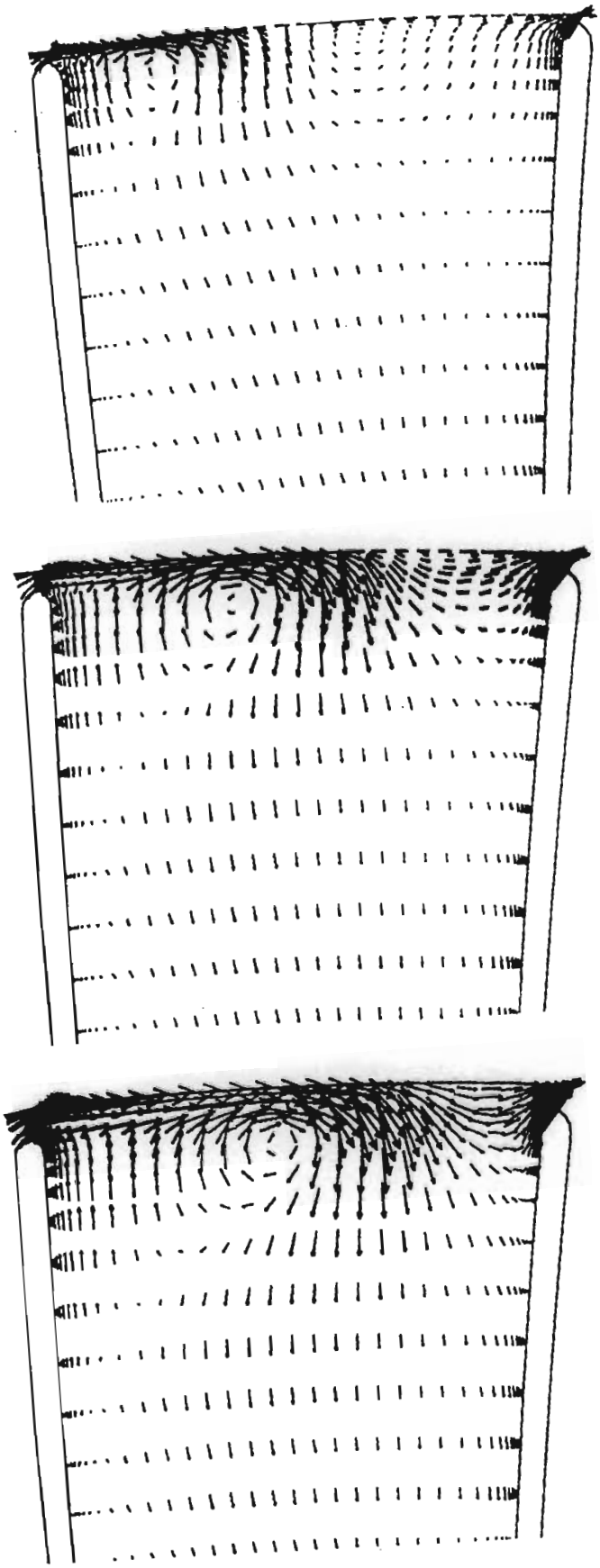

Figure 2.9 The predicted leakage vortex structure and vortex position for varying clearance, Bindon (1994).

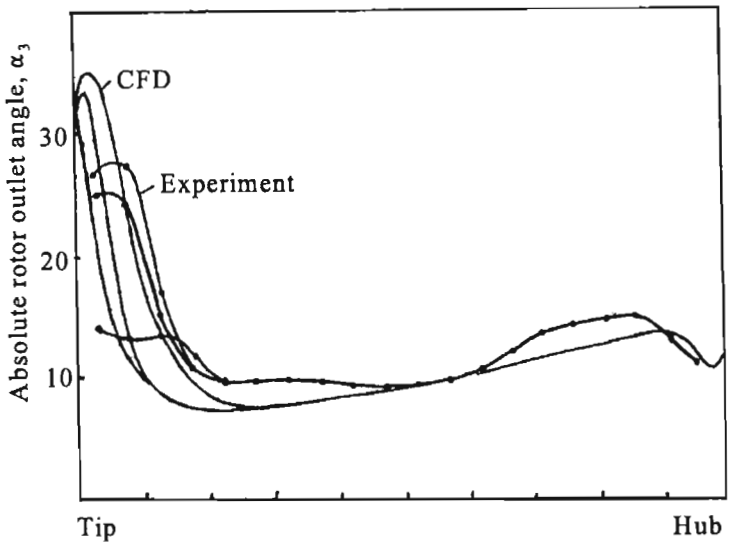

Figure 2.10 The predicted results of Bindon (1994) for the radial variation of the rotor absolute outlet angle at varying clearance compared to the experimental measurements of Morphis (1993).

CHAPTER 3

INSTRUMENTATION AND DATA ACQUISITION

1. Introduction

A low speed axial turbine was developed by Morphis (1993) to examine the effects of tip clearance and tip shape on the overall performance of the turbine. The flow was traversed with a pneumatic five-hole probe connected to 5 differential pressure transducers in a specific arrangement to minimise measuring errors. A miniature 3-hole probe was also used to traverse the region close to the endwall where the larger 5-hole probe could not be used. In order to obtain numerous results that were highly repeatable, the control of the turbine operating parameters as well as data acquisition was fully automated using stepper motors and a personal computer.

2. Description of the 1.5 stage turbine

The vertical research turbine illustrated in Figure 3.1 indicates the traverse measuring points as well as the arrangement of the blade rows of the vertical research turbine used in this investigation. The positions of the measuring stations are presented in Table 3.3. Air is drawn into the turbine and through the blade rows by a radial fan driven by a hydraulic power pack. The amount of hydraulic power required to drive the fan was controlled by a stepper motor driven swashplate pump which in turn regulated the flow rate or axial velocity through the turbine. The torque developed by the rotor was transferred by a shaft to a torque transducer through a special zero backlash and self aligning coupling which

absorbed no power from the rotor. The torque transducer also measured the shaft speed to enable the rotor power to be determined. The power developed by the rotor was absorbed by a hydraulic pump which expanded the high pressure hydraulic oil through a valve thus creating heat which ultimately was rejected in a water cooling circuit. The governing of the valve was accomplished with a stepper motor which then resulted in a computer controllable rotor speed.

The nozzle and rotor blades were designed by Morphis (1993) according to the free vortex criterion assuming incompressible flow conditions and hence twisted blades were manufactured. The blade profiles were designed with a commercial package, Northern Research and Engineering Corporation (1972) (NREC). The NREC program "BLADE" was used to design the blade profiles at five radial stations for the inlet and outlet angles presented in Table 3.1. Additional design parameters required were the inlet and outlet Mach numbers as well as the Mach number distribution on the blade surfaces. The design procedure was an iterative one that required the Mach number distribution as the starting point. A blade profile was then obtained and the Mach number distribution was then modified until a suitable profile was found. The profile selection criteria included the trailing edge thickness, blade chord length and blade area. The intermediate blade profiles were then found by linear interpolation to create a total of 29 radial profiles and, after CNC machining, were carefully blended to obtain the final blade shapes.

For simplicity, the second nozzle was designed exactly the same as the first. A zero-shrink epoxy resin was used to cast the blades and very good tolerances were obtained with a complex curing process developed by Morphis (1993). A summary of the turbine aerodynamic data is presented in Table 3.1 and the geometry specifications for the nozzle and turbine blades are presented in Table 3.2. A

detailed description of the iterative blade design procedure and the technique of casting and the subsequent curing of the blades is documented in Morphis (1993).

Table 3.1 Turbine aerodynamic data

	Hub		**Mid**		**Tip**
Radius (mm)	142.0	157.3	172.5	187.8	203.0
α_1	0.0	0.0	0.0	0.0	0.0
α_2	66.1	63.9	61.7	59.6	57.6
α_3	0.0	0.0	0.0	0.0	0.0
β_2	42.8	29.5	13.6	-2.93	-17.9
β_3	53.1	55.8	58.2	60.4	62.3
Reaction	0.15	0.31	0.42	0.51	0.58
V_x/U	0.752	0.680	0.617	0.568	0.526

Table 3.2 Nozzle and Rotor blade geometry specifications

	Hub		**Mid**		**Tip**
Radius (mm)	142.0	157.3	172.5	187.8	203.0
Nozzle chord (mm)	36.8	39.5	41.8	44.8	46.5
Rotor chord (mm)	46.3	46.2	46.0	46.0	46.0
Nozzle thickness max (% chord)	18.5	19.0	15.8	14.7	14.3
Rotor thickness max (% chord)	17.3	16.5	15.3	15.3	15.3
Nozzle blade area (mm^2)	143	154	164	180	195
Rotor blade area (mm^2)	248	233	201	186	162

	Nozzle	Rotor
Trailing edge thickness (mm)	1.0	0.7
Mid Pitch/Chord ratio	0.55	0.63
Number of blades	41	43

The leading edge of both the rotor and nozzle blades was given a 1mm radius to compensate for varying inlet incidence. This effectively reduced the blade chord by 1mm.

Table 3.3 Measurement positions relative to blade rows

Station	Percentage axial chord measured at		Based on tip chord of
	Hub	Tip	
Plane 1	198.6	70.3	Nozzle
Plane 2	26.0	16.3	Nozzle
Plane 3	9.7	33.6	Rotor
Plane 4	22.9	13.1	Nozzle

Based on the above data, an aerodynamic measurement grid was defined to coincide with the nozzle pitch and is represented in Figure 3.2. Due to the effect of the boundaries at the tip and hub, it was not possible to traverse closer than 2mm with the 3.175mm diameter 5-hole probe. To resolve the flow close to the endwall behind the rotor, it was necessary to use a miniature 3-hole pneumatic probe with a width of 0.3mm. Both probes were operated in the null-yaw mode using the same traverse mechanism.

To examine the effect of tip shape on the leakage flow and the subsequent mixing loss, Morphis (1993) created three rotors, one with a flat tip shape and two low entropy tip rotors, namely a radiused pressure corner tip and a contoured suction squealer tip. A leakage flow rate reducing tip, namely a double squealer tip has also been tested in this study. All the rotors were final machined to a nominal diameter of 406.1mm, which in the nominal outer casing bore of 203.5mm gave a gap of 0.45mm or 1% of the blade chord at the tip.

To test the effect of clearance at 2% and 3% of blade chord, two other outer casing rings of aluminium were progressively machined to increase the internal bore instead of reducing the rotor diameter to give the required gap between the rotor and endwall as illustrated in Figure 3.3. It was felt that this would not affect the nature of the leakage flow and any extra loss due to the blending of the larger bore back to the nominal bore behind the rotor was believed to be negligible compared to the loss associated with the leakage flow.

3. Data acquisition

The performance of the turbine was examined using time averaged aerodynamic data obtained from pneumatic probes as well as mechanically measuring the shaft power developed by the rotor and the blade speed. These were used in various efficiency definitions presented in Chapter 4 to resolve the differences in tip leakage effects.

The individual pressures from each of the two probes used were connected to differential pressure transducers in a particular way to minimise the measuring error as illustrated in Figure 3.4 after Morphis (1989). Another commonly used method is a scani-valve diverting the various pressure leads to a single pressure transducer.

In the locality of the experimental turbine, unstable atmospheric conditions often experienced were found to cause pressure fluctuations within the laboratory and since the scani-valve was a relatively slower system, it was more susceptible to atmospheric fluctuations which would introduce a significant variability in the results. The pressure transducers in this case were measured by a high speed analogue to digital (A/D) card fitted into a PC which allowed high speed, effectively simultaneous measurements to be taken by software.

Besides the aerodynamic data at the probe measurement point, a reference dynamic pressure was measured at the inlet to the turbine by a United Sensor KBC-6 Kiel total pressure probe and four equally spaced static pressure holes drilled into the outer casing. To obtain the instantaneous mass flow through the turbine, it was necessary to determine density. This in turn required the measurement of the ambient pressure and temperature to obtain the density from the perfect gas law. The temperature was obtained by a single LM 335 Celsius temperature sensor with a 10mV/°C resolution. The ambient absolute pressure was obtained with a Kulite ITQ-1000(0-100mV) pressure transducer.

The rotor developed torque was measured by an enhanced accuracy Himmelstein MCRT 2800(35-1) torque transducer with a speed sensor. The voltage output proportional to torque was generated by a Himmelstein transducer amplifier (Model 6-201). This was measured directly by the A/D card system. It was found necessary to use a temperature compensating high accuracy Phillips PM2519 multimeter to measure the shaft speed. This required the addition of a GPIB IEEE-488 I/O card to the PC to measure the shaft speed.

In following up the results of Morphis (1993) it was found that the ambient pressure transducer was the source of a significant variability in the results. The nature of the problem and the effect on the results of Morphis (1993) is presented in Appendix A along with a new estimate of the repeatability of various quantities.

4. Automation and operating point control

The 5-hole and 3-hole probe were both yawed and advanced radially by the same traverse mechanism with stepper motor control. These motions were achieved with gearing and screw feeds respectively and special care was taken to eliminate backlash to ensure highly repeatable positioning. The tangential positioning of the probes was achieved by rotating the outer casing shown in Figure 3.1 to which the traverse mechanism was attached at the relevant axial position. Backlash in the gears for the tangential motion was compensated for by the data acquisition software. Table 3.4 presents the accuracy of each of the positioning systems. Each was coupled to the resolution created by the gear ratios and the minimum increment of each stepper motor. Due to the discrete step of the stepper motors, the repeatability of each of the motions was very good, being less than a quarter of the resolution.

Table 3.4 Summary of probe traversing resolutions

Motion	**Minimum resolution**
Tangential	0.00378° (or 0.0134mm at the tip radius)
Radial	0.005mm
Null yaw	0.036°

In addition to the probe traversing mechanism, two other critical turbine operating point parameters were controlled to ensure reliable and repeatable data. These were the V_x/U ratio and the axial velocity V_x Both were controlled independently of each other to ensure that the relative velocity triangles for the rotor remained close to the design value.

However, it was noticed that another change in operating conditions was significantly affecting the trends observed in the data. This was found to be precipitated by a change in the viscosity of the hydraulic oil during warming up the turbine as well as an increase in the ambient temperature over a time span of about 2 hours and can also be seen in Appendix A, Figure A-4.

The change in viscosity of the hydraulic oil caused a reduction of the opposing torque of the pump driven by the rotor, thereby increasing the shaft speed. This problem was alleviated by allowing a warm up period of about 30 minutes at full power. The heating of the room presented another problem not previously noticed. The increased room temperature caused a reduction of the ambient air density which then lowered the Reynold's number. The control routine previously ensured that the Reynold's number was kept constant and this resulted in an increased axial velocity to compensate for the reduction.

As will be seen in Appendix A, the power developed by the rotor is physically dependent on the cube of the axial velocity and only linearly dependent on the density. A changing flow rate then caused large variations in the shaft power which even though non-dimensionalised, resulted in an unrepeatability that critically affected the comparison of the various blade tip shapes. It was therefore decided to maintain a constant axial velocity which proved to be a successful control parameter

that enabled some small differences between the various rotors not previously noted to be observed. With the improved accuracy in measuring the various quantities and the enhanced stability of the axial velocity and V_x/U ratio during the measurement period, a reliable accuracy presented in Table 3.4 was maintained throughout the data acquisition process.

Table 3.4 Resolution of rig operating point parameters

Parameter	**Accuracy**
Axial velocity	± 0.06 m/s (nominal value 30 m/s)
V_x/U	± 0.007 (nominal value 0.526)

5. Inlet conditions

A one-dimensional traverse at the inlet to the turbine was conducted to reveal the inlet axial velocity profile, total pressure loss and the radial and tangential angles which are presented in Figures 3.5 and 3.6. Morphis (1993) conducted hot wire anemometer tests and, from a Fast Fourier Transform utility, found 3.8% inlet turbulence over a broad spectrum of frequencies with no specific peaks.

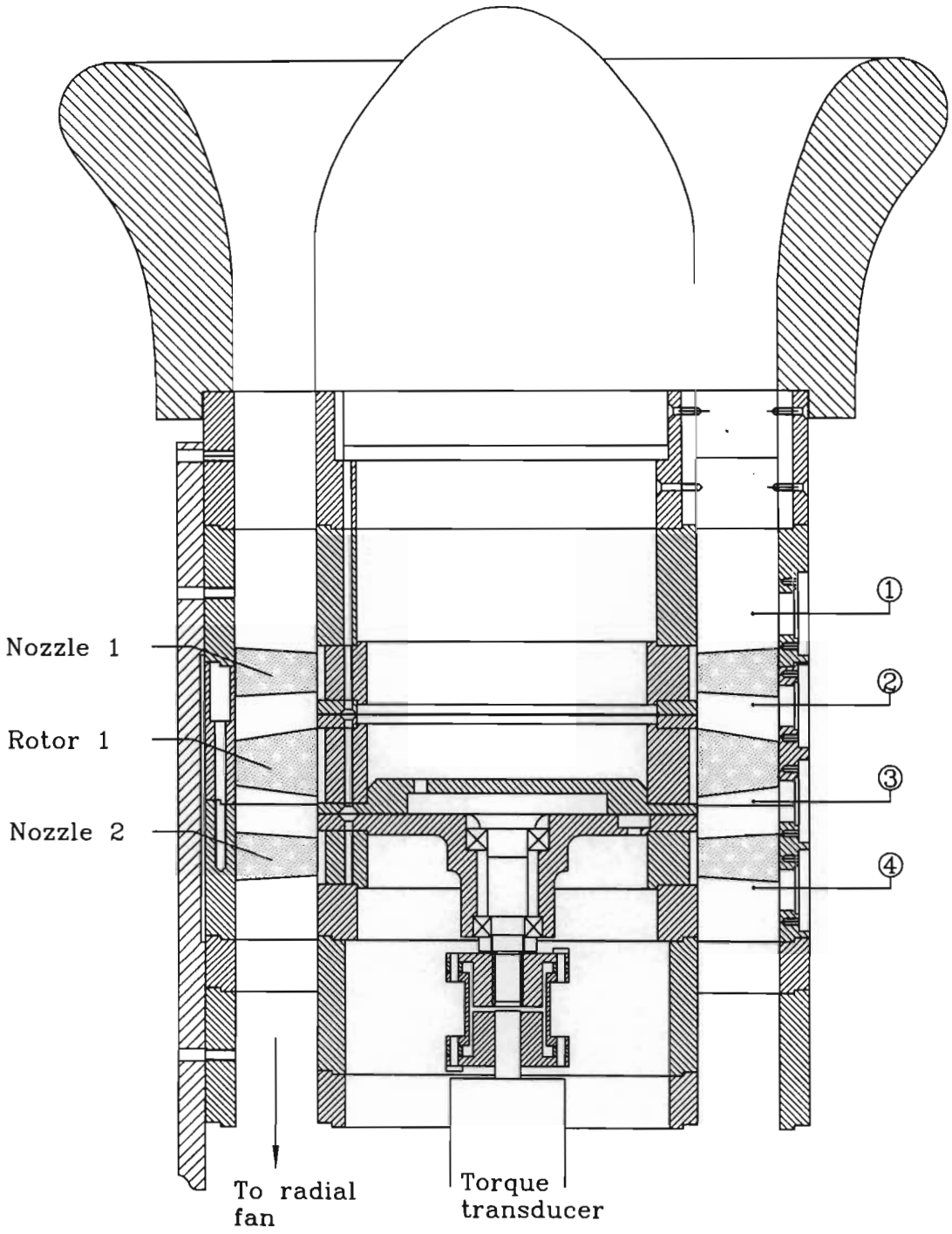

Figure 3.1 A schematic of the 1.5 stage turbine showing the traverse positions.

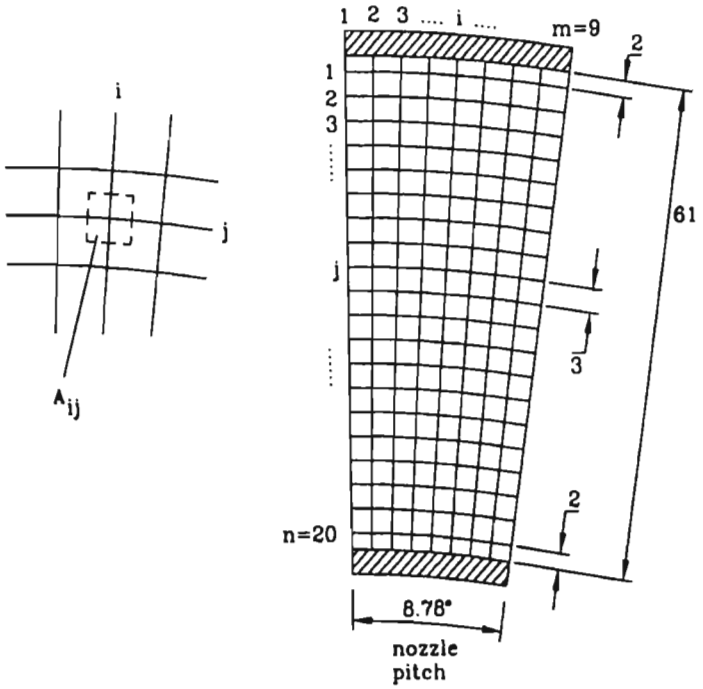

Figure 3.2 The radial measurement grid showing the incremental area about each point.

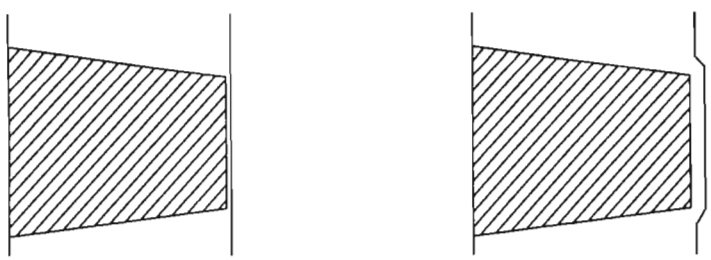

The nominal casing
1% clearance

The bore was carefully increased
and blended for larger clearance

Figure 3.3 The clearance was increased by modifying the outer casing bore.

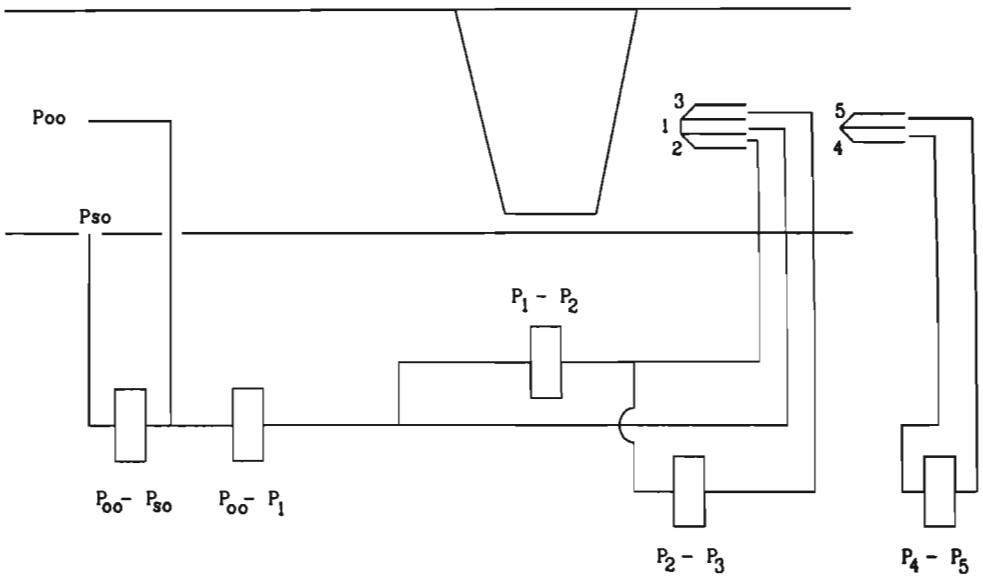

Figure 3.4 The pressure transducers were connected for minimum error after Morphis (1989)

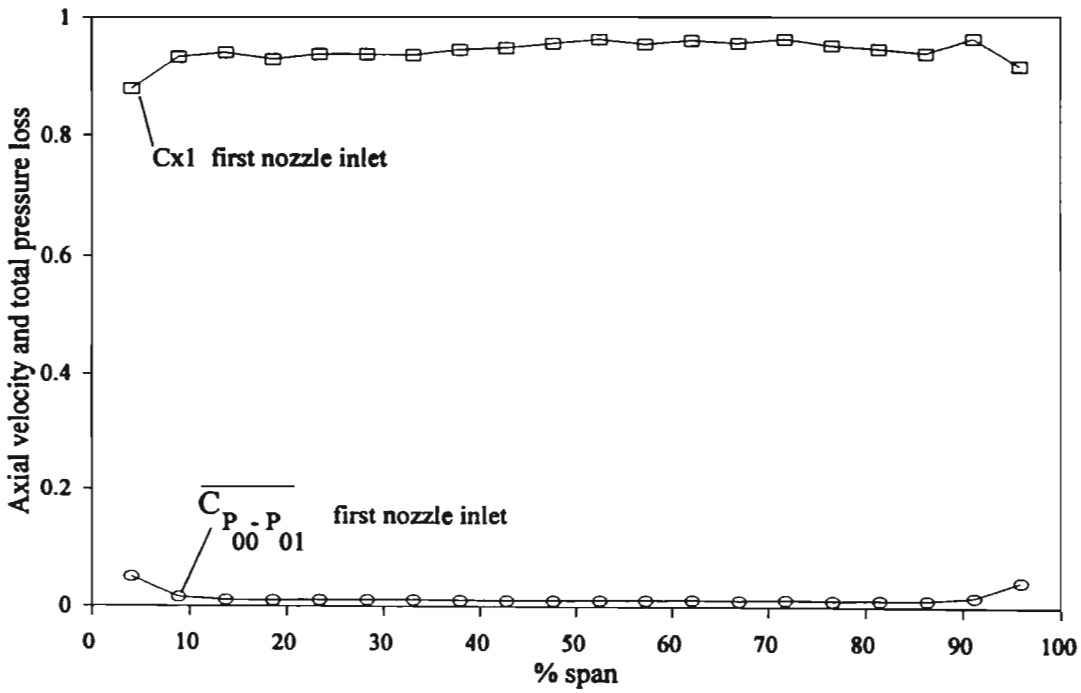

Figure 3.5 The tangentially averaged axial velocity and total pressure loss coefficient at the inlet to the first nozzle.

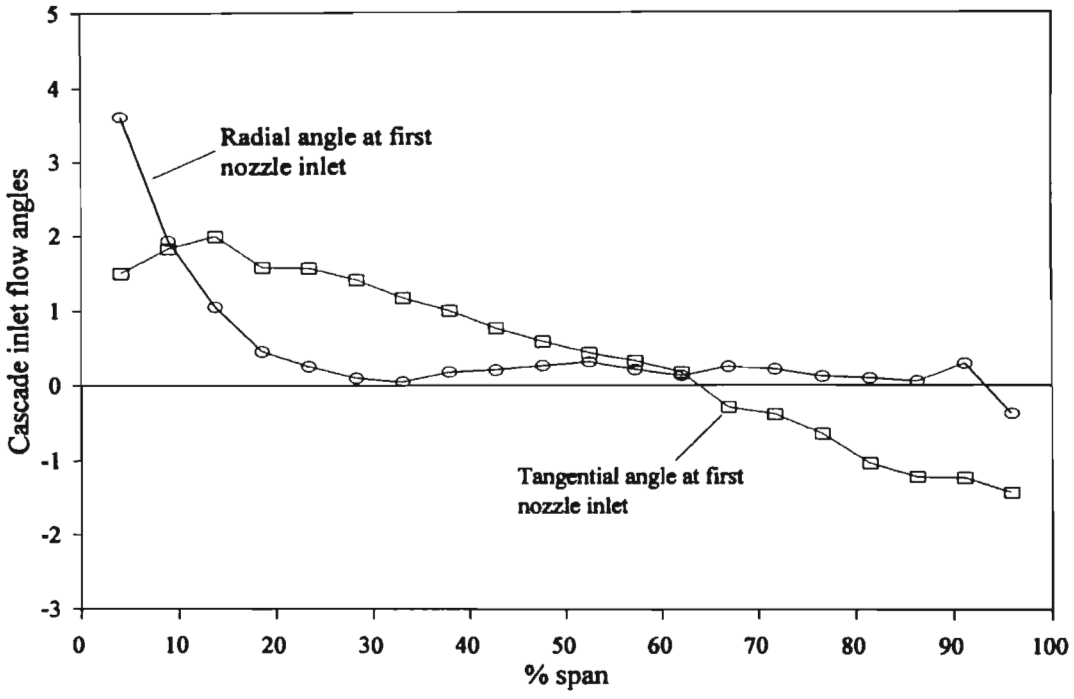

Figure 3.6 The pitchwise variation of the radial (pitch) and tangential (yaw) angle at the inlet to the first nozzle

CHAPTER 4

FLOW COEFFICIENTS AND PERFORMANCE INDICATORS

1. Introduction

To assess the performance of the turbine it was necessary to consider a number of yardsticks by which to evaluate the respective rotors and the effect of tip clearance. These took the form of various flow coefficients and efficiency definitions for the rotor alone, a nozzle alone, the single stage and the overall one and a half stages.

The performance of the machine reflected the work developed by the rotor with respect to the isentropic work determined from aerodynamic measurements using the time averaging 5-hole and 3-hole probes. The work developed was determined in two ways, the first being calculated from the rotor torque and speed and the second from the Euler equation based on the flow deflection.

It was found necessary to eliminate the effect of atmospheric variations as well as the time varying ambient temperature. To this effect, a technique of non-dimensionalising the inlet velocity was used. This essentially referenced the mass flow at the measuring point to the mass flow at the inlet to the turbine.

Figure 4.1 presents the enthalpy-entropy diagram for the 1.5 stage machine where the numerical subscripts refer to the measuring planes defined in Figure 3.1. The flow sign conventions used in this thesis are introduced in Figure 4.2.

2. Flow coefficients

2.1. The definition of the flow coefficients

It is necessary to first introduce the definitions of a number of flow coefficients. The reference total pressure is obtained by a measurement in the inlet freestream flow. The loss in total pressure from reference point 0 to point 1 can be expressed as

$$P_{00} - P_{01} \qquad (1)$$

non dimensionalising this with the reference velocity V_0 yields the total pressure loss coefficient

$$C_{P_{00}-P_{01}} = \frac{P_{00} - P_{01}}{\frac{1}{2}\rho V_0^2} = \frac{P_{00} - P_{01}}{q_{ref}} \qquad (2)$$

This can be converted into a static pressure component (or coefficient) and a velocity component (or coefficient)

$$\frac{P_{00} - P_{01}}{q_{ref}} = \frac{P_{00} - P_{S1} - \frac{1}{2}\rho V_1^2}{q_{ref}}$$

$$= \frac{P_{00} - P_{S1}}{q_{ref}} - \frac{\frac{1}{2}\rho V_1^2}{q_{ref}} \qquad (3)$$

$$C_{P_{00}-P_{01}} = C_{P_{00}-P_{S1}} - C_{V1}$$

or expressed as

total pressure loss coefficient (at 1) = static pressure coefficient (at 1) - velocity coefficient (at 1)

Equation 3 also demonstrates the relationship between these coefficients and enables any one to be determined from knowledge of the others, in particular, to deduce the total pressure loss at a wall boundary given that the local velocity is zero.

2.2. Mass averaging the flow coefficients

To evaluate the performance of the turbine, it was necessary to use overall aerodynamic data to represent quantities such as the driving pressure between planes 1 and 2 for instance. This was achieved by mass averaging the local coefficients with the local mass flow contained in the envelope of the measuring point around the probe tip.

While measurements were being taken, the varying ambient conditions caused the inlet conditions to fluctuate and hence those at the measuring point as well. This resulted in corresponding variations of the non dimensionalised coefficients. To render the local mass flow independent of atmospheric conditions, it was normalised with the reference mass flow based on the freestream velocity at the inlet to the turbine. The normalised mass flow at the (ij)th measuring point was therefore defined as $\frac{\dot{m}_{ij}}{\dot{m}_{ref_{ij}}}$ (4)

Both incremental mass flows are based on the inlet density (ρ_{ij}) and the incremental area (A_{ij}) around the (ij)th measurement point defined in Figure 3.2. The subscript ij also represents the time at which the (ij)th measurement was taken. $\dot{m}_{ref_{ij}}$ however is based on the inlet freestream axial velocity $V_{x_{ref\,ij}}$ whereas $\dot{m}_{ij}$ is based on the local axial velocity measurement.

Hence each of the aerodynamic coefficients was mass averaged with the normalised mass flow coefficient to render the mass flow independent of varying conditions. This is expressed by

$$\overline{Y} = \frac{\sum_{i=1}^{m}\sum_{j=1}^{n} Y_{ij} \frac{\dot{m}_{ij}}{\dot{m}_{ref\,ij}}}{\sum_{i=1}^{m}\sum_{j=1}^{n} \frac{\dot{m}_{ij}}{\dot{m}_{ref\,ij}}} \qquad (5)$$

where Y is any dimensionless coefficient

To observe radial trends in the flow structure, the coefficients were mass averaged in the tangential direction only and this is expressed by

$$\overline{Y_j} = \frac{\sum_{i=1}^{m} Y_{ij} \frac{\dot{m}_{ij}}{\dot{m}_{ref\,ij}}}{\sum_{i=1}^{m} \frac{\dot{m}_{ij}}{\dot{m}_{ref\,ij}}} \qquad (6)$$

The driving pressure between say planes 1 and 2 can now be obtained from the following relationship

$$\overline{C_{P_{01} - P_{S2}}} = \overline{C_{P_{00} - P_{S2}}} - \overline{C_{P_{00} - P_{01}}} \qquad (7)$$

and similarly the total pressure loss between plane 1 and 2 can be found from

$$\overline{C_{P_{01} - P_{02}}} = \overline{C_{P_{00} - P_{02}}} - \overline{C_{P_{00} - P_{01}}} \qquad (8)$$

A similar radial comparison was made by comparing the radially averaged coefficients at the same radius and while radial transport of fluid was expected, it was felt that the results would be representative of the true trends.

3. The single stage efficiency

The single stage efficiency reflects the work developed by the rotor and is established from the familiar concept of total-to-total and total-to-static conditions where the outlet velocity is also considered in the latter. With reference to Figure 4.1, the total-to-total efficiency is therefore

$$\eta_{tt} = \frac{\overline{w}}{\overline{h_{01} - h_{03}}} = \frac{\overline{w}}{\overline{h_{01} - h_{3is}} - \overline{\tfrac{1}{2} V_{3\,is}^{\,2}}} \qquad (9)$$

where w is the averaged specific work based on shaft power or on aerodynamic measurements. Morphis (1993) showed that for <u>incompressible</u> flow, this may be represented by the various corresponding pressure differences. After normalising each of the components with a reference dynamic pressure (q_{ref}) the incompressible equation is

$$\eta_{tt} = \frac{\overline{\dfrac{w}{q_{ref_{ij}} / \rho_{ij}}}}{\overline{\dfrac{P_{01} - P_{S3}}{q_{ref_{ij}}}} - \overline{\dfrac{\tfrac{1}{2} V_3^{\,2}}{q_{ref_{ij}} / \rho_{ij}}}} = \frac{\overline{C_w}}{\overline{C_{P_{01} - P_{S3}}} - \overline{C_{V_3}}} \qquad (10)$$

The work coefficient C_w is defined as the work per unit mass flow normalised with the reference dynamic pressure. Note that it does not take account of the driving pressure expended to achieve it or of the kinetic energy leaving the rotor. The efficiency expressions take these effects into account. The work coefficient is based on either mechanical work

$$\overline{C_w} = \frac{w}{q_{ref_{ij}} / \rho_{ij}} = \frac{(\tau\,\omega)_{ij} / \dot{m}_{ref_{ij}}}{q_{ref_{ij}} / \rho_{ij}} \qquad (11)$$

or is obtained by the summation of aerodynamic work over the measurement grid

$$\overline{C_{w_{aero}}} = \sum_{i}^{m} \sum_{j}^{n} \frac{w_{ij\,aero}}{q_{ref_{ij}} / \rho_{ij}} = \sum_{i}^{m} \sum_{j}^{n} \frac{\dot{m}_{ij} U_{ij} \Delta V_{\theta_{ij}} / \dot{m}_{ref_{ij}}}{q_{ref_{ij}} / \rho_{ij}} \qquad (12)$$

where $w_{ij\,aero}$ is the Euler work at the present measuring point.

The total-to-static efficiency is accordingly

$$\eta_{ts} = \frac{\overline{C_w}}{\overline{C_{P_{01} - P_{S3}}}} \qquad (13)$$

4. The rotor efficiency

Two definitions similar to the single stage efficiencies are used. The rotor total-to-total efficiency is defined as

$$\eta_{tt} = \frac{\overline{w}}{\overline{h_{02} - h_{03_{is}}}} = \frac{\overline{w}}{\overline{h_{02} - h_{3_{is}}} - \overline{\tfrac{1}{2} V_{3\,is}^{2}}} .$$

It can be assumed that $V_3 \approx V_{3_{is}}$. The incompressible form of the above equation then becomes

$$\eta_{R_{tt}} = \frac{\dfrac{\overline{w}}{q_{ref}/\rho_{ij}}}{\dfrac{\overline{P_{02} - P_{S3}}}{q_{ref}} - \dfrac{\overline{\tfrac{1}{2}\rho_{ij} V_3^{2}}}{q_{ref}}} = \frac{\overline{C_w}}{\overline{C_{P_{02} - P_{S3}}} - \overline{C_{V_3}}} \qquad (14)$$

where $\overline{C_{P_{02} - P_{S3}}}$ is the driving pressure across the rotor determined from Eq 7.

The total-to-static similarly becomes

$$\eta_{R_{ts}} = \frac{\overline{C_w}}{\overline{C_{P_{02} - P_{S3}}}} \qquad (15)$$

5. The 1.5 stage efficiency

A one and a half stage efficiency was defined as the ratio of the sum of the work output and the flow exit kinetic energy to the enthalpy difference (driving pressure) across the 1.5 stage turbine and with reference to Figure 4.1 is expressed as follows.

$$\eta_{1.5} = \frac{\overline{w} + \overline{\tfrac{1}{2}V_4^2}}{\overline{h_{01} - h_{4_{is}}}}$$

and for incompressible flow becomes

$$\eta_{1.5} = \frac{\overline{w} + \overline{\tfrac{1}{2}V_4^2}}{\overline{(P_{01} - P_{S4})/\rho}} = \frac{\overline{C_w} + \overline{C_{V_4}}}{\overline{C_{P_{01} - P_{S4}}}} \qquad (16)$$

6. The nozzle efficiency

The nozzle efficiencies relate the mass averaged velocity at the outlet from each nozzle to the isentropic enthalpy difference or driving pressure across the nozzle and for incompressible flow are defined as follows

$$\eta_{N1} = \frac{\overline{\tfrac{1}{2}V_2^2}}{\overline{h_{01} - h_{2_{is}}}} = \frac{\overline{\tfrac{1}{2}V_2^2}}{\overline{(P_{01} - P_{S2})/\rho}} = \frac{\overline{C_{V_2}}}{\overline{C_{P_{01} - P_{S2}}}} \qquad (17)$$

and similarly,

$$\eta_{N2} = \frac{\overline{\tfrac{1}{2}V_4^2}}{\overline{h_{03} - h_{4_{is}}^*}} = \frac{\overline{\tfrac{1}{2}V_4^2}}{\overline{(P_{03} - P_{S4})/\rho}} = \frac{\overline{C_{V_4}}}{\overline{C_{P_{03} - P_{S4}}}} \qquad (18)$$

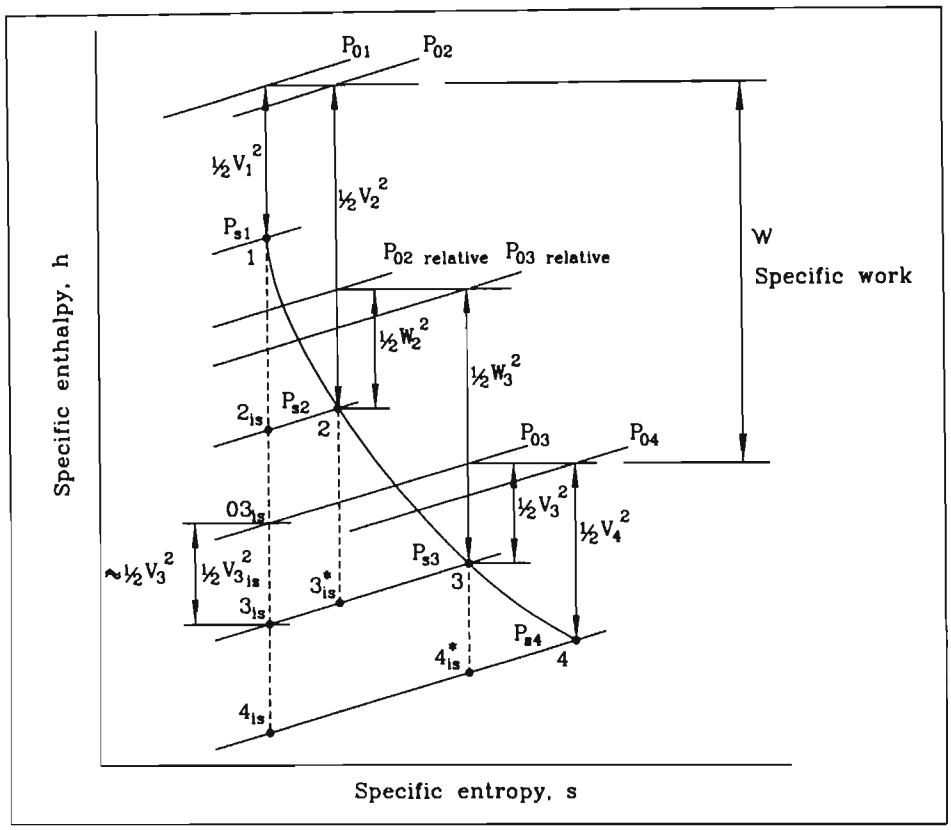

Figure 4.1 The specific enthalpy-entropy diagram for the expansion of a gas through an axial 1.5 stage turbine.

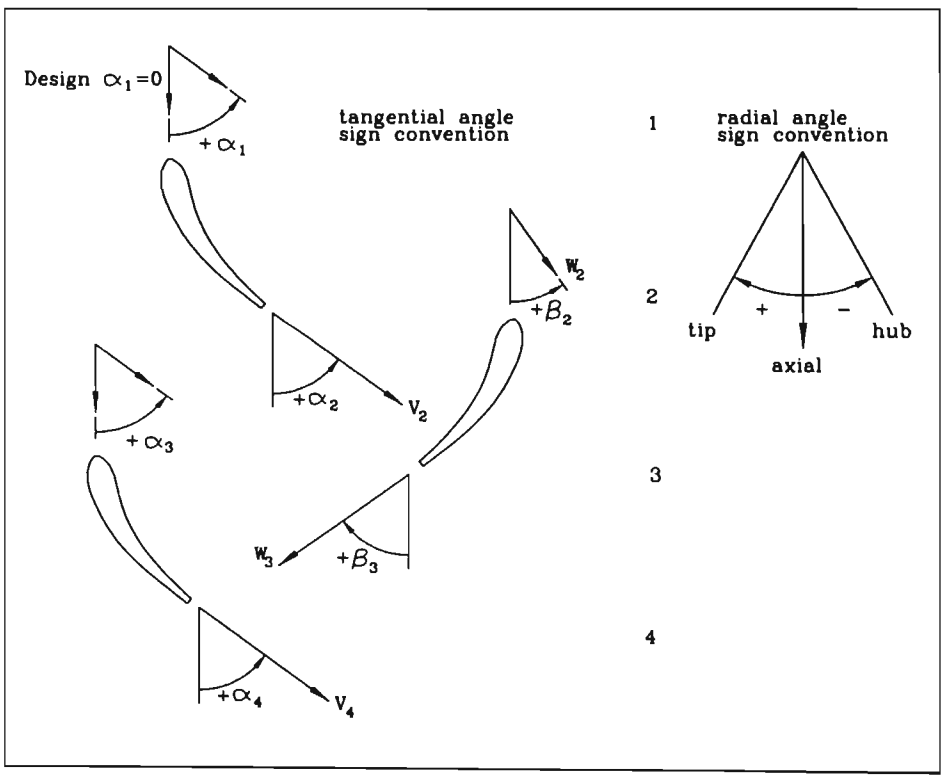

Figure 4.2 The absolute and relative flow angle sign conventions used.

CHAPTER 5

A COMPARISON OF TIP GEOMETRY AND CLEARANCE EFFECTS ON THE OVERALL MACHINE PERFORMANCE

1. Introduction

A direct comparison of the performance of the experimental turbine with various rotor tip shapes is obtained by comparing the overall total-to-total and total-to-static efficiencies for the rotor, single stage and 1.5 stage turbine as defined in the previous chapter. The total-to-total and 1.5 stage quantities provide a guide for multistage machines or for the last stage of a jet engine where the exit kinetic energy is put to good use. The total-to-static efficiency is a guide to the performance of a single stage turbine without an exit diffuser.

The most significant difference between tip shapes and varying clearance is expected to be seen within the rotor, hence the rotor efficiency is presented on its own to isolate the differences in machine performance. This then lends itself to an analysis of the single stage machine as well as the flow development downstream of the 1st stage. In an attempt to interpret the 1.5 stage efficiencies, it is also necessary to obtain an understanding of how the second stage nozzle interacts with the complex, time dependent flows emerging from the rotor and to compare this to the situation of a turbine final stage.

2. The effect of tip geometry and clearance on the turbine performance

2.1. The rotor performance

Figure 5.1 and Figure 5.2 show that the total-to-total and total-to-static efficiency show a monotonic reliance on tip clearance with a reduction in efficiency of approximately 1.5% and 1% per 1% reduction in clearance which compares favourably with the data mentioned in Booth (1985). The relationship between tip shape and machine performance is not as clearly defined, suggesting that the effect of changing the tip gap geometry may not be as critical on the overall machine performance as previously thought. It is important to reiterate that although the differences between the tip shapes may be somewhat negligible due to the uncertainty, as detailed in Appendix A, these figures are presented as a numerical average of a number of experiments and it is believed they fairly represent the trends observed

As reviewed in Chapter 2, researchers in the past have tended to base an overall tip leakage loss correlation simply on the gap mass flow or discharge coefficient. This predicts that the low entropy tip shapes which produce a higher leakage flow rate would ultimately degrade the machine performance compared to a low leakage flow rate tip such as a double squealer or flat tip shape. It can be seen from the two figures that the flat tip does show a slight advantage over the other tip shapes at the smallest tip clearance.

It is interesting to recall the results of Bindon & Morphis (1990) who found that at 2.5% clearance, a radiused tip and suction squealer tip produced a leakage flow rate about 19% and 7% respectively greater than that of a flat tip whereas the

discharge coefficients were both about 12% greater than that of the flat tip. Extending these findings to the present situation, it is reasonable to expect that the radiused and suction squealer tips would perform in a similar way to the cascade experiment and, if the loss due to tip clearance were a linear function of the discharge coefficient, the mixing loss could be expected to be roughly 12% greater as well. With increasing tip clearance, the leakage flow rate increases linearly (Storer (1989) and Yaras & Sjolander (1988), and can be expected to produce a proportionately higher mixing loss component. Therefore, at the larger clearances, the efficiency of low entropy tip rotors should reflect a deficit compared to the flat tip rotor than at 1% clearance.

However, as seen in Figures 5.1 and 5.2, this is not the case and the trend in the efficiency for the low entropy tips is essentially the same as that of the flat tip. In fact, the radiused tip shows a slight advantage over the flat tip at 3% clearance, suggesting that the leakage loss cannot be simply related to the gap discharge coefficient.

At 1% clearance, the double squealer tip shape does not perform as well in total-to-total efficiency as the other tip shapes whereas the flat tip shape appears to have a slight advantage of approximately 0.2% over the other tip shapes. This is somewhat contrary to expectations in that both the flat and double squealer tips were anticipated to offer a similar performance and it was presumed that the two leakage flow rates were comparable. The apparent advantage of the flat tip over the low entropy tips may be due to the additional profile loss that is generated by the increased tip surface area of the low entropy tips.

At 3% clearance, the slight advantage of the radiused tip over the other shapes is a surprising result. Yaras et al (1988) found that with increasing clearance, the discharge coefficient for a flat tip decreased linearly. This is understandable considering the results of Bindon & Morphis (1990) who found that the width of the separation bubble increased at larger clearances. This is then responsible for a relative reduction in the leakage cross flow area. The radiused tip on the other hand, does not limit the leakage flow and instead minimises the internal gap loss such that the only hindrance to the leakage flow is the development of the boundary layers on the endwall and tip surface. It is therefore reasonable to expect that the radiused tip would create a proportionately larger leakage flow rate at the higher clearances with subsequently higher mixing loss. This should then be reflected as a lower efficiency for the radiused tip compared to the flat tip.

The above result can possibly be explained by comparing the situation for a small and a large tip clearance. At a small clearance, the boundary layer deficit near the tip and endwall surfaces is relatively large compared to freestream leakage fluid within the cross flow area. The separation bubble on the flat tip surface then plays an important role in reducing the cross flow area and thus the leakage flow rate. However, at a very large clearance the boundary layers on the respective surfaces are now relatively thin compared to the freestream leakage flow cross sectional area. The separation bubble of the flat tip can be expected to play a proportionately lesser role in reducing the leakage flow rate and thus the flow rates for both tip shapes become comparable in magnitude.

In this situation, the magnitude of the resulting mixing loss for both tips can be expected to be similar as well, however, the separation bubble is a major contributor to the generation of entropy within the gap. Since this is not present

in the radiused tip, it is possible that the radiused tip would perform slightly better than the flat tip because of a lower internal gap loss.

Although the nature and structure of the leakage fluid is determined by the gap shape and interaction of the boundary layers in the gap, it is possible that at 1% clearance, the leakage mass flow is more influenced by viscous effects than at larger clearances and evidence of this is shown later. With viscous effects dominating, the double squealer could be expected to produce more entropy at the gap exit than the radiused tip but potentially will have the advantage of lower mixing losses further downstream which would be indicated as a slight improvement in the 1.5 stage and second nozzle efficiency. At 3% clearance, the gap leakage fluid may be inviscid and the internal gap loss not as dependent on tip shape as previously thought, thus explaining the comparable performance of the double squealer tip to the other tips at larger clearances.

It is seen in both Figures 5.1 and 5.2 that the contoured tip does not exhibit any advantage over either the flat or radiused tip shapes. Morphis & Bindon (1990) demonstrated that the contoured suction squealer had similar internal gap losses to the radiused tip but had a lower leakage flow rate. This was thought to be able to reduce the mixing losses and hence the overall loss, possibly giving this tip shape a slight advantage. Again the slightly lower performance of the suction squealer tip may be caused by the loss of work extraction in the tip region, in which the modification of the blade profile in the tip region is more severe than that of the radiused tip. Evidence to support this will be shown later.

2.2. The single stage performance

The single stage efficiency was not expected to differ from the rotor efficiency since this quantity incorporates the first stage nozzle efficiency which is obviously constant. Figure 5.3 and Figure 5.4 indeed show that the trends for total-to-total and total-to-static efficiencies are similar to that of the rotor.

The radial variation of the single stage total-to-static efficiency shown in Figures 5.5 and 5.6 was determined by considering the Euler work absorbed by the rotor at a constant radius. The radial transportation of fluid is expected to complicate the results slightly, however, the findings shown later indicate that for each tip shape and clearance, the radial flows were similar and relatively small compared to the main flow, allowing a reasonable comparison of tip clearance effects.

Of interest in Figure 5.5 is the reduction of efficiency in the tip region with an increase in clearance. This is an expected result since an increasing gap will give rise to a larger leakage flow rate which in turn gives rise to a greater amount of fluid that is poorly deflected, hence a reduction of work extraction occurs in the tip region.

Apart from the tip region, all the performances are essentially the same regardless of tip shape.

The poor performance of the double squealer tip in the tip region is possibly due to increased internal gap entropy which mixes into the mainstream flow. It is interesting that the double squealer was expected to reduce the leakage flow rate,

however, it will be shown in Chapter 6 that in fact the leakage flow rate was slightly higher than that of the flat tip, possibly contributing to a moderately higher mixing loss.

By minimising the leakage flow rate, the double squealer tip was expected to increase the overall passage flow deflection and ultimately the work extraction. The unexpected increase in the leakage flow rate may be explained by the mixing model of Heyes et al (1991) for the case of a flat tip shape. Essentially, if a greater amount of mixing of the leakage fluid has occurred by the gap exit, then the discharge coefficient for the tip is increased, which could lead to a greater leakage mass flow and subsequently a higher mixing loss

The particular design of double squealer tip may in fact be causing a greater amount of mixing in the clearance gap leading to an increase in the leakage flow rate. These results also confirm the findings of Morphis & Bindon (1990) and Bindon (1988) that the internal gap loss must be considered in the overall performance of a particular tip shape as well as highlighting the importance of the deflection of the leakage fluid.

It is interesting to note that the flat and radiused tip shapes perform similarly in the tip region at 1% clearance. Even though the nature of the two tip leakage flows are different, it appears that in the case of the radiused tip shape, the increase of the downstream mixing loss may be offset by the reduction of the internal gap loss.

2.3. The 1.5 stage performance

The one and a half stage performance is evaluated using the definition of Morphis (1993) described in Chapter 4 and essentially is a measure of the rotor work extraction and the kinetic energy available at the second nozzle outlet with reference to the enthalpy difference (driving pressure) across the 1.5 stage machine.

It is apparent from Figure 5.7 that the flat tip rotor delivers a slender advantage over the other tip shapes for all clearances. At 1% clearance, the double squealer tip delivers a slightly poorer performance, however, this tip shape does not incur an overall penalty at larger clearances when compared to the radiused and suction squealer tips.

The trend in the 1.5 stage efficiency shown in Figure 5.7 is not at first obvious, especially when it was seen in Figures 5.1 and 5.2 that the radiused tip showed a slight advantage over the other tip at 3% clearance. This can be better understood when the performance of the second stage nozzle is taken into account.

3. The performance of the second stage nozzle

Morphis & Bindon (1994b) showed a significant improvement in the second stage nozzle efficiency over the first stage nozzle due to a poor resolution of a transducer and insufficient data points in the tip region. However, Figure 5.8 does suggest a moderately increased efficiency especially at 1% clearance. This result indicates that the second nozzle may well be operating at a slightly higher efficiency due to the reduction of secondary flow losses as discussed in the review.

A detailed investigation of the flow structure to confirm this is presented in Chapter 6.

The flat tip again demonstrates a slightly improved performance over the other tip shapes, although, at 1% clearance it is moderately lower and is within the experimental uncertainty. Interestingly, the double squealer tip shows a small advantage over the other tip shapes at 1% clearance. The suction squealer tip also shows a moderate advantage over the radiused tip, again confirming that a slightly lower leakage flow rate generates less mixing loss. Figure 5.9 confirms that apart from the result at 2% clearance, the overall total pressure loss caused by the suction squealer tip is lower than that of the radiused tip confirming the previous finding. The flat tip produces the lowest overall total pressure loss compared to the other tip shapes.

Figure 5.8 suggests that the efficiency of the second nozzle remains reasonably constant and moderately higher than that of the first stage nozzle. This in itself is a somewhat surprising result considering the time dependent flows such as the leakage vorticity and the 'chopping' of the rotor blade wake effects all of which have been confirmed by various researchers to increase the turbulence level and generate a higher loss.

4. The development of the flow downstream of the first stage

As noted in Denton (1993), a nozzle accelerates the flow causing thinning of the boundary layers and stretching of other forms of low energy fluid eg tip clearance induced vortices and blade wakes. It is probable that this mechanism also minimises the losses due to vortex chopping and the leakage flow mixing loss. In

the absence of the second nozzle, however, the flow behind the rotor must mix out at constant area with further total pressure loss and it is interesting to see whether the loss production in either case is comparable.

Figure 5.10 depicts the total pressure loss that occurs from a measuring plane at the rotor outlet to a measuring plane approximately 1.5 blade chords further downstream in the absence of the second nozzle. It can be seen that the double squealer and flat tip rotors produce a slightly higher total pressure loss than the other two low entropy tip shapes at 1% clearance, however, the flat tip produces moderately lower loss at 3% clearance. This is a somewhat surprising result because the low entropy tips were expected to create a higher mixing loss due to the higher leakage flow rate. This was in fact seen previously in the discussion of the second nozzle efficiency where clearly the low entropy tips produced a higher mixing loss resulting in the slightly lower nozzle efficiency.

Again, it should be remembered that the low entropy tips differ from the flat and double squealer tips by the internal gap entropy generation. The double squealer in particular is expected to produce slightly more entropy at the gap exit compared to the flat tip and interestingly this is reflected as a higher overall total pressure mixing loss compared to the flat tip. It will be shown in the next chapter, however, that the leakage flow has not fully mixed out at the downstream measuring plane which could therefore result in a slightly higher total pressure losses for the low entropy tips.

5. The flow blockage effect of the leakage flow

Two other overall machine performance indicators were examined, these being the driving pressure across the machine and the rotor work extracted for the same reference mass flow. In Figure 5.11, the overall driving pressure is represented by the static pressure coefficient across the machine and the work extraction by the work coefficient. It is interesting that to maintain a constant mass flow rate through the machine, the low entropy tip shapes required a higher driving pressure thus confirming the findings of Peacock (1983) who indicated that the leakage flow caused a blockage. However, it can also be seen that although the driving pressure increases, the work output also increases proportionately, hence explaining why the efficiency of each tip was similar in magnitude.

A higher leakage flow rate thus creates a greater blockage giving rise to a higher driving pressure. The tip shape is therefore an important parameter in determining the driving pressure required because the pressure ratio and consequently the mass flow through the turbine are determined by the compressor characteristics which generally are not variable.

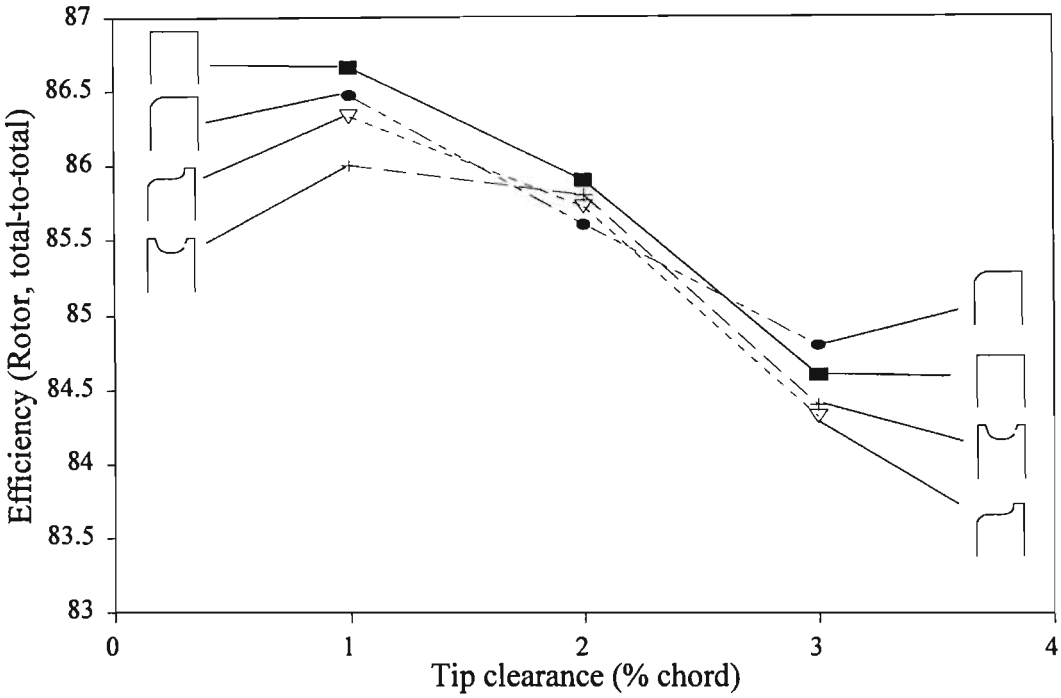

Figure 5.1 The rotor total-to-total efficiency for various tips and changing tip clearance.

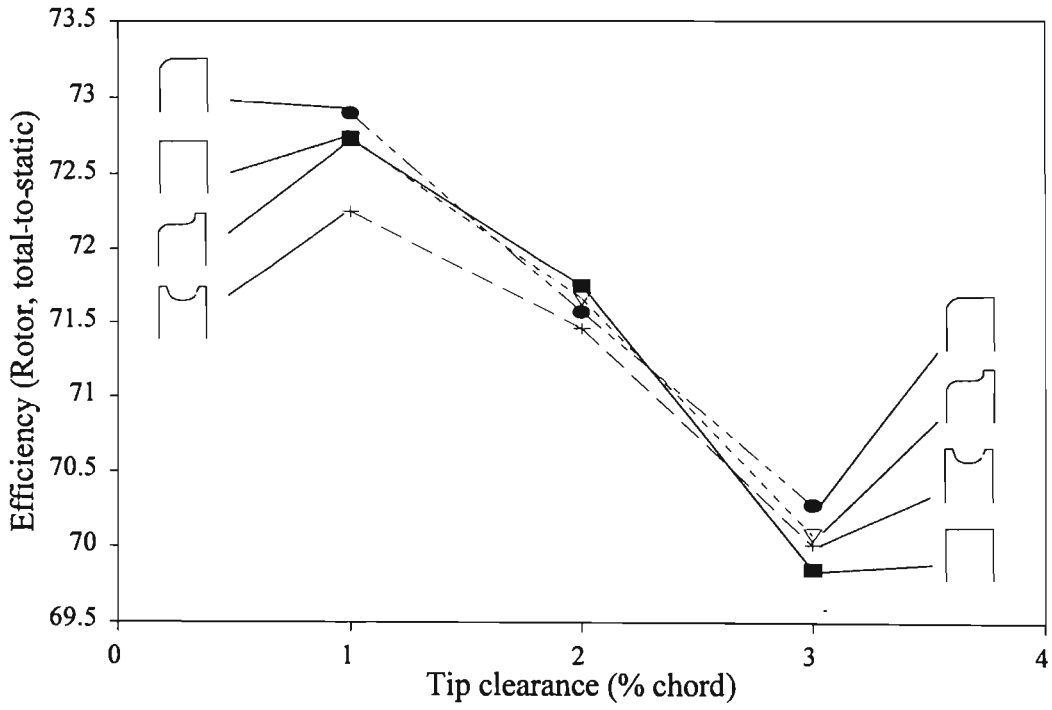

Figure 5.2 The rotor total-to-static efficiency for various tips and changing tip clearance.

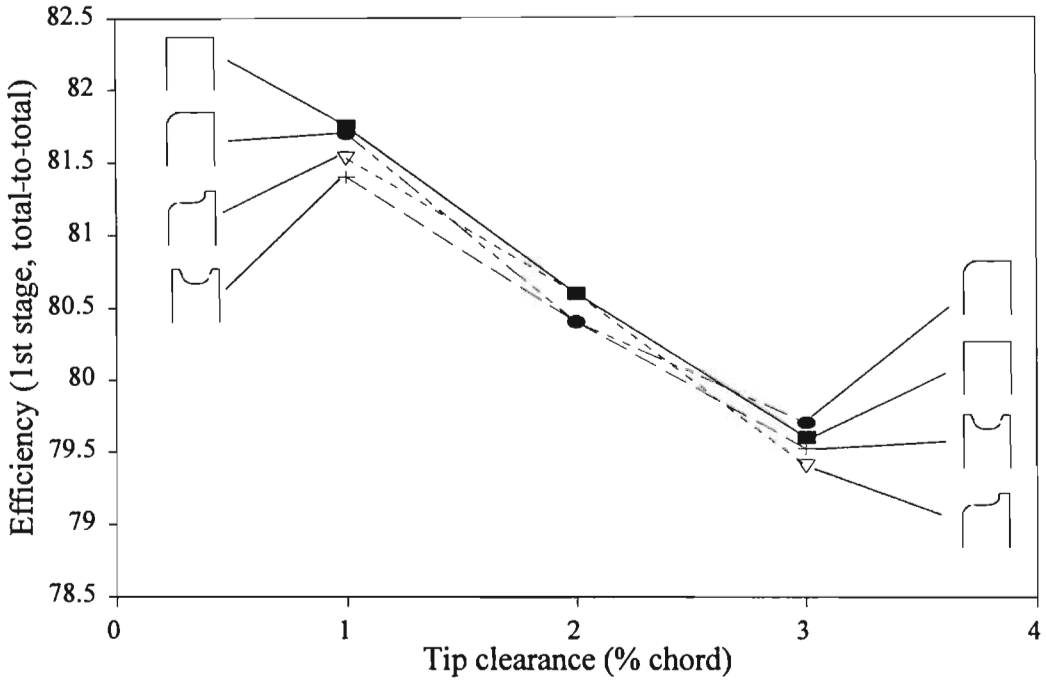

Figure 5.3 The single stage total-to-total efficiency for various tips and changing tip clearance.

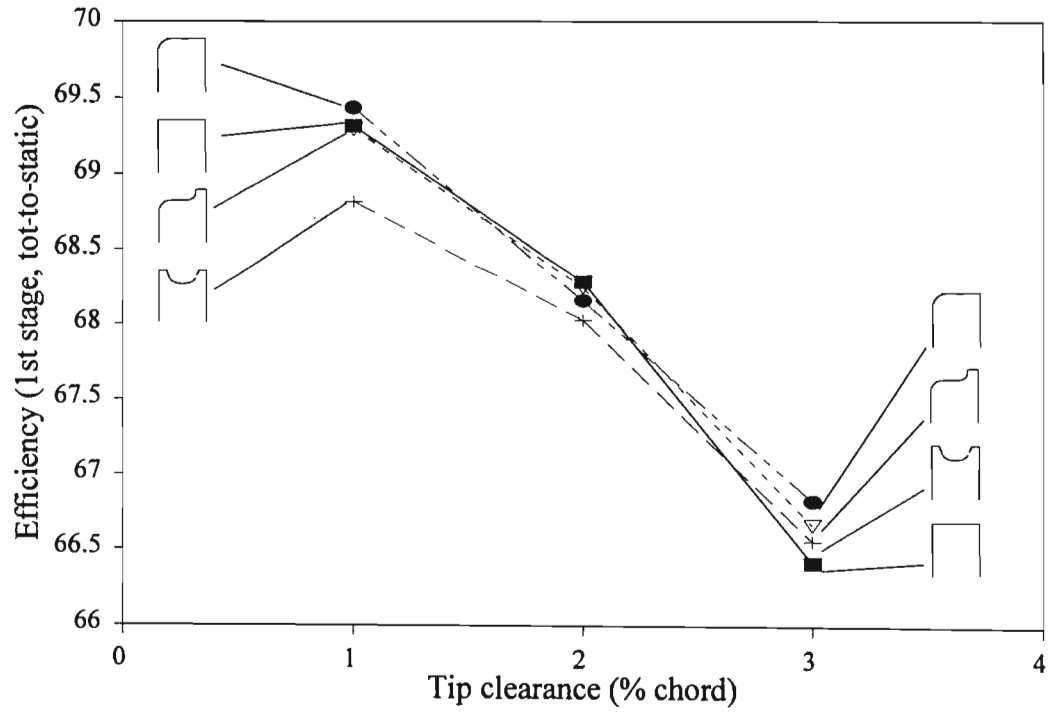

Figure 5.4 The single stage total-to-static efficiency for various tips and changing tip clearance.

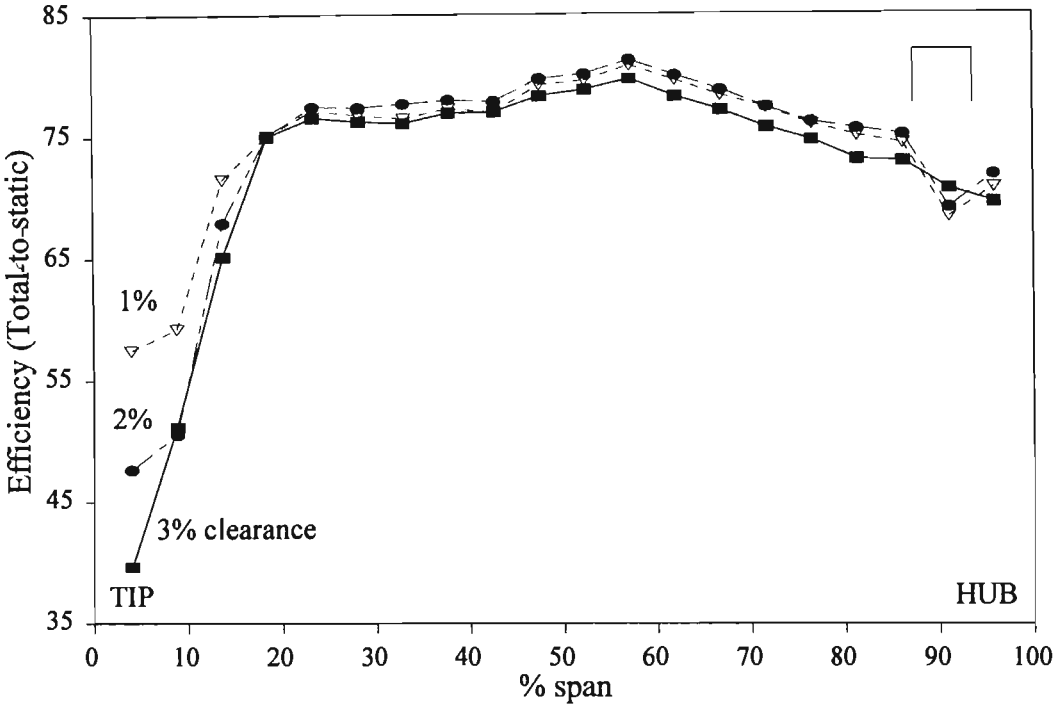

Figure 5.5 The radial variation of the tangentially averaged single stage total-to-static efficiency for the flat tip at varying tip clearance.

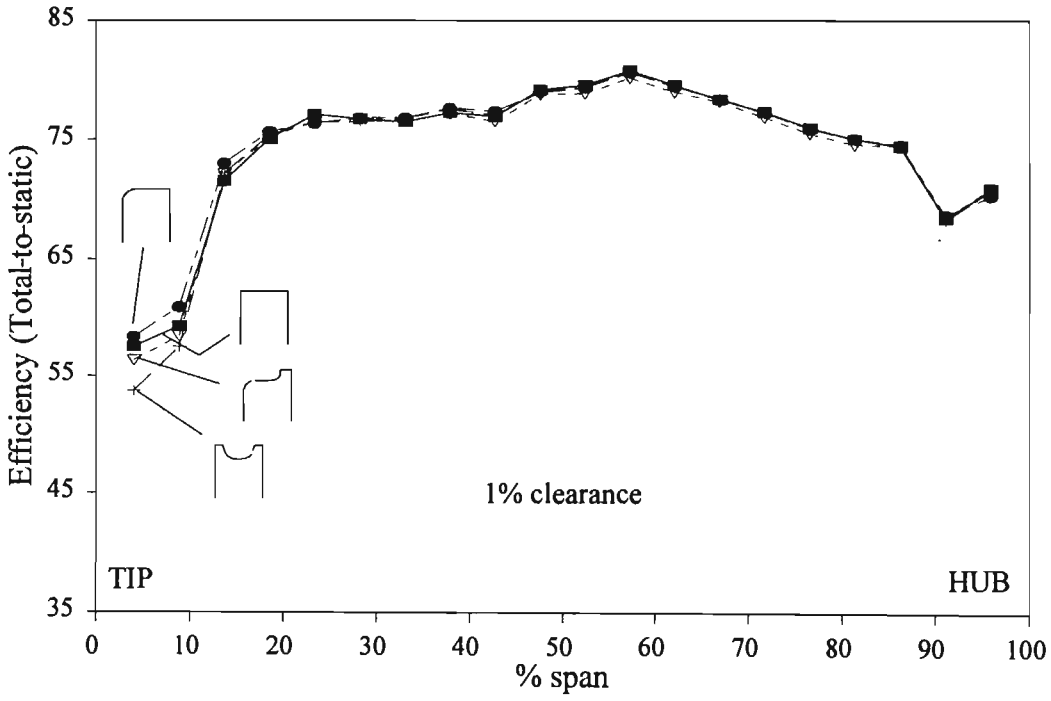

Figure 5.6 The radial variation of the tangentially averaged single stage total-to-static efficiency for various tips at 1% clearance.

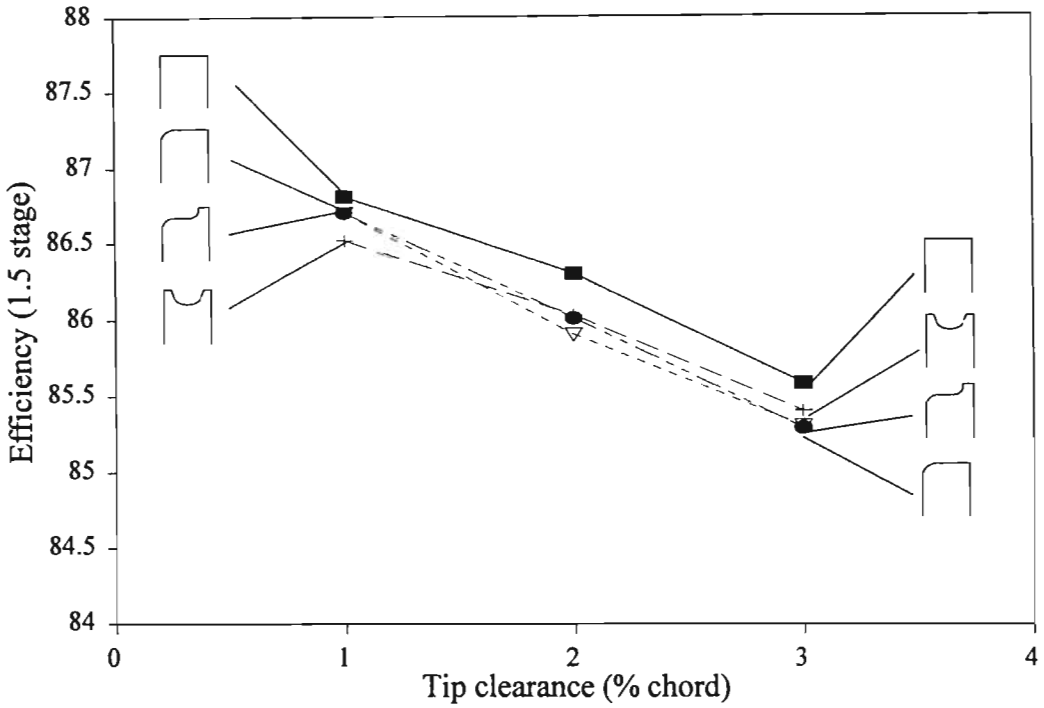

Figure 5.7 The 1.5 stage efficiency for various tips and changing tip clearance.

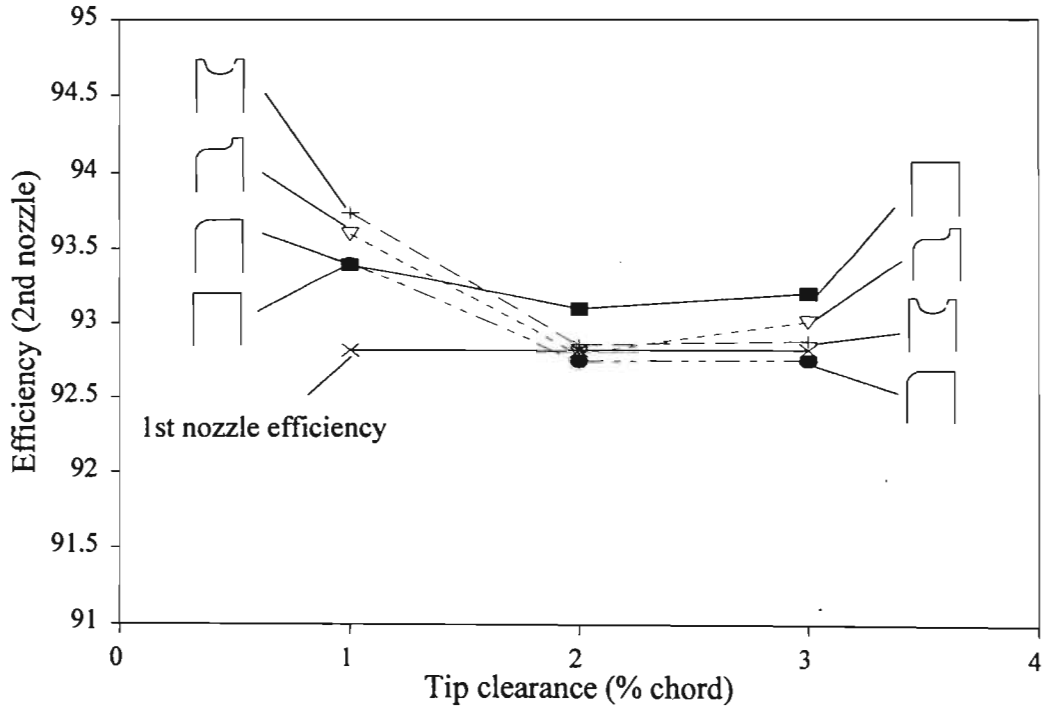

Figure 5.8 The 2nd nozzle efficiency for various tips and changing tip clearance compared to the 1st nozzle efficiency.

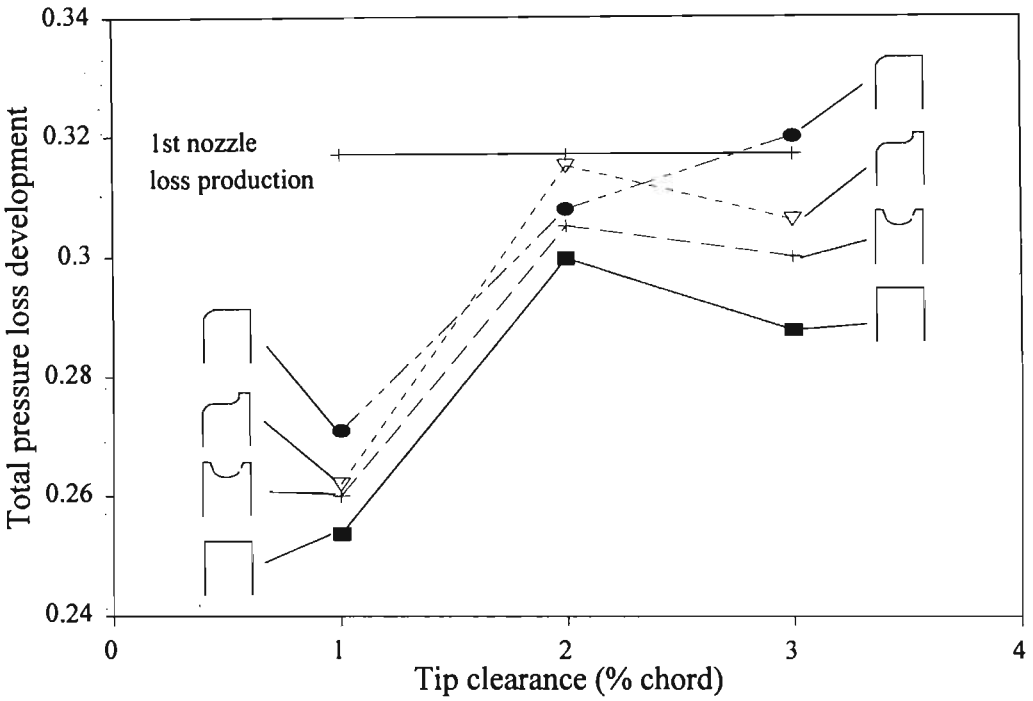

Figure 5.9 The development of total pressure loss across the 2nd nozzle for various tips and changing tip clearance compared to the 1st nozzle.

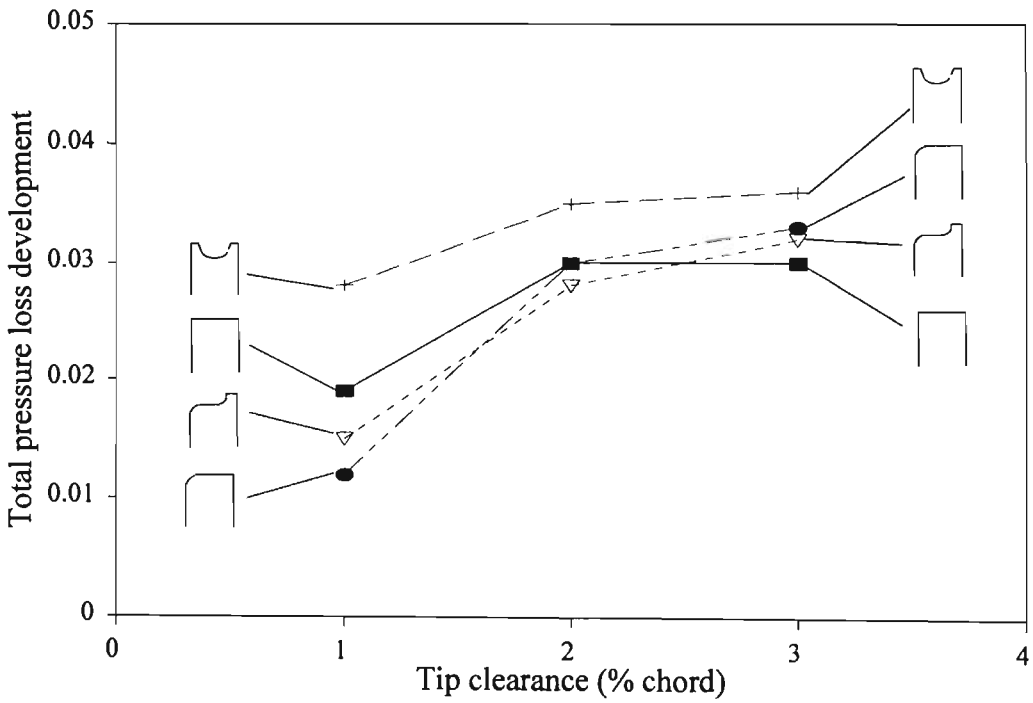

Figure 5.10 The development of total pressure loss downstream of the rotor for various tip shapes and changing tip clearance.

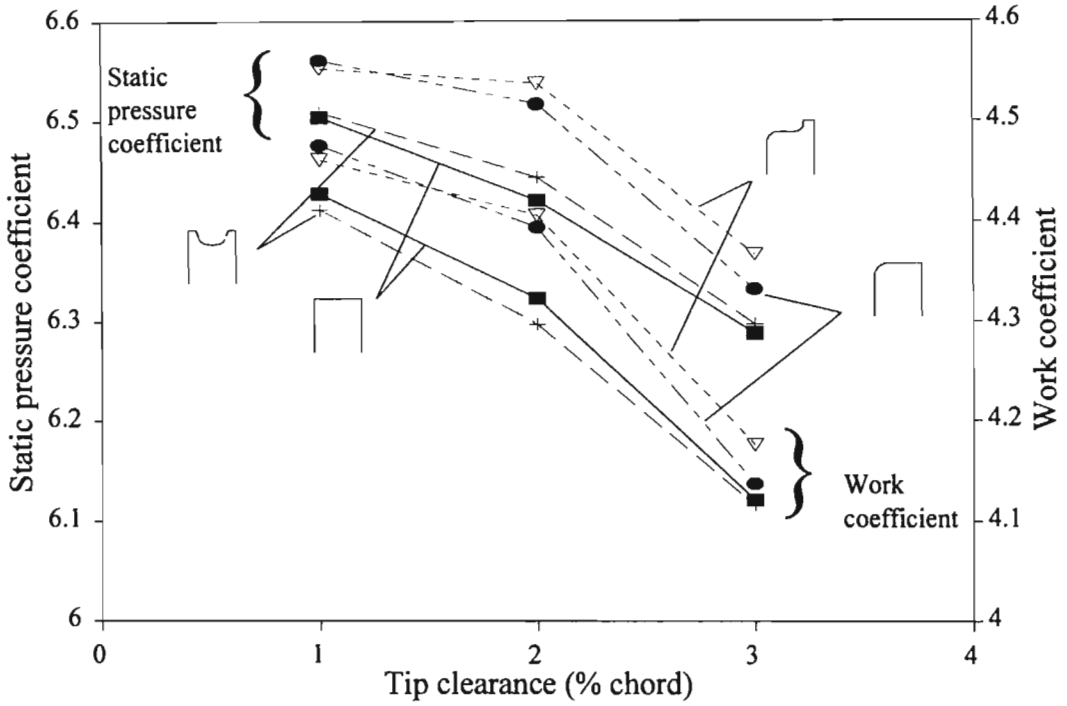

Figure 5.11 The driving pressure across the rotor and turbine work extraction for various tips and changing tip clearance.

CHAPTER 6

THE FLOW FIELDS AND LOSS DEVELOPMENT FOR THE 1 &1.5 STAGE TURBINE

1. Introduction

In the previous chapter, the overall performance of the machine was examined and, in this chapter, the flow field details are examined in an attempt to explain the effect of clearance and the differences between the tip shapes. Tangentially averaged quantities behind the rotor are compared and the results of Morphis (1989) from a linear cascade are also used to clarify the results obtained. Additionally, use is made of loss contours and flow vectors to illustrate the influence of the leakage flow at the rotor outlet.

2. The rotor outlet flow

2.1. A comparison of linear cascade data

Figure 6.1 indicates the rotor relative outlet flow structure for a linear blade row with 2% tip clearance. Morphis (1993) identified two envelopes of the flow near the endwall where each was thought to be formed by the leakage flow over the length of the gap as shown in Figure 6.2. The leakage flow in the first 63% of the blade chord was observed to wrap up almost completely into the passage vortex and contained approximately 51% of the leakage flow as illustrated in Figure 6.3. Over the remaining 37% of the chord, however, 49% of the leakage flow was seen to exit the rotor as a poorly deflected jet and, only further downstream, was found

to wrap up into a vortex. It was postulated that this poorly deflected jet could possibly be utilised in a subsequent nozzle if the kinetic energy of the leakage jet could be partially recovered as the results of Yaras & Sjolander (1989) suggest.

Figures 6.4 & 6.5 are reproduced from Morphis (1993) and indicate the absolute incidence angle and velocity coefficient respectively at inlet to the second nozzle. These values were obtained by transforming the stationary cascade data to the moving frame by the consideration of a hypothetical blade speed at design conditions, detailed in Morphis & Bindon (1990). Representative curves are presented at various percentages of chord measured from the endwall. From these graphs, it is seen that between 35-80% of the pitch, a relatively large negative incidence flow occurs in the range of 1.1-6.9% of blade chord from the endwall. This is seen to be related to the poorly deflected leakage jet contained in the endwall envelope shown in Figure 6.1 and is explained graphically in Figure 6.6. Conversely, between 11.9% and 16.9% of chord from the endwall, the inlet incidence is positive, due to the overturned flow within the inner region of the passage vortex. This is shown in the envelope with dashed line boundaries as identified by the author.

Figure 6.5 indicates that the flow at the linear cascade exit has a relatively high velocity near the endwall between 40-80% of blade pitch which is attributed to the envelope of leakage flow adjacent to the endwall identified in Figure 6.1. Further in from the endwall, there is a slight deficit in the similar pitchwise location, corresponding approximately to the overturned region of the passage vortex. Near mid span, it is seen that the velocity coefficient approaches the design value of approximately 1.0.

When these results are mass averaged to give a radial distribution of the axial velocity coefficient, a previously unnoticed phenomenon can be seen in Figure 6.7. Firstly, the axial velocity coefficient from 0-10% of blade span ranges from a maximum of approximately 1.5 down to a minimum of 0.8. This is caused by the high velocity of the leakage flow adjacent to the endwall and corresponds to an increase of mass flow in the tip region at the linear cascade outlet which confirms the assertion of Heyes & Hodson (1992). At approximately 13% of blade span, there is a minimum axial velocity, corresponding to the low velocity coefficient observed at 11.9-16.9% of blade chord in Figure 6.5. This also confirms the findings of Peacock (1983) who showed that the tip leakage flow caused a flow blockage due to the passage vortex. At mid span, the axial velocity coefficient appears to reach a steady value of approximately 0.91. These results are also represented graphically in Figure 6.6. The consideration of the conservation of mass flow requires that an increase of axial velocity at the tip region must be accompanied by a decrease of axial velocity elsewhere. It is important to realise that this axial velocity deficit represents the underturned flow in the passage vortex at the cascade outlet.

The time averaged radial distribution of axial velocity in the present experimental turbine at the rotor outlet is also presented in Figure 6.7 to compare to the linear cascade result. The basic trends are similar, however, two differences are worth noting. Firstly, the maximum axial velocity measured in the real rotor is not as great as that for the simulated rotor and occurs some way in from the endwall. This is due to the effect of relative motion in the tip gap and can be clearly seen. The scraping effect of the endwall is hence responsible for a slightly lower leakage flow rate due to a reduced wall jet in the tip region. Another possible reason for the reduced maximum velocity could be that the experimental turbine better

incorporates the aspects of radial pressure gradients and spatial and dynamic similarity may not be strictly observed.

The second difference is in the relative position of the passage vortex by determination of the velocity deficit. The turbine rotor produces a similar axial velocity deficit but this is closer to the endwall than that of the linear cascade. This may be occurring because, in the experimental turbine, the leakage flow does not lift off the endwall and dissipate as rapidly as in the linear cascade as observed by Bindon (1994), possibly due to radial effects.

The effects of relative motion can again be seen in Figure 6.8 where the inlet incidence is reduced close to the endwall. The scraping effect of the endwall opposes the direction of the leakage jet and would enhance the turning of the passage flow albeit with a reduction in velocity due to the boundary layer close to the endwall.

The reduction of incidence corresponds directly to the increase in the rotor outlet angle shown in Figure 6.9. This again confirms that relative motion at the tip of the blade is responsible for overturning adjacent to the endwall by viscous shearing. Besides these difference in the results adjacent the endwall, the overall trends in the second nozzle inlet incidence for the turbine and linear cascade are similar and confirm that the overturned flow region is precipitated by the leakage flow and corresponds to an axial velocity deficit.

The simulated rotor results clearly do not reveal any wall effects since the gap leakage flow was seen to be primarily inviscid and no experimental modelling of a moving wall was undertaken. For both the linear cascade and experimental

turbine, however, the flow at the outlet from the rotor suggests that the mixing of the leakage jet will be far from complete at the inlet to the second nozzle.

2.2. The effect of tip clearance on the rotor outlet flow

In order to investigate the effect that tip clearance has on the flow at the rotor outlet, various coefficients are examined for the case of the flat tip shape only. The overall trends were found to be similar for the other tip shapes and these will be later compared at 3% clearance to differentiate between the tip shape effects.

In Figure 6.10, the second nozzle inlet angle near the tip shows a large negative incidence, clearly depending on the tip clearance. This is not unexpected because a larger gap will cause a greater leakage flow with less deflection and, consequently, greater negative incidence at the second nozzle inlet. It is also of interest that close to the endwall (0-4%chord), the incidence is reduced for all clearances, an effect attributed to relative motion.

An aspect that can be seen in Figure 6.8 for both the simulated rotor data and the turbine data is that the resulting incidence from about 25% span up to the hub of the second nozzle is significantly off design. In the original investigation of Morphis (1993), a similar trend was noticed but was not examined further. It was discovered in the course of this investigation that the supposition of an axial velocity coefficient of unity through the turbine was not valid due to the measurement plane of the reference velocity.

The error occurred because the measurement was taken between support blades fixing an inner casing ring relative to the outer ring which essentially reduced the

flow area and increased the axial velocity at that point for the particular reference mass flow. Subsequently, a slight diffusion of the flow occurred behind the support blades with a reduction in the axial velocity through the remainder of the turbine. The operating V_x/U ratio was therefore incorrectly based on a slightly higher axial velocity, leading to the rotor operating in an overspeed condition and resulted in the underturned flow observed. However, this study has continued with the same V_x/U ratio of Morphis (1993) since a comparison of the results was needed and it was felt that the effect of clearance and tip shape was not significantly affected by the slightly off-design operating point.

Interestingly, Figure 6.10. shows an apparent linear variation of the second nozzle inlet angle from 25% blade span up to the hub which suggests that a clearance related mechanism is responsible for the trend. (Note that the inlet angle to the second nozzle was designed to be axial and therefore incidence corresponds directly to the negative of the fluid inlet angle as defined in Figure 4.2).

It is also interesting that in general, linear cascade work has suggested that tip clearance effects are limited to the region from the tip up to about 25% of span from the endwall and significant spanwise effects were not anticipated. Figure 6.11 also demonstrates that the velocity coefficient at each clearance is slightly lower with increasing clearance from about 25% span up to the hub.

Figure 6.12 further emphasises the difference in axial velocity at each clearance where it is observed that at 1% clearance, the mid span axial velocity is higher than those at the greater clearances. These variations are in excess of the uncertainty of the results mentioned in Appendix A. Figure 6.13 shows that the leakage flow does not significantly influence the relative flow outlet angle from

25% chord up to the hub as expected from linear cascade work thus indicating that deviation at the rotor outlet is not the cause of the change in the absolute outlet angle. Rather, the change in the second nozzle inlet angle is due to a deficit of mass flow that is experienced from about 25% span up to the hub, again confirming the assertion of Heyes & Hodson (1992).

This leakage flow model is represented graphically in Figure 6.14. A larger tip gap causes a larger leakage flow rate which was seen to be linear by Yaras et al (1988) and Storer (1989). The increase in the mass flow in the tip region is therefore accompanied by a deficit over the remaining blade span due to conservation. This deficit thus gives rise to a rotor absolute outlet flow with less overall deflection and therefore lower work extraction over the entire blade length.

The model is supported in Figure 6.15 by consideration of the tangentially averaged radial angle at the rotor inlet (first nozzle outlet) and the rotor outlet (second nozzle inlet). At the inlet to the rotor, the radial angle is positive, indicating a net migration of fluid from the hub to the tip according to the sign convention adopted in Figure 4.2. At the rotor outlet, the radial angle shows a net flux towards the hub, confirming the mechanism suggested in Figure 6.14.

The leakage flow adjacent to the endwall (0-8% chord), as identified in Figure 6.1 remains to be analysed and will be seen to be an important aspect of the leakage flow. In Figure 6.11 and 6.12, increasing tip clearance increases the axial velocity in the tip region and hence the mass flow rate. The swirl component of this relatively high velocity flow can be seen in a vector plot representation of the secondary flow at the rotor exit in Figure 6.16. These vectors represent the local time averaged radial and tangential velocity components from the 5 hole probe.

Again, an overall impression of a radial flow from tip to hub is obtained in accordance with the mechanism suggested in Figure 6.14. It can also be seen that the leakage jet manifests itself as a high swirl velocity in the form of a ring of fluid adjacent to the endwall. Figure 6.17 indicates a low total pressure loss corresponding to this ring of fluid adjacent to the endwall. This is synonymous with a higher kinetic energy compared to the mid span flow.

The concept of total pressure is somewhat objectionable considering that work has been extracted from the rotor. However, the work extraction for this turbine was based on a free vortex design thus the change of enthalpy or total pressure can be expected to be constant per unit span of blade. A local perturbation of total pressure loss can therefore be considered as a change in velocity in the presence of a uniform static pressure field behind the rotor. Measurements behind the rotor confirmed that the static pressure field was indeed uniform. Total pressure is thus a reasonable evaluation of the effectiveness of work extraction across the rotor if the entropy generation by the walls and rotor blade profiles is ignored.

In Figure 6.17, it is immediately apparent that at 2% and 3% clearance, the total pressure of the ring of fluid adjacent the to endwall is lower than that at mid span. As the clearance is reduced to 1%, the loss of total pressure increases to a wall value of approximately 6.2. This can be interpreted as the leakage jet exiting the gap with a high total pressure, or high kinetic energy as a result of less work extraction. This in itself is an important result because it shows that the leakage flow will energise the flow in the rotor blade passages and further downstream. It must be emphasised here that this is significantly different from the results in a linear cascade. Measurements of the leakage flow downstream of a linear cascade blade row will not record a relatively higher total pressure but will be similar or

slightly lower than that at the inlet to the cascade blade row due to viscous friction in the clearance gap.

The difference in total pressure loss from 25% of span up to the hub is again an indication of the effect that clearance has on the overall flow. The higher leakage flow rate was seen to reduce the deflection of the flow and thus the work of the rotor (see Figure 6.14) which is then manifested as a lower total pressure loss at exit to the rotor.

2.3. The effect of tip shape on the rotor outlet flow

The rotor tip shape was seen in Chapter 5 to have a marginal effect on the machine efficiency, however, it was found that the low entropy tip shapes produced a greater work output and required a higher driving pressure. Comparative results for the various tip shapes are presented for 3% clearance since the effects of clearance were found to be similar for all tip shapes and the differences between the tip shapes were more pronounced at a larger clearance.

If the second nozzle inlet angle is examined in Figure 6.18, two distinct differences are seen between the tip shapes. The first concerns the trend from 25% span up to the hub which again is caused by a mass flow rate deficit across the blade span where each tip shape gives rise to a leakage flow with a slightly differing flow rate at the gap exit.

The second significant difference in results is in the tip region. From 0-8% span from the endwall, the contoured suction squealer tip causes a greater inlet angle (or negative incidence) when compared to the other tips and, in particular, the

radiused tip. This is interesting because although the velocity coefficient in the tip region for the contoured suction squealer is similar in magnitude to that of the radiused tip (shown in Figure 6.19), it can be seen in Figure 6.20 that the axial velocity is slightly lower, suggesting a slightly lower leakage flow rate. The reason for the increased inlet angle, therefore, is due to a slightly poorer deflection of the leakage flow. This confirms the work of Morphis (1989) who found a reduction of the leakage flow rate for a contoured suction squealer.

At approximately 10% of span from the endwall, the absolute outlet angle of the contoured suction squealer is similar to the other tip shapes, however, there is a significant deficit of velocity and corresponding axial velocity as indicated in Figures 6.19 & 6.20 respectively. This suggests that the resulting passage vortices have a slightly stronger rotation than those produced by the other tips shapes. This is confirmed in Figure 6.21 where it can be seen that at 10% of span from the endwall, the rotor deflection is significantly greater than that of the other tip shapes and corresponds to the overturned flow in the passage vortex.

As expected, a similar trend is observed for the radiused tip when compared to the square tip shape, however, the double squealer tip is seen to be somewhat in between the radiused tip and the square tip in terms of the magnitude and direction of the outlet flow in the tip region.

In Figure 6.19, the velocity coefficient for the double squealer tip from 0-8% of span from the endwall is slightly greater than that of the square tip shape and a similar trend is found in the axial velocity plot in Figure 6.20. This is a surprising result because previous research has shown that the double squealer tip had the potential to reduce the tip leakage flow rate in a linear cascade. In the range 8-

15% chord, Figure 6.21 shows that the relative angle of the double squealer tip rotor outlet flow is also greater than that of the square tip, suggesting that a slightly stronger passage vortex exists. These results imply that the cross sectional shape of the cavity as well as the reduction of the highly sheared flow on the tip surface are important factors in the reduction of the leakage mass flow rate as suggested by Chen et al (1993).

A comparison of the total pressure loss coefficient at the rotor exit for the various tip shapes is presented in Figure 6.22. The contoured suction squealer exhibits a slightly larger total pressure loss at 10% of span compared to the other tip shapes. From this it may again be deduced that the passage vortex is moderately greater than those of the other tip shapes. The evidence again confirms that the low entropy tip shapes cause a higher tip clearance mass flow which gives rise to a stronger passage vortex. This in turn is responsible for a slightly larger deficit in axial velocity or mass flow at about 10% of span from the endwall.

The above observations suggest a possible explanation for the difference in driving pressure across the different tip shape rotors and a tentative model is presented in Figure 6.23 based on the findings of Peacock (1983). The increased tip leakage flow rate causes an increased mass flow in the tip region behind the rotor. This is accompanied by a deficit of mass flow corresponding to the overturned flow in the passage vortex. This deficit can be regarded as a flow blockage and can be compared to reducing the cross sectional area of a nozzle. Because the control routine used for the turbine essentially maintained a constant mass flow rate through the turbine, the reduction of the flow area within and behind the rotor would then require a higher driving pressure which, at the same time, raises the differential pressure across the rotor and thus increases the work from the rotor.

3. The development of the rotor exit flow in the absence of a second nozzle

The development of the rotor exit flow in the absence of a further stage is of importance when considering certain turbine applications for example in a jet engine. In the previous chapter, it was seen that the overall changes in machine performance for varying clearance were similar and thus only the effect of tip shape is investigated at 3% clearance.

The flow angle downstream of the various tip rotors is presented in Figure 6.24. If this is compared to the situation immediately behind the rotor represented in Figure 6.18, a number of differences may be observed. Firstly, the outlet angle of flow in the tip region has been reduced from a value of approximately 32° down to a value of 25°. This apparent change in angle can be understood by comparing Figures 6.25 and 6.26 to Figures 6.19 and 6.20, where it is obvious that the high energy leakage jet has significantly dissipated to form a more conventional velocity profile near the surface of the endwall. The axial velocity deficit noted immediately behind the rotor has also been eliminated as a result of the mixing of the ring of fluid adjacent to the endwall with the main stream flow. This is confirmed again in Figure 6.27 by comparing the swirl component to that in Figure 6.16. The high energy ring of fluid has also penetrated further into the mainstream flow.

With reference to Figure 6.24 and Figure 6.18, another interesting phenomenon can be seen near the hub. The flow angles have been reduced from approximately 15° to about 10°. This reduction is possibly due to the development of the leakage flow which induces a number of counter-rotating vortices as identified in Figure 6.27 by the dashed line envelopes. The reduction in the flow angle at the

hub corresponds to the increase in axial velocity at 80-90% span seen in Figure 6.26 which obviously has been brought about by the radial transport of fluid by the vortex formations. The resulting counter-rotating vortices would give rise to overturning at the hub and this will precipitate a lower axial velocity there as noted by Joslyn & Dring (1990). Interestingly, the pitch between the time averaged vortices corresponds to the nozzle blade pitch, suggesting that the time averaged vortex formation is seeded by the interaction of the rotor with the upstream nozzle wakes.

Further evidence of the influence of the upstream nozzle may also be seen in Figure 6.28 which presents a contour plot of the total pressure loss development in the downstream rotor outlet flow. The loss contours were obtained by subtracting the local loss coefficient at the downstream position from the upstream tangentially averaged loss coefficient at the same radius. It can be seen that an apparent negative total pressure loss occurs as represented by the shaded areas. What this gain in total pressure indicates is the mixing of the high energy leakage jet with the mainstream flow. Also shown are apparent wake remnants from the upstream nozzle indicating the effect of the blade wakes on the mixing losses in the flow downstream of the rotor.

The radial distribution of the tangentially averaged loss development of the flow downstream of the rotor is presented in Figure 6.29. It is seen that close to the endwall, there is a large loss formation, similar for each tip shape and is synonomous with the rapid dissipation of the wall jet. In the region of 10% span from the tip there is an apparent gain in total pressure due to the high energy leakage jet mixing with the mainstream flow. Also of importance in Figure 6.29 is the fact that the squealer tip profile appears to produce the highest gain in total

pressure at 10% span but then appears to produce slightly more total pressure loss from 15-25% span in comparison with the other tip shapes. This may be interpreted as a slightly higher mixing loss caused by the dissipation of the higher swirl velocity in the mainstream flow.

In Chapter 5, the overall total pressure loss in the downstream flow for each of the low entropy tips was lower than that of the flat tip, suggesting that they may have a slight advantage if used in a final stage. It appears that the lower total pressure loss is due to the energisation of the passage flow and suggests that possibly more of the kinetic energy of the leakage fluid has been recovered than that of the flat tip. This may be a property of the entropy gradient within the leakage flow caused by the rate of the internal gap entropy generation. However, it is worth mentioning that the flow has obviously not mixed out fully and additional mixing losses can be expected which may negate this slight advantage. It is also interesting that the effect of tip clearance on the loss development is limited to about 25% span from the tip.

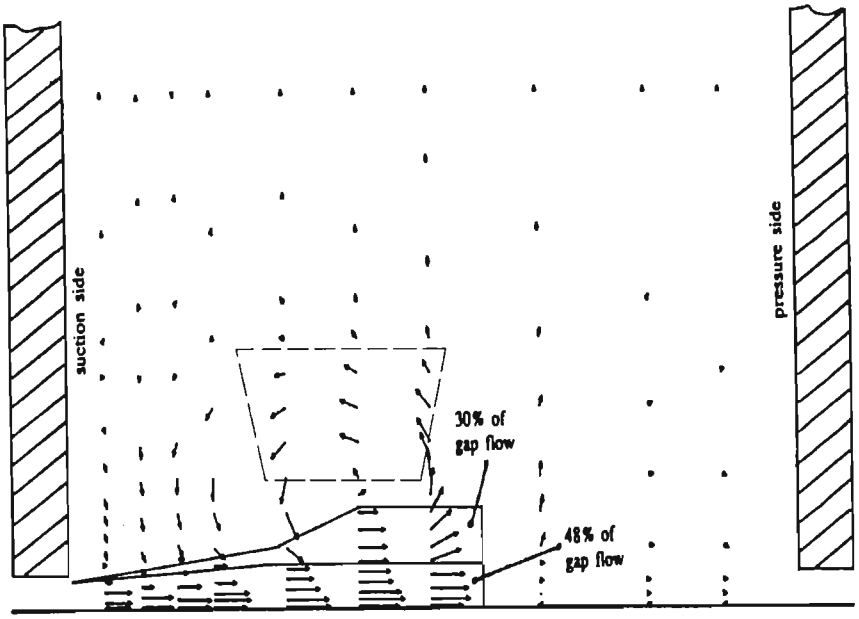

Figure 6.1 The secondary flow structure at the linear cascade exit showing the two envelopes identified by Morphis (1993) as well as the envelope of overturned flow in the passage vortex indicated by the dashed line polygon.

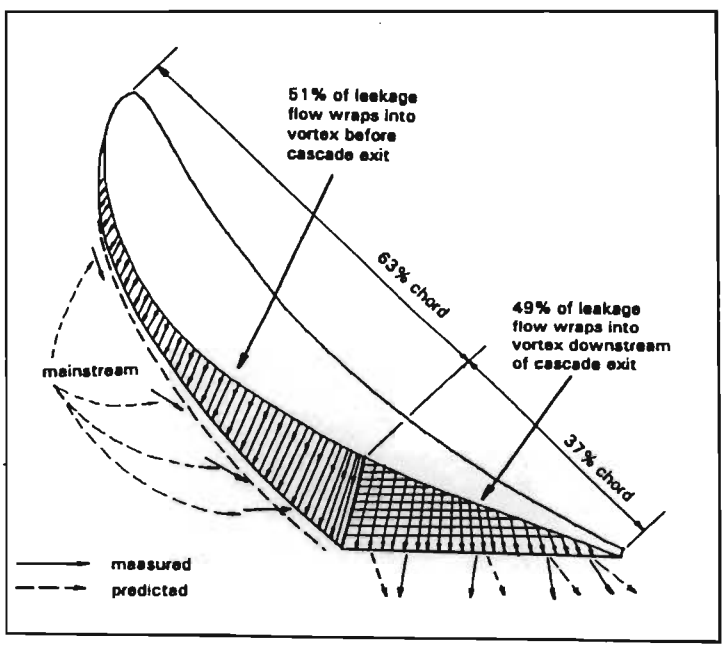

Figure 6.2 Morphis (1993) identified the proportion of the leakage flow that did not wrap up into the passage vortex.

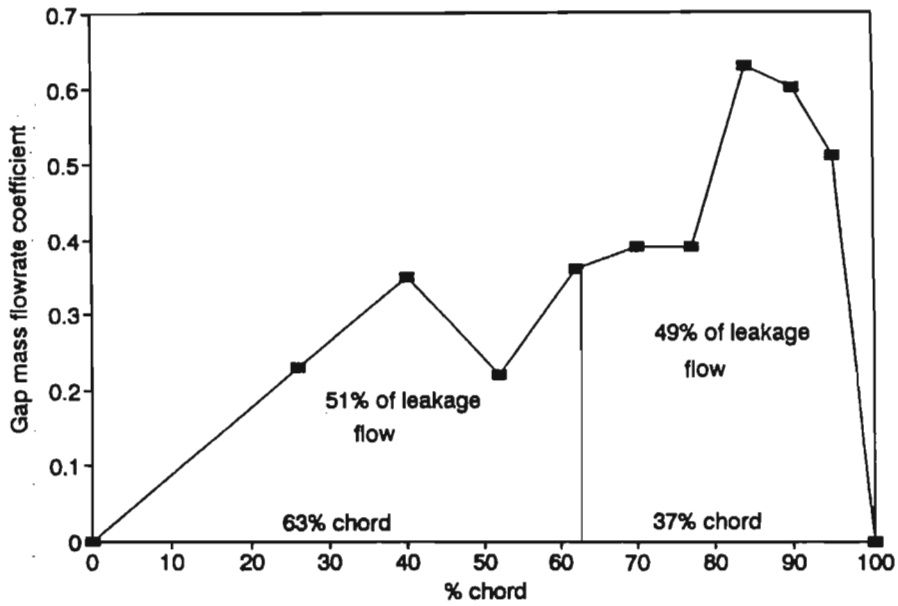

Figure 6.3 The leakage flow rate distribution at the gap exit of the linear cascade

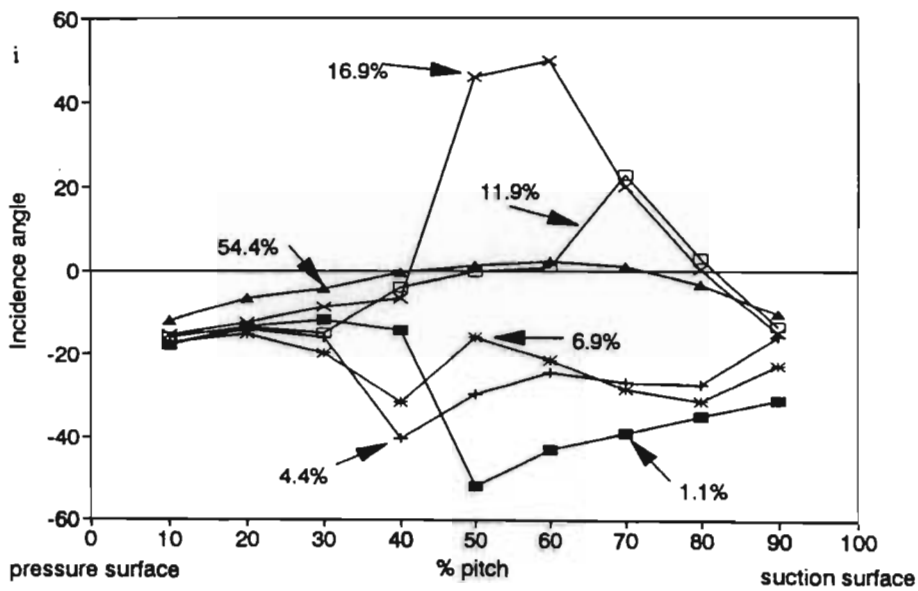

Figure 6.4 The hypothetical second nozzle incidence angle simulated from the linear cascade data with 2% clearance.

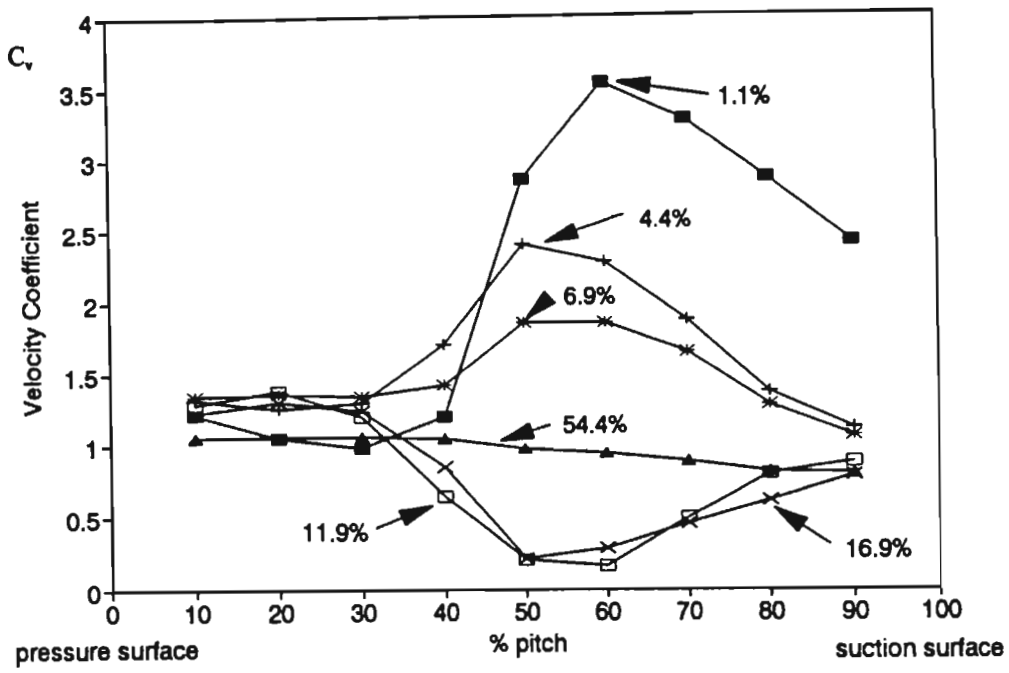

Figure 6.5 The hypothetical second nozzle inlet velocity coefficient simulated from the linear cascade data with 2% clearance.

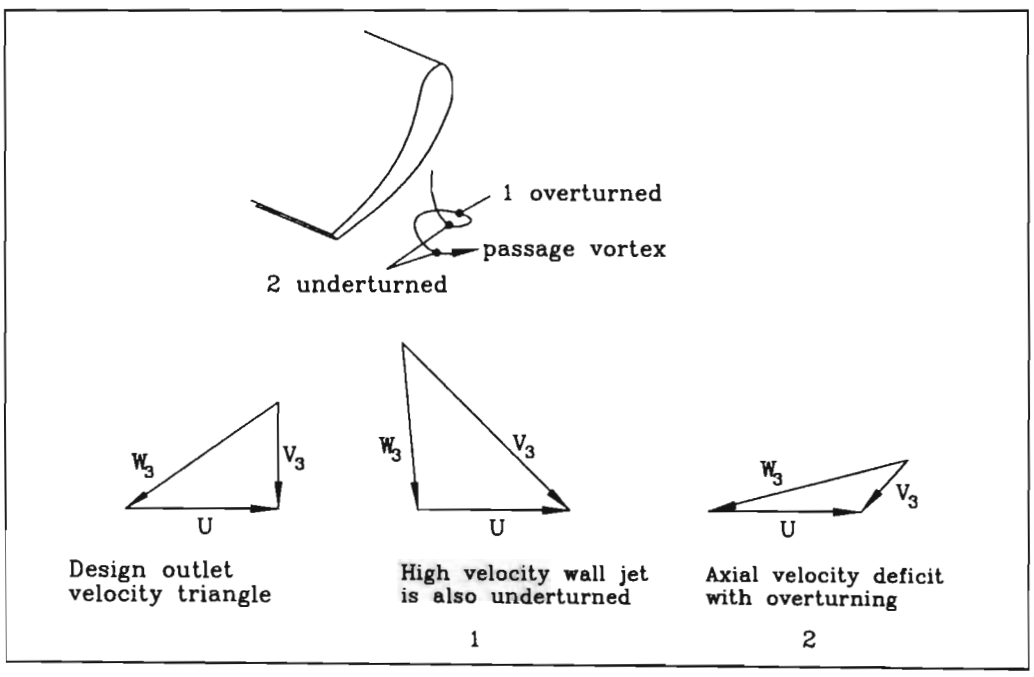

Figure 6.6 The effect of the leakage flow on the design velocity triangle

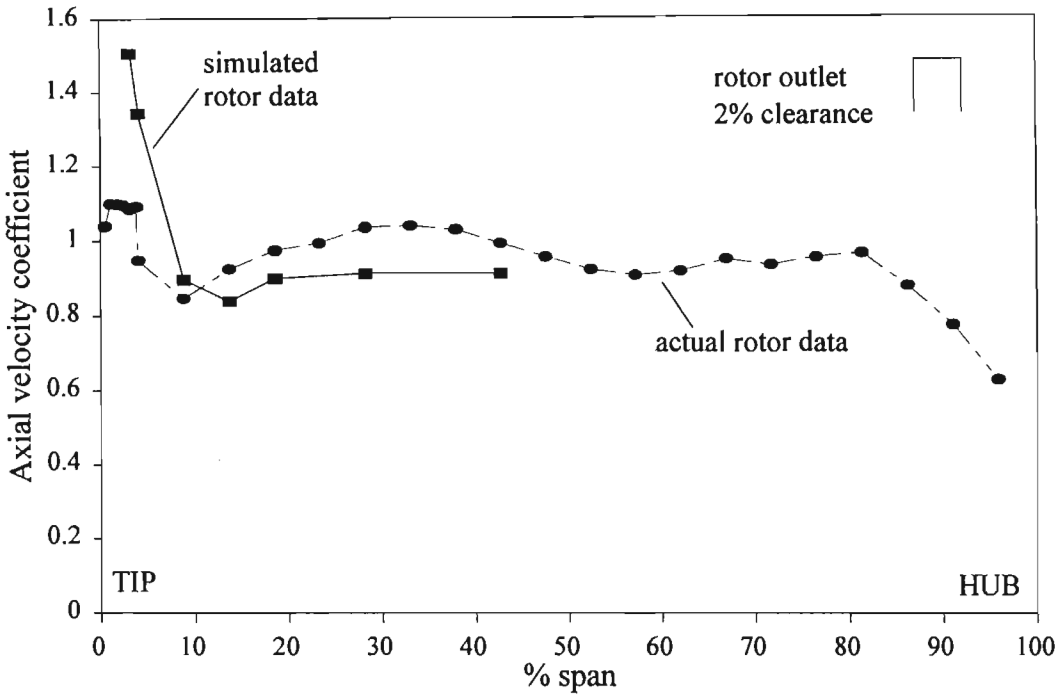

Figure 6.7 The radial variation of the tangentially averaged axial velocity coefficient at the hypothetical rotor outlet compared to actual rotor data.

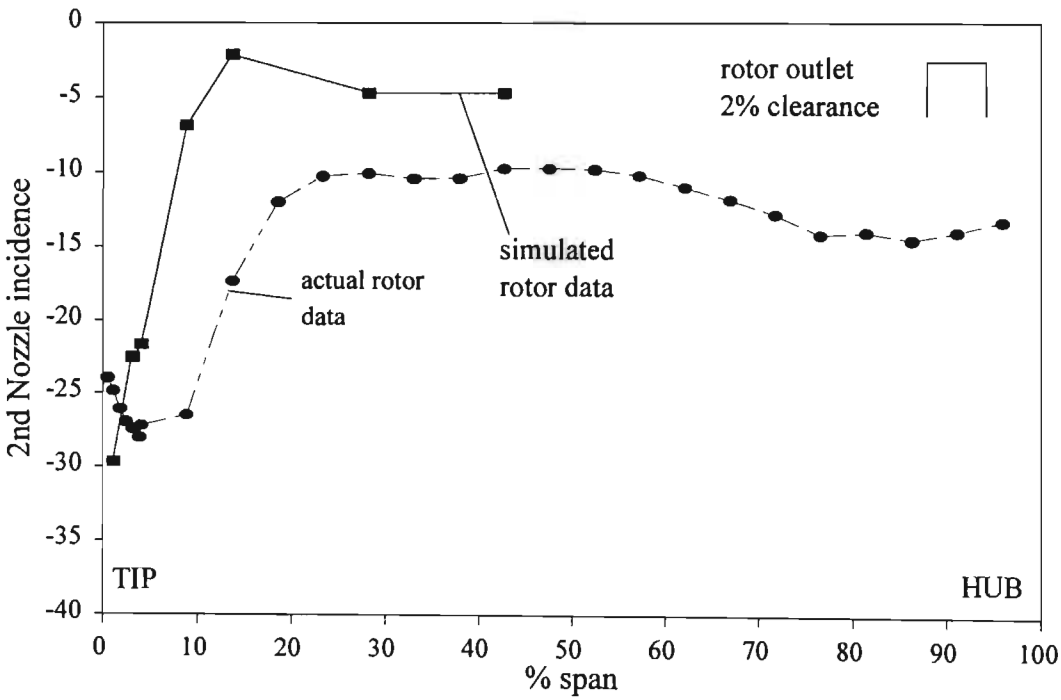

Figure 6.8 The radial variation of the tangentially averaged 2nd nozzle incidence angle behind the hypothetical rotor compared to actual rotor data.

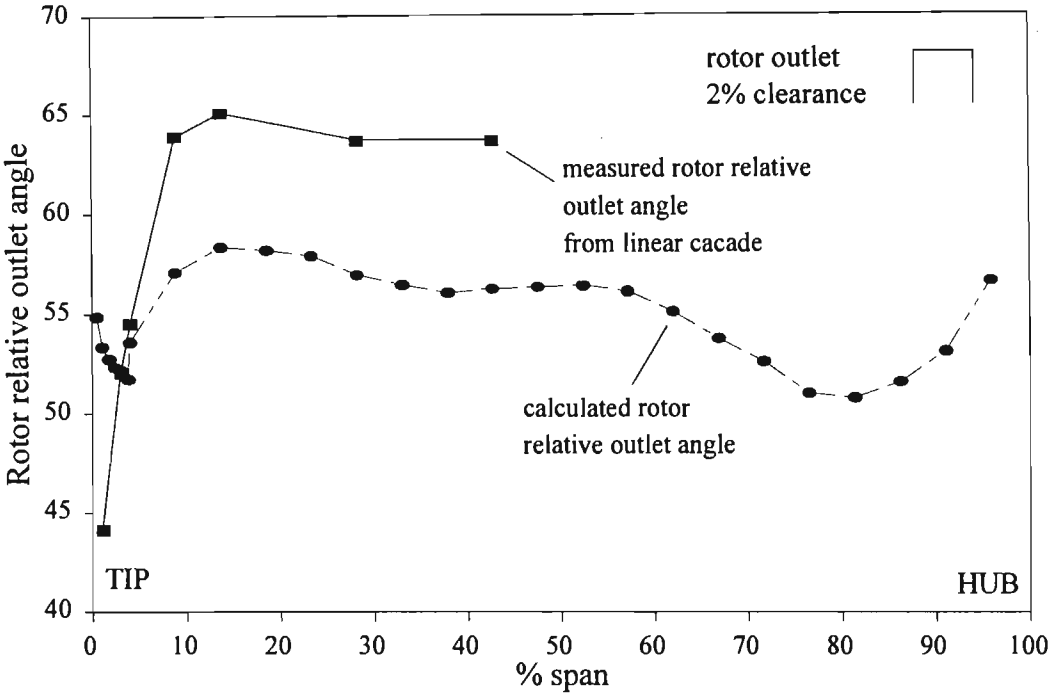

Figure 6.9 The radial variation of the tangentially averaged rotor relative outlet angle behind the hypothetical rotor compared to actual rotor data.

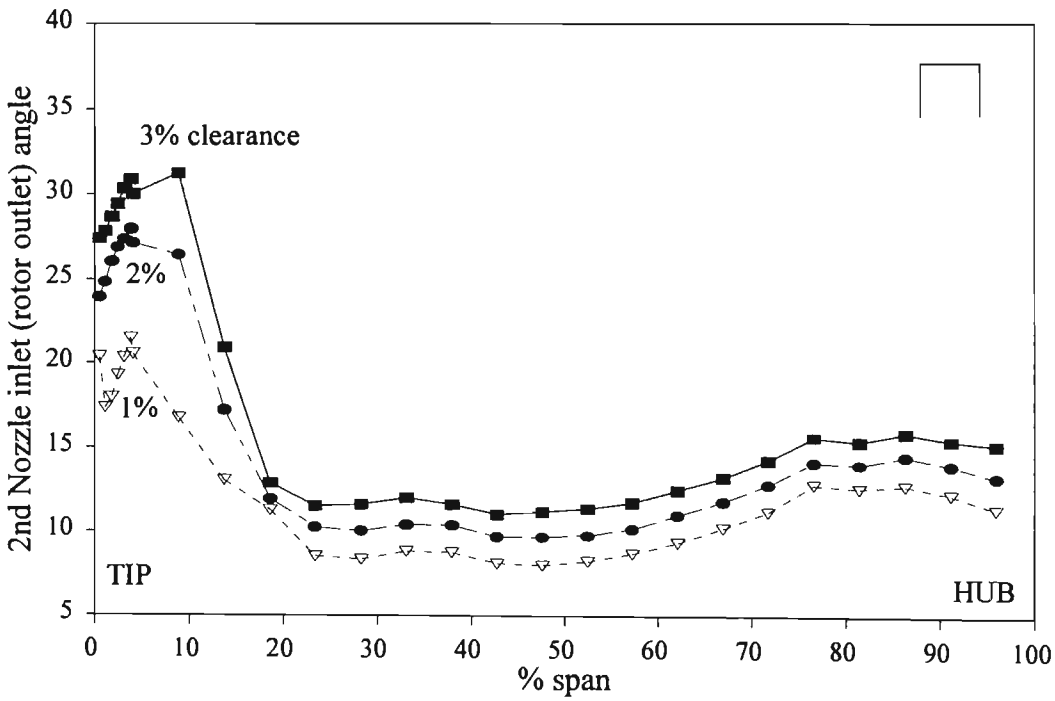

Figure 6.10 The radial variation of the tangentially averaged 2nd nozzle inlet angle for the flat tip rotor with varying tip clearance.

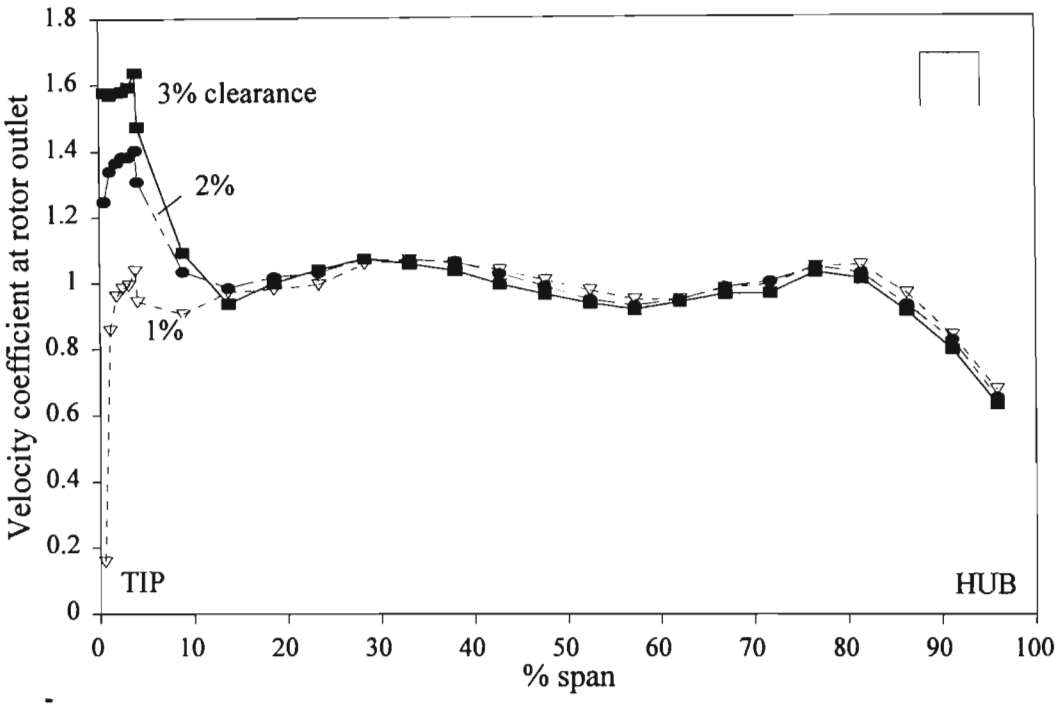

Figure 6.11 The radial variation of the tangentially averaged velocity coefficient at the flat tip rotor outlet for varying tip clearance.

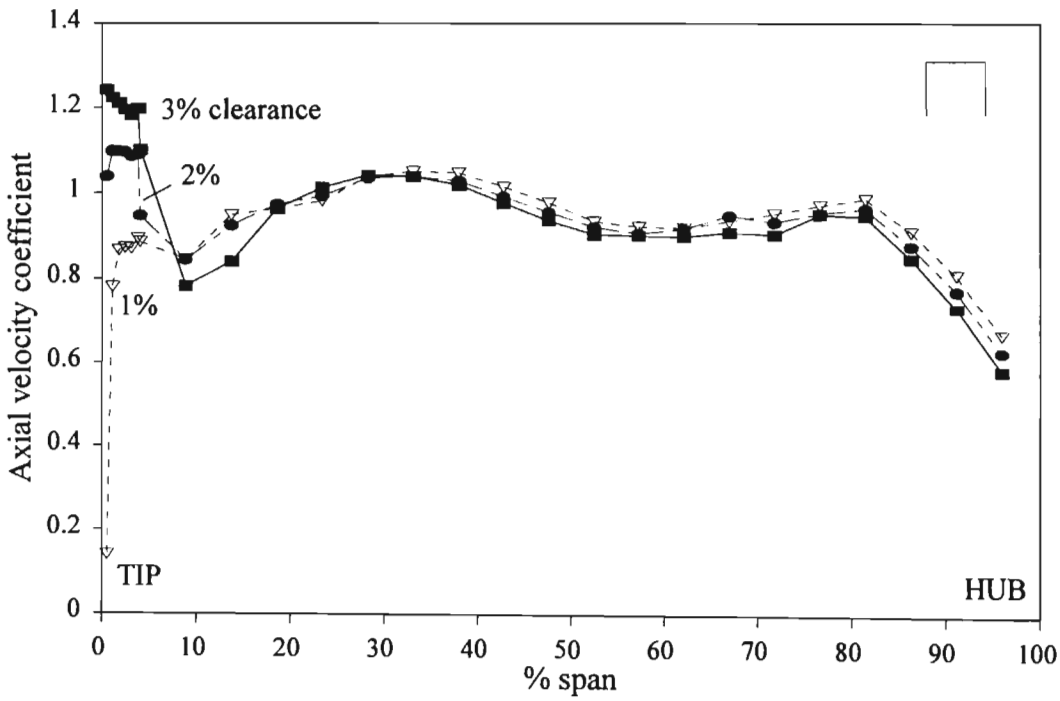

Figure 6.12 The radial variation of the tangentially averaged axial velocity coefficient at the flat tip rotor outlet for varying tip clearance.

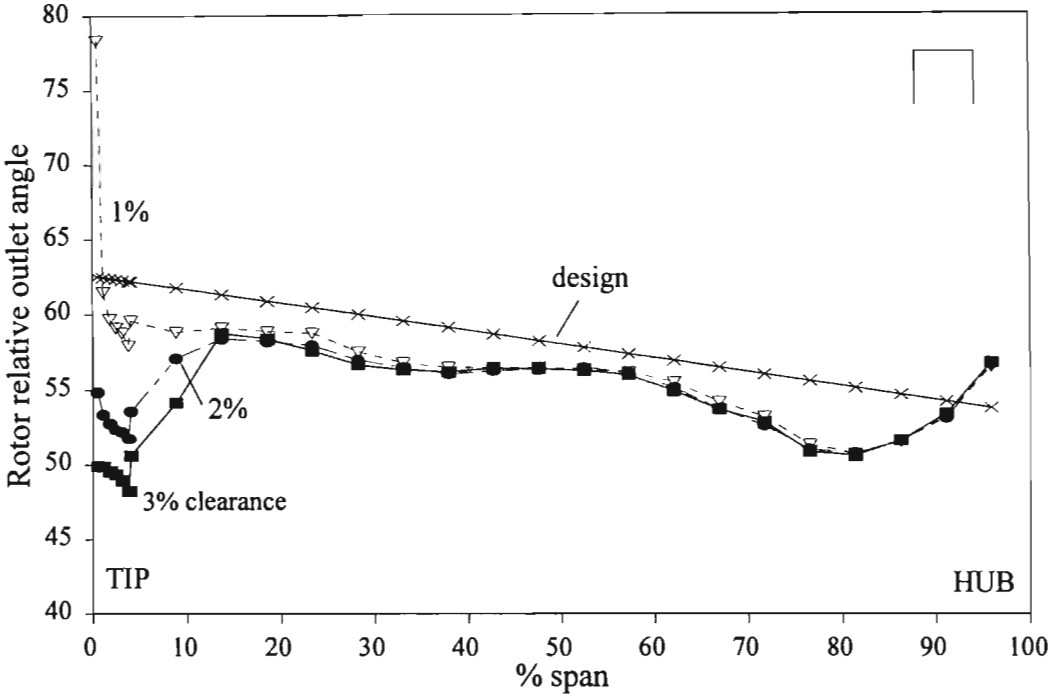

Figure 6.13 The radial variation of the flat tip rotor relative outlet angle for varying tip clearance.

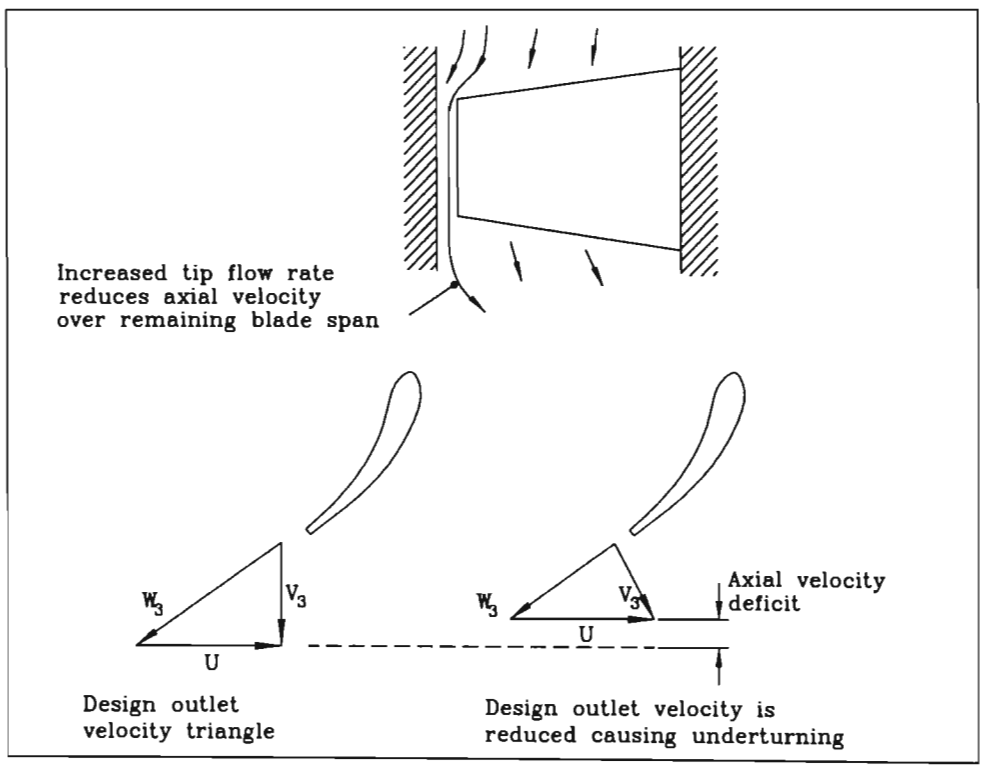

Figure 6.14 The gap increases the mass flow rate in the tip region with an accompanying reduction in the axial velocity across the remaining blade span.

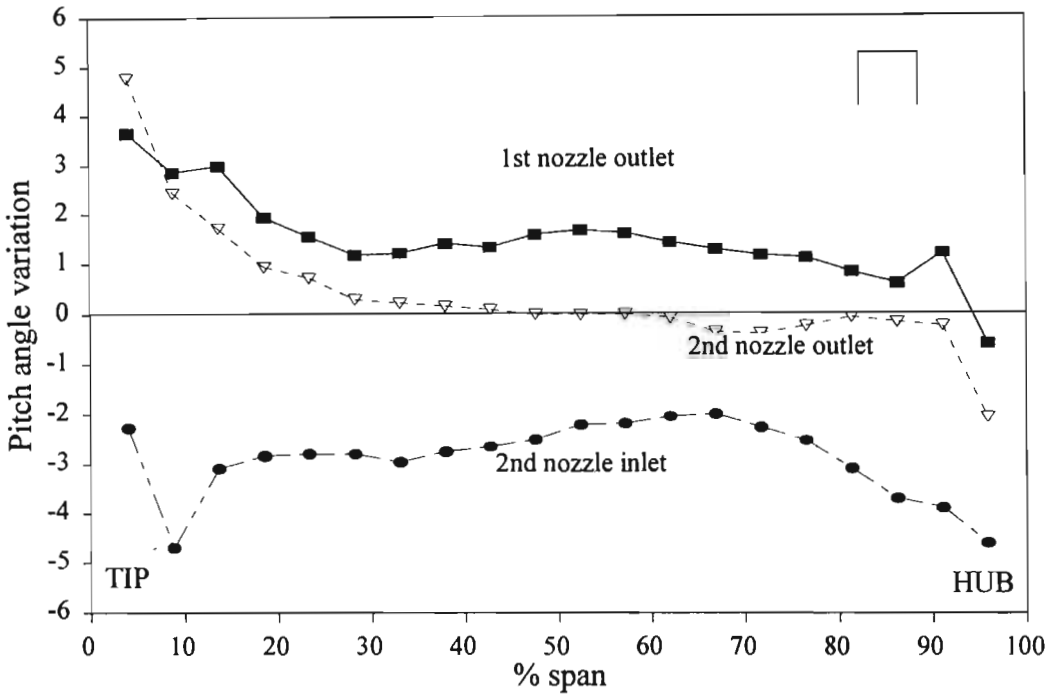

Figure 6.15 The radial variation of the tangentially averaged radial angles at various axial stations for the flat tip rotor at 3% clearance.

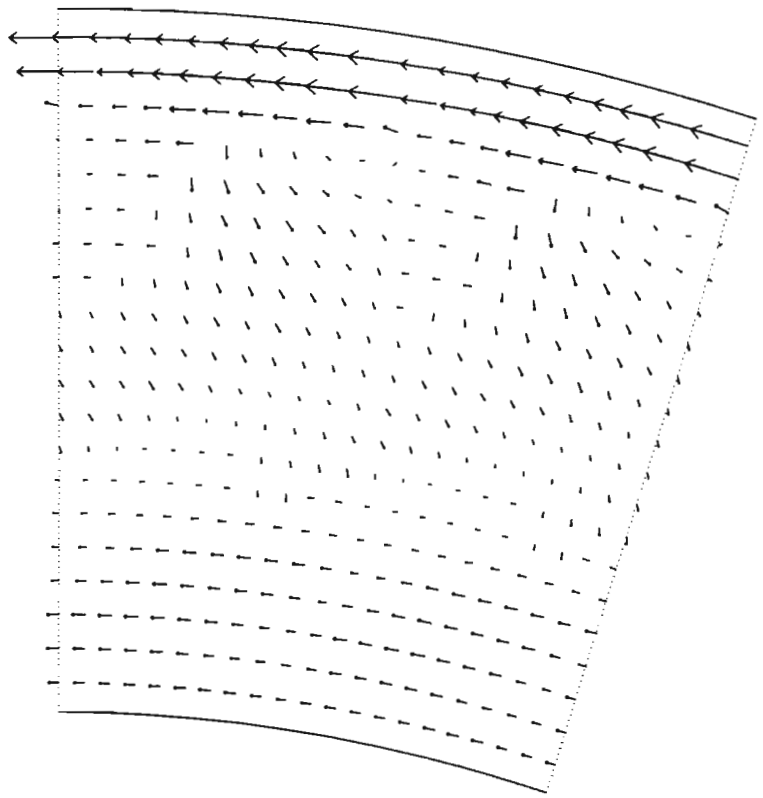

Figure 6.16 The time averaged secondary flow structure at the flat tip rotor outlet for 3% clearance showing the relatively large swirl component of the leakage flow.

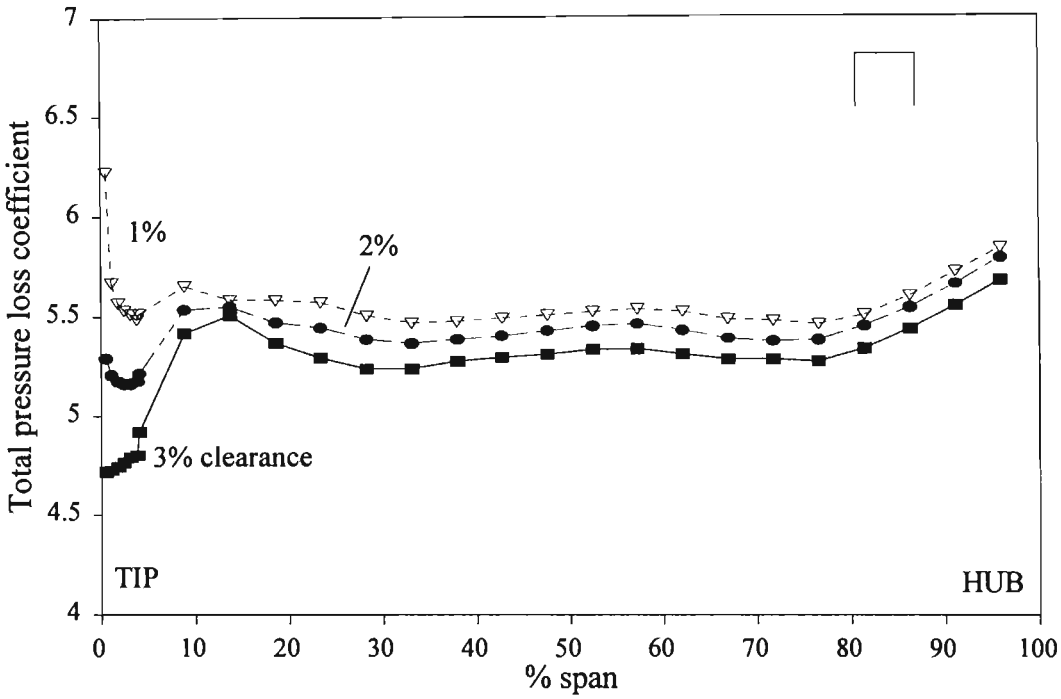

Figure 6.17 The radial variation of the tangentially averaged total pressure loss coefficient at the flat tip rotor outlet for varying tip clearance.

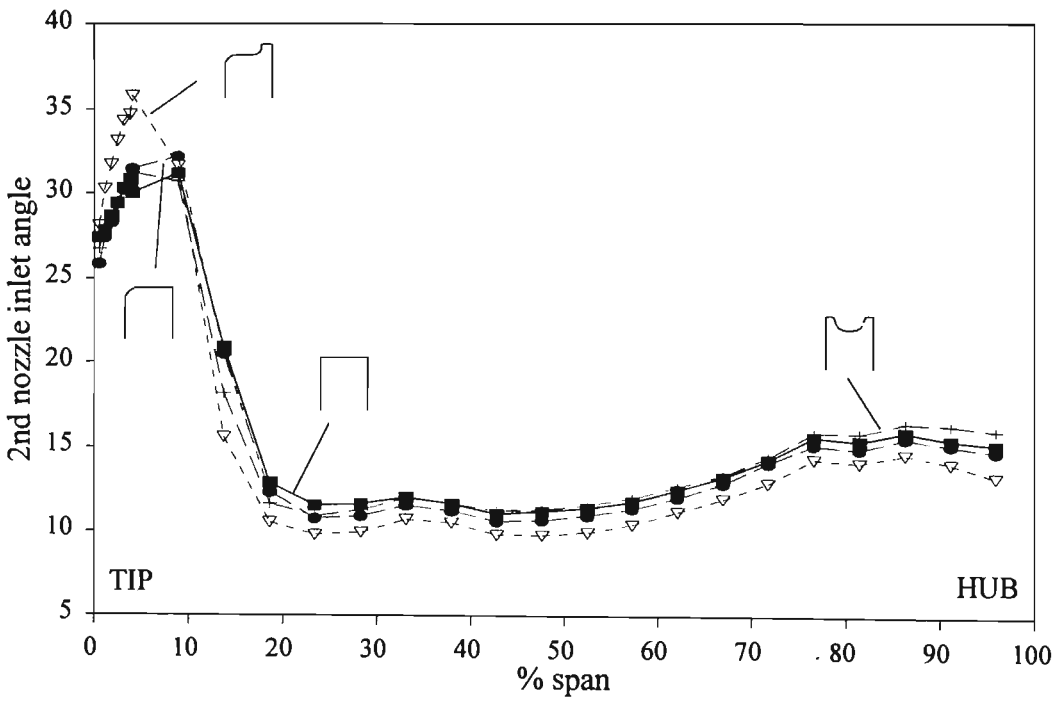

Figure 6.18 The radial variation of the tangentially averaged 2nd nozzle inlet angle for various tip shapes at 3% clearance.

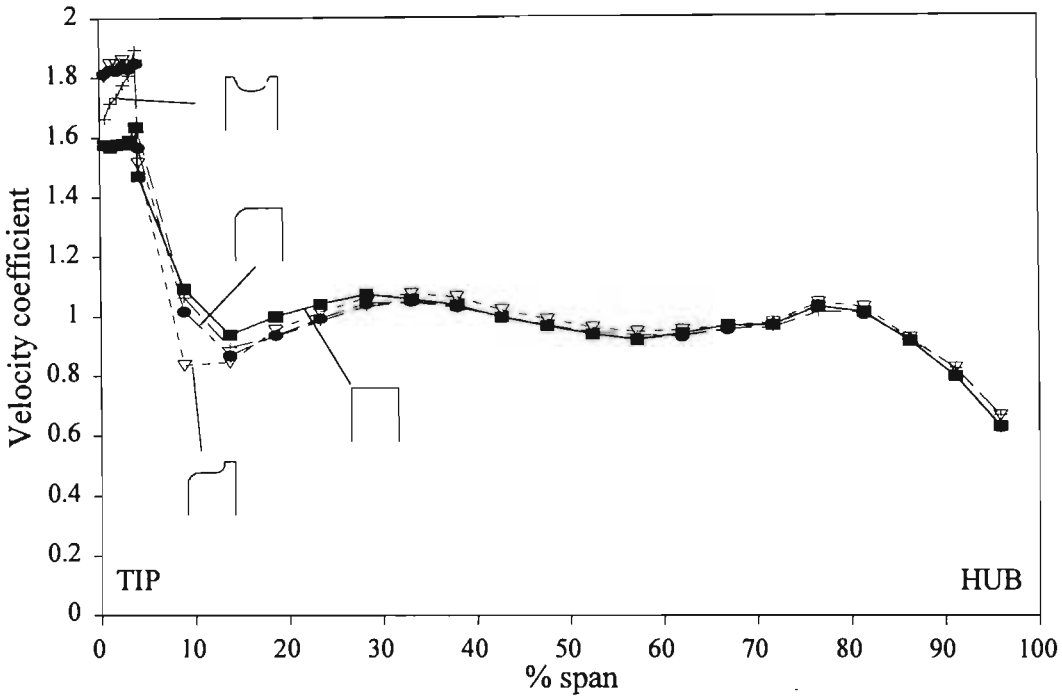

Figure 6.19 The radial variation of the tangentially averaged velocity coefficient at the rotor outlet for various tip shapes at 3% clearance.

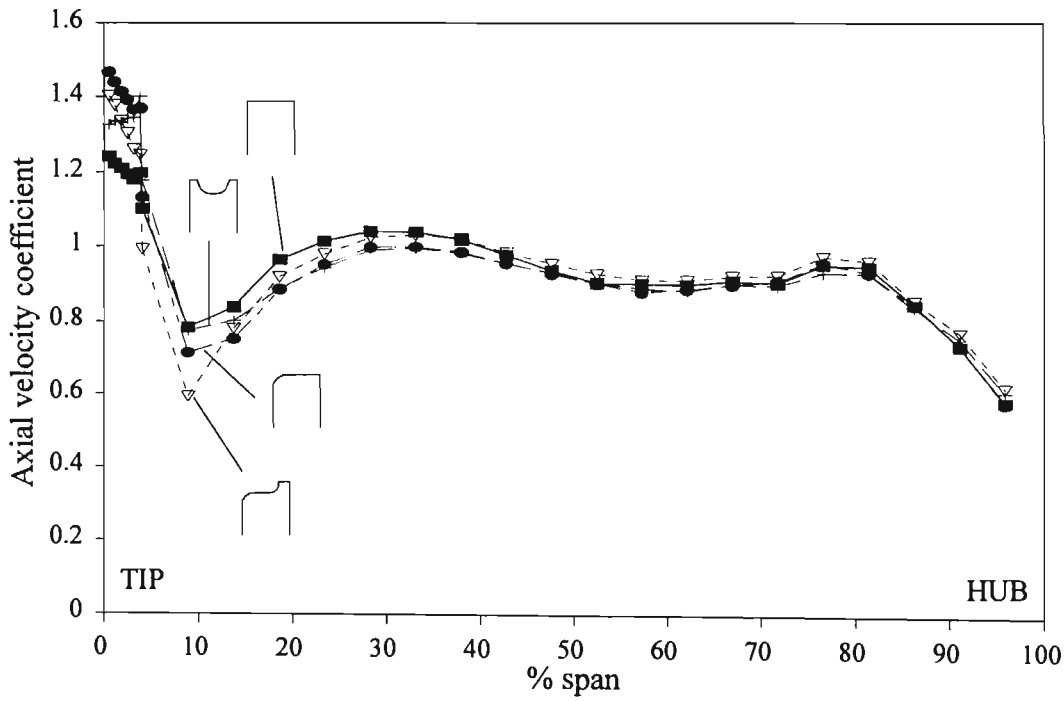

Figure 6.20 The radial variation of the tangentially averaged axial velocity coefficient at the rotor outlet for various tip shapes at 3% clearance.

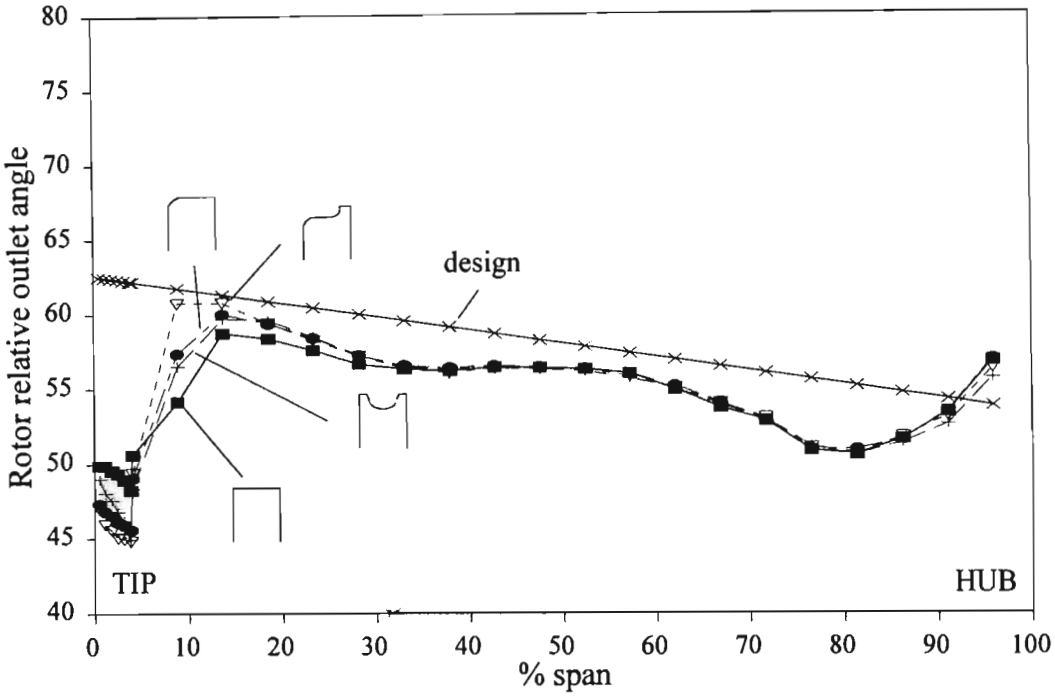

Figure 6.21 The radial variation of the tangentially averaged rotor relative outlet angle for various tip shapes at 3% tip clearance.

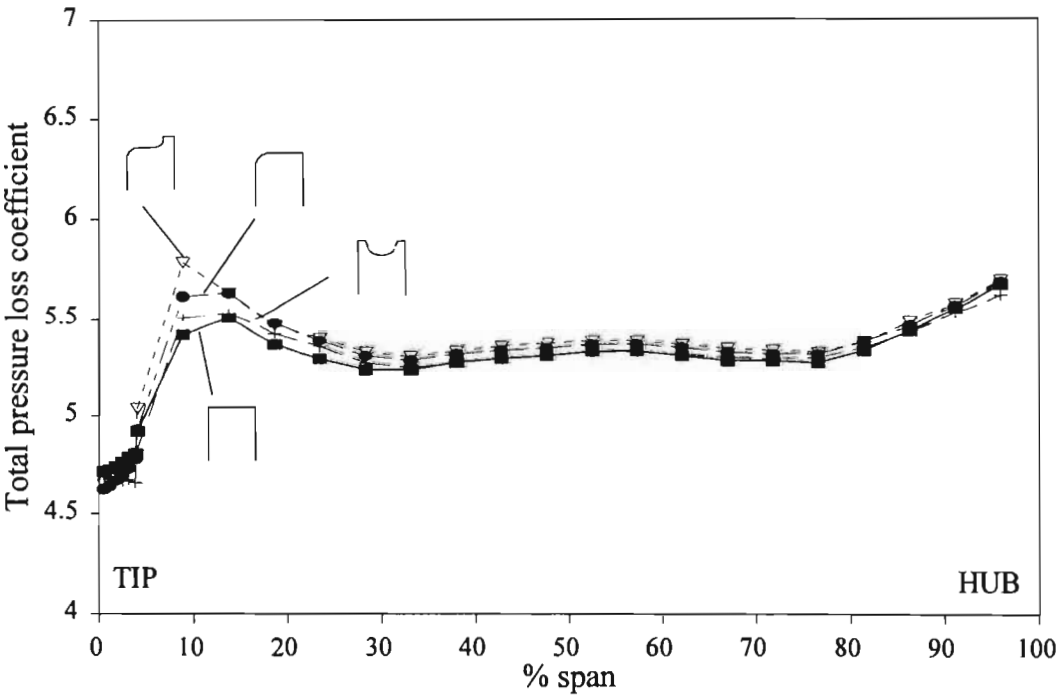

Figure 6.22 The radial variation of the tangentially averaged total pressure loss coefficient at the rotor outlet for various tip shapes at 3% clearance.

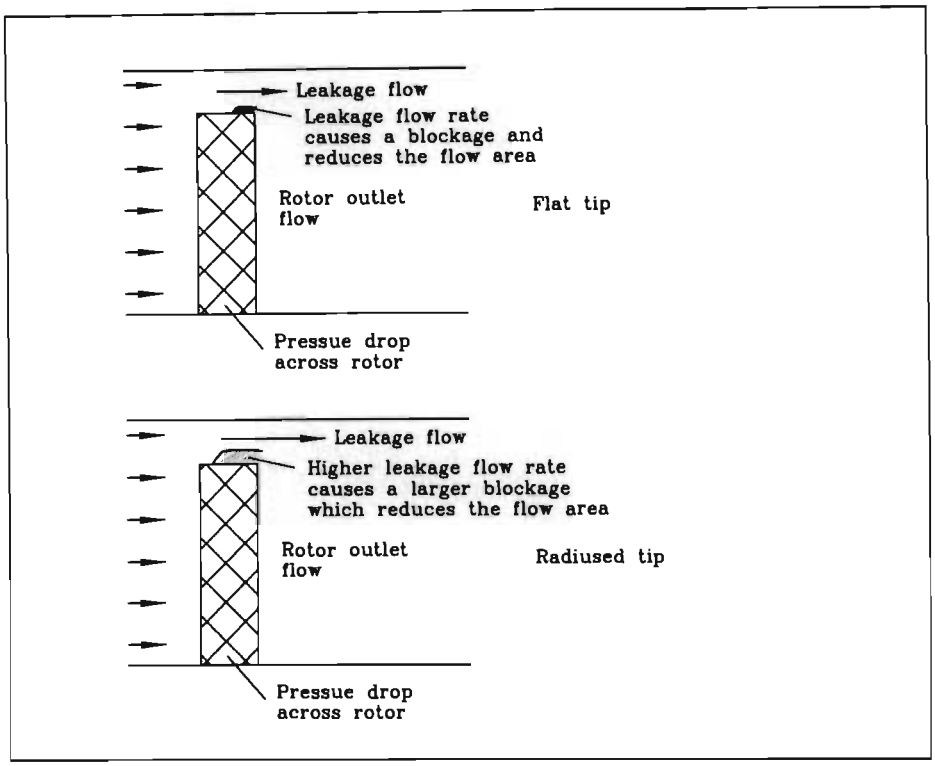

Figure 6.23 A higher leakage flow rate causes a larger flow blockage which effectively reduces the flow area, requiring a higher driving pressure for the same turbine mass flow rate.

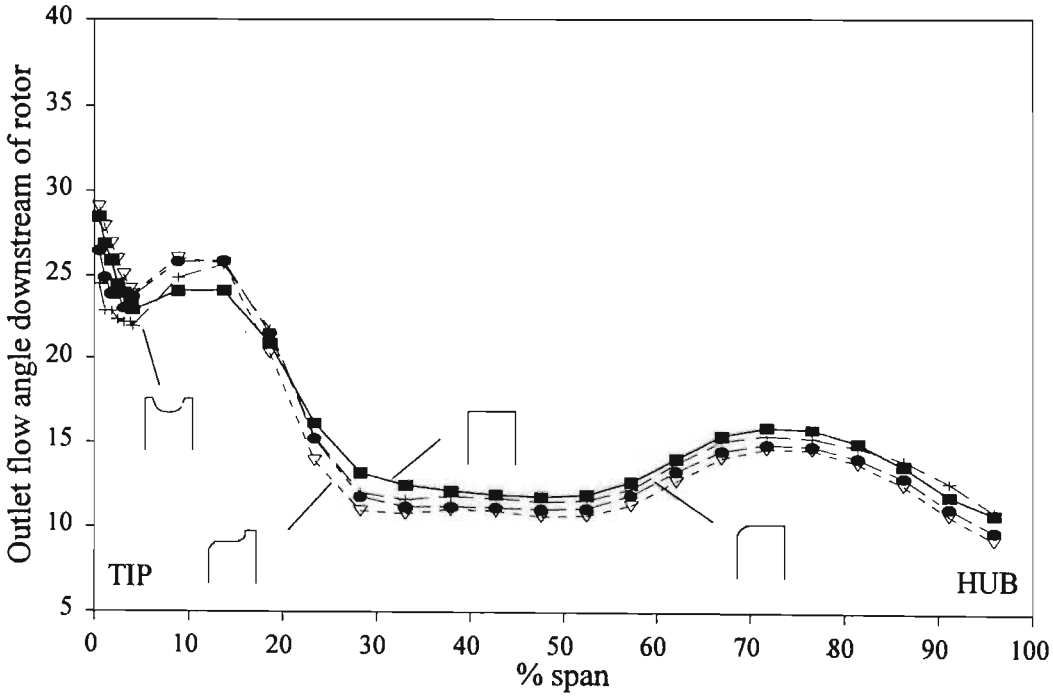

Figure 6.24 The downstream development of the tangentially averaged rotor absolute outlet angle for various tip shapes at 3% clearance.

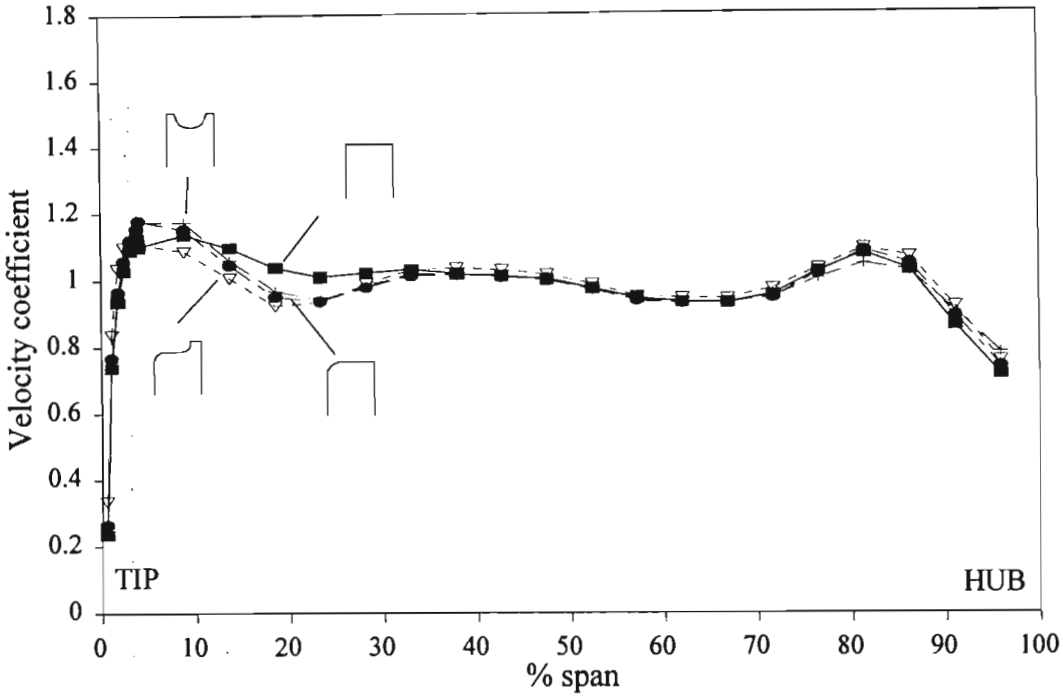

Figure 6.25 The downstream development of the tangentially averaged velocity coefficient for various tip shapes at 3% clearance.

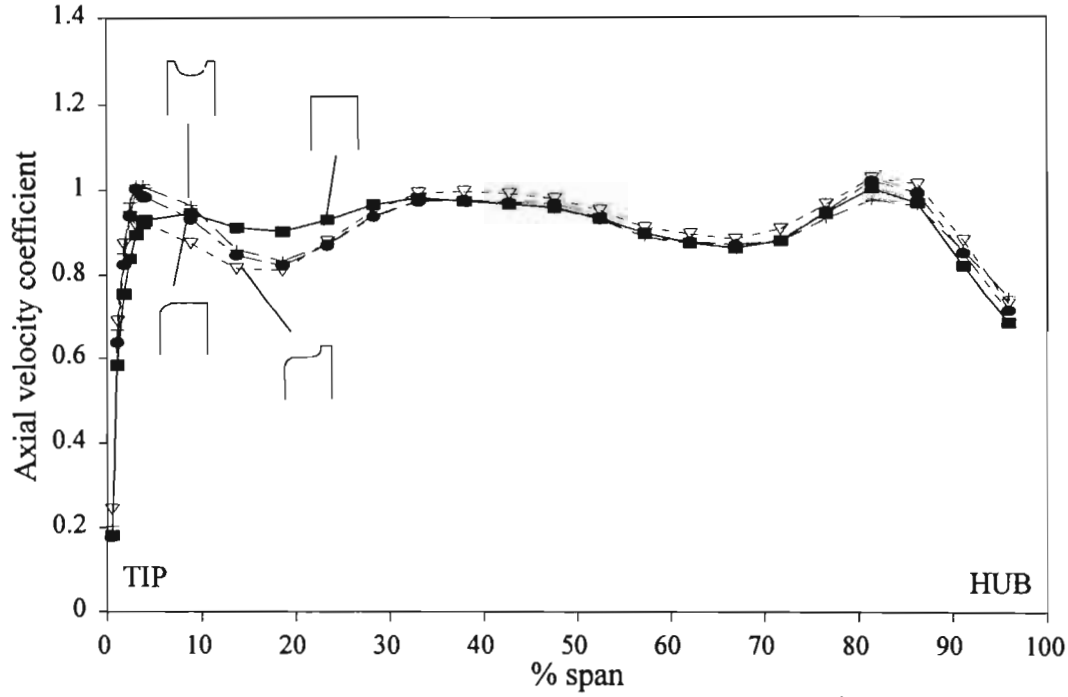

Figure 6.26 The downstream development of the tangentially averaged axial velocity coefficient for various tip shapes at 3% clearance.

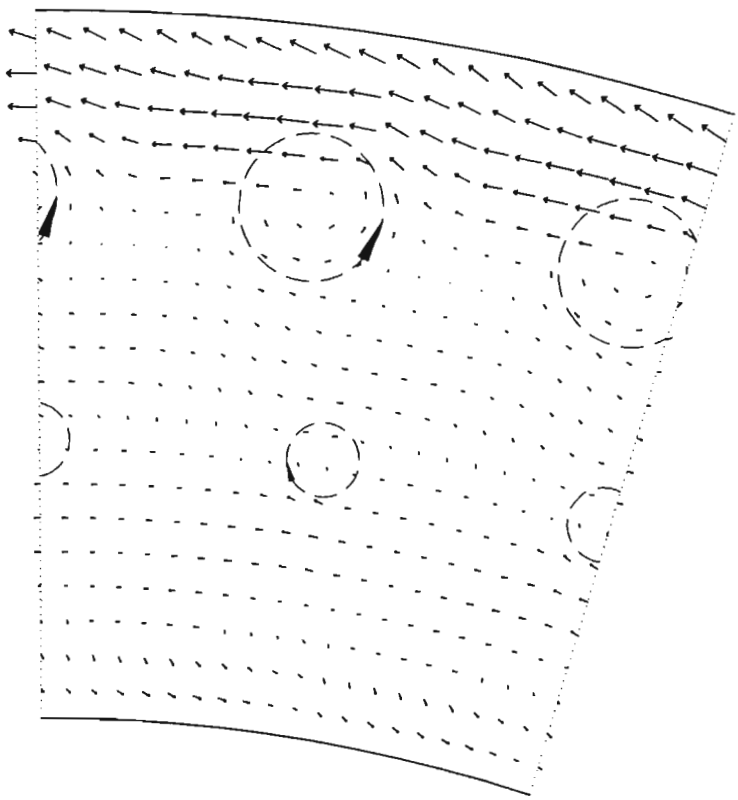

Figure 6.27 The downstream development of the time averaged secondary flow vectors of the flat tip rotor at 3% clearance.

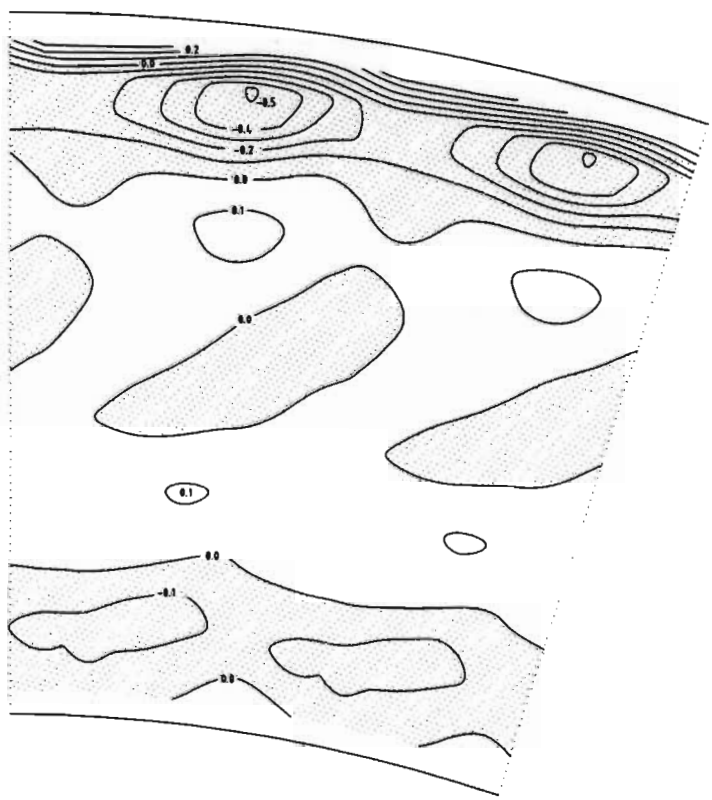

Figure 6.28 Contours showing the subsequent development of the total pressure loss behind the flat tip rotor at 3% clearance in the absence of a second nozzle.

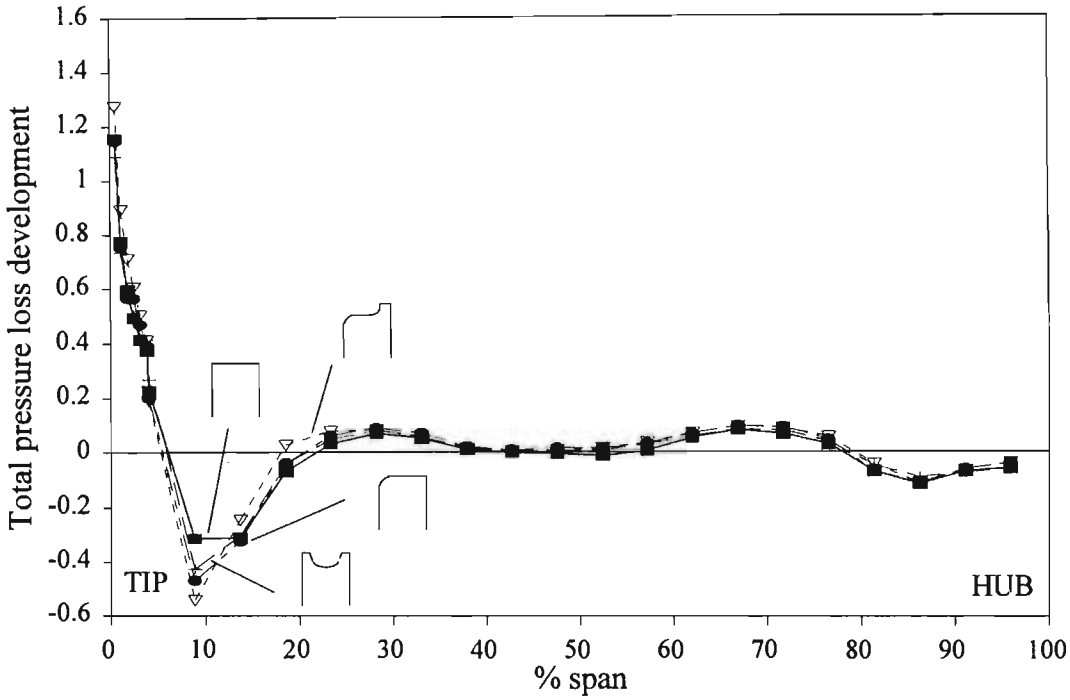

Figure 6.29 The radial variation of the tangentially averaged total pressure loss coefficient downstream of the rotor for various tip shapes at 3% clearance.

CHAPTER 7

THE FLOW FIELDS AND LOSS DEVELOPMENT BEHIND THE SECOND NOZZLE

1. Introduction

The relative performances of the first and second nozzle are compared and radially averaged quantities and contours of loss and flow vectors are used to explain the possible flow mechanisms within the second nozzle.

Again the effect of clearance on the second stage nozzle is investigated by comparing results at various clearances for the flat tip shape rotor. A comparison of the different tip treatments is done at 3% clearance. Results are also compared to the first nozzle outlet flow in an attempt to explain the apparently high second nozzle efficiency.

2. The performance of the second stage nozzle

2.1. The effect of tip clearance on the performance of the second stage nozzle

In the discussion of the rotor outlet flow, it was seen that the second nozzle ingests a rather complex flow which, besides varying with time, also contains a ring of poorly deflected fluid in the tip region close to the endwall. This endwall ring of fluid was seen to be closely dependent on the tip clearance and showed only a moderate relationship to the tip shape used.

Figure 7.1 shows the influence of tip clearance on the second nozzle outlet angle. A number of phenomena can be noticed from this, the first being the shift of a local minimum outlet angle near the endwall from 25-35% from the tip. This movement from tip to hub is directly related to the tangential velocity of the ring of fluid near the endwall and this is verified in Figures 7.14, 7.16 and 7.18 which indicate a time averaged vortex structure in the secondary flow vector plots at the second nozzle outlet. These figures show that the centre of each vortex appears to move further from the endwall. Taking the case of 2% clearance in Figure 7.16, by observation, the vortex structure is centred at approximately 23% of span from the endwall. The minimum outlet angle in Figure 7.1 occurs at approximately 30% span from the endwall corresponding to the underturned flow in that vortex.

Figure 7.1 also shows that beyond 50% span from the endwall, the tangentially averaged curves do not indicate a significant variation, confirming that the leakage flow effect is limited up to 50%. It is interesting to recall that the limiting region behind the rotor was found to occur up 25% of span from the endwall. Obviously, the second nozzle exercises a considerable mixing effect on the flow behind the rotor due to the radial transportation of fluid within the blade passages.

The third feature of Figure 7.1 is the overturning evident between 50-85% span. This overturning corresponds directly to another vortex flow structure observable in each of Figures 7.14, 7.16 and 7.18 and appears to be centred about 55% span. This rotational flow can not be attributed to classical secondary flow at the hub and appears to be an induced vortex structure by the previously mentioned one centred at approximately 23% span. Figures 7.14, 7.16 & 7.18 also show evidence of tip-hub radial flows within the blade wakes behind the second nozzle. This is

an expected phenomenon since low momentum fluid on the blade surfaces will migrate in this direction due to the significant radial pressure gradient.

It is interesting that the vortex structure centred at 55% span opposes the formation of the classical hub secondary flow vortex. This may reduce the formation of the hub secondary flow which would ultimately reduce the pressure losses within the second nozzle. This is suggested in a comparison of the secondary flow structure at outlet to the first nozzle shown in Figure 7.26 in which the hub secondary flow vortex is evident as well as the expected secondary flow structure at the tip. The migration of low momentum fluid in the blade wakes appears to slightly oppose the hub secondary flow vortex which is not as large in appearance as the tip secondary flow vortex.

Figure 7.2 shows that the tangentially averaged velocity coefficient is only slightly affected by tip clearance, however, the axial velocity in Figure 7.3 shows that there is a significant effect up to 50% of span. It can be seen that the large axial velocity near the endwall at the inlet to the nozzle has been mixed out within the nozzle passages. The perturbations in axial velocity can also be seen to correspond to the under and overturning of the vortex structures as noted by Joslyn & Dring (1992).

Figure 7.4 shows that the effect of tip clearance on the total pressure loss across the second nozzle is also limited up to 50% span from the endwall. The largest clearance appears to have energised the flow in the region of 10-25% span indicating of the that the high energy leakage ring of fluid adjacent to the endwall has mixed out within the nozzle. Figures 7.15, 7.17 & 7.19 illustrate the total pressure loss contours at outlet from the second nozzle. Each figure demonstrates

that there are a number of regions between the hub and tip that experience a total pressure gain due to the high energy leakage flow behind the rotor and are represented in the figures by the shaded areas.

At 1% clearance it is seen that there is a high energy zone near the tip, near mid span and also near the hub. At 2% clearance, the tip and mid span zones have merged as shown and also indicate a slightly higher total pressure gain corresponding to a pressure loss coefficient of -0.2. This is also shown in Figure 7.19 with a minimum loss coefficient just under -0.4, confirming that the high energy leakage jet has mixed into the passage flow within the nozzle blades.

Morphis (1992), indicated the existence of an extended loss formation on the suction surface side of the blade wakes and noted the dependence of the size of the loss formation on the magnitude of the tip clearance. A similar finding was shown by Boletis & Sieverding (1991). In comparing these contour plots to that of the first stage nozzle shown in Figure 7.27, a number of conclusions can be drawn about the nature of this formation.

In Figure 7.27, no negative loss zones are observed behind the first stage nozzle, confirming that the leakage flow is responsible for the apparent gains seen in Figures 7.15, 7.17 & 7.19. It was also confirmed that the first stage nozzle indicates evidence of the classical secondary flow vortices at the tip and hub and a significant thickening of the wake loss can be seen at the tip and hub. This can be attributed to the low momentum fluid on the endwall and hub surfaces being swept into the corresponding suction corner with an accumulation of low energy fluid in those regions.

At 1% clearance in Figure 7.15, the loss formation on the suction surface of the second nozzle (Morphis (1993)) is not immediately apparent, but two interesting phenomena can be observed. Firstly, the thickening of the blade wake at the tip is significantly reduced when compared to that of the first nozzle. This is probably due to the high energy leakage fluid energising and sweeping the boundary fluid into the blade wake. The second phenomenon is a similar version of the loss formation as noted by Morphis (1992) but this is seen to occur at approximately 75% span from the endwall. This also is as a result of the sweeping effect that occurs due to the formation of the previously mentioned counter-rotating vortex that exists at about 55% span from the endwall. By comparison too, it is noted that the blade wakes behind the second nozzle are slightly thicker than those of the first nozzle, potentially as a result of the low energy fluid being swept into the blade wakes as well as a higher profile loss due to increased viscous shearing. By increasing the tip clearance, the loss formation on the suction side thus progressively increases in size, corresponding to increased shearing due to the sweeping effect of the leakage flow on the endwall and suction surface.

The trends suggest a model of the manner in which the leakage flow is ingested by the second nozzle and the resulting outlet flows. This model is presented in Figure 7.28. It is interesting that even though the resulting tip vortex at the outlet from the second nozzle is essentially of the same rotation as that expected in classical secondary flow, the nature of the two is entirely different. The classical secondary flow vortex is caused by the blade tangential pressure gradient and contains low energy fluid from the endwall. The leakage flow adjacent to the endwall contains high energy fluid that is poorly deflected by the rotor and because of this does not induce the same blade loading at the tip of the second nozzle. The resulting vortex structure is therefore caused by the flow straightening

effect that the second nozzle has on the rotor outlet flow as suggested in Figure 7.28.

2.2. The effect of tip shape on the second nozzle

The squealer tip was observed to cause the slightly more underturning (5-22% span) and overturning (22-40% span), conforming to a vortex structure of greater rotational strength because of slightly poorer deflection of the leakage flow at the rotor outlet. Figure 7.5 shows that this gives rise to a greater degree of overturning at the second nozzle outlet corresponding to a larger vortex structure observed at 23% span.

The secondary flow vector plots for the radiused, suction squealer and double squealer tip are shown in Figures 7.20, 7.22 & 7.24 respectively, however, the differences are not easily identifiable and the tangentially averaged results are more indicative of the small differences, which again confirms the overall similarity of the flow with various tip shapes.

Again Figure 7.6 shows that the outlet velocity coefficient for the various tip shapes is similar, however, Figure 7.7 shows a moderate difference in the axial velocity distribution at the nozzle outlet. These differences can again be attributed to the corresponding strength of rotation of the leakage induced vortices at the nozzle outlet which in turn is a linear function of the swirl component of the leakage flow. Again the effects are limited up to 50% span.

Figure 7.8 shows an expected trend with regards to the effect of tip shape on the total pressure loss across the second nozzle. It can be seen that at 10% span, the

lowest loss coefficient is due to the suction squealer tip which causes the highest leakage swirl velocity. This trend is repeated for the other tip shapes as well, but it is interesting that the radiused tip produces slightly higher losses from about 20-30% span. This is probably due to the increase of mixing losses of the leakage flow. This effect can also be seen in Figure 7.21 which indicates the pressure loss contours at the second nozzle outlet for the radiused tip. It can be seen that in relation to Figures 7.19, 7.23 & 7.25 for the flat, suction squealer and double squealer tip, the overall energised zone for the radiused tip is moderately smaller than that of the other tips. When comparing this figure to that of the square tip, it is seen that the high energy zone near the endwall is of a greater magnitude, possibly indicating that mixing of the high energy jet has not progressed as far as that for the square tip. This may indicate that although the radiused tip causes a higher leakage flow rate, this occurs with a greater axial component thus reducing the swirl component of the leakage flow and lowering the mixing loss due to the flow straightening effect of the second nozzle.

2.3. A comparison of the first and second stage nozzles

Figure 7.9 illustrates that, adjacent to the endwall and hub, the total pressure loss in the boundary regions is significantly lower for the second nozzle which is a similar result to Dossena et al (1993). It is interesting, though, to note that the second nozzle has a higher total pressure loss from 25-80% span. The overall reduction of the total pressure coefficient illustrates the importance of the high energy fluid due to tip clearance and confirms that the reduction of the secondary flow at the tip and hub may well be responsible for the apparent improvement in the second stage nozzle efficiency. It must also be added that this improvement in secondary flow loss occurs in spite of the additional entropy generation expected

due to the rotor-stator wake interaction and the time varying flow as well as the increased viscous shearing expected from the leakage flow.

As an additional aid to evaluating the performance of the second nozzle, the flow relative to a second rotor is considered. Figure 7.10 shows the absolute flow outlet angle for the first and second stage nozzle compared to the design condition. The first stage nozzle shows the expected deviations due to over and underturning at the tip and hub caused by the secondary flow effects. The second stage nozzle does not indicate overturning at either the tip or hub, due to the fact that the secondary flow at the hub is potentially retarded for the reasons mentioned previously. The slight overturning in the region 60-80% span is due to suction corner vortex and the induced counter-rotating vortex at 55% span as mentioned previously.

A slight compressibility effect can be seen in Figure 7.11 where the velocity coefficient at the second nozzle outlet is about 5% greater than that of the first nozzle. The relative outlet angle from each nozzle is compared in Figure 7.12 where it can be seen that the second nozzle will also reduce the incidence angle of a hypothetical second rotor. Additionally, in the region from 5-15% span from the tip, the incidence is approximately 5 degrees better which theoretically will reduce incidence loss.

The question of mixing losses has not been addressed in this investigation. Figure 7.13 indicates the axial velocity at inlet and outlet to the first nozzle and a significant increase can be observed at the outlet from the first nozzle from 5-25% span which relates to the underturning of the secondary flow near the tip. In the case of the first nozzle, given the uniform outlet flow, the mixing loss based on the conservation of momentum could be expected to be reasonably small.

Also in Figure 7.13, however, the variation of axial velocity at the inlet and outlet of the second stage nozzle is observed to be considerably greater than that for the first stage nozzle. At inlet, the variation in axial velocity is due to the effect of the high velocity leakage flow annulus near the endwall and the relative flow effects within the rotor. The variation at outlet is caused by the flow straightening effect of the second nozzle and the over and underturning of the vortex structures. It can be expected that in the event of almost complete mixing of the axial velocity variations, considerably more mixing losses would be incurred for the second stage nozzle. It was seen, however, that the mixing process was far from complete, even at the outlet from the second nozzle and illustrates the importance of a mixing model that can accurately predict the amount of mixing at a particular distance. If the second stage rotor is located as close as possible to the preceding nozzle, it is also conceivable that, with the lower incidence expected, slightly more work could be extracted from the second stage rotor due to a moderately improved efficiency.

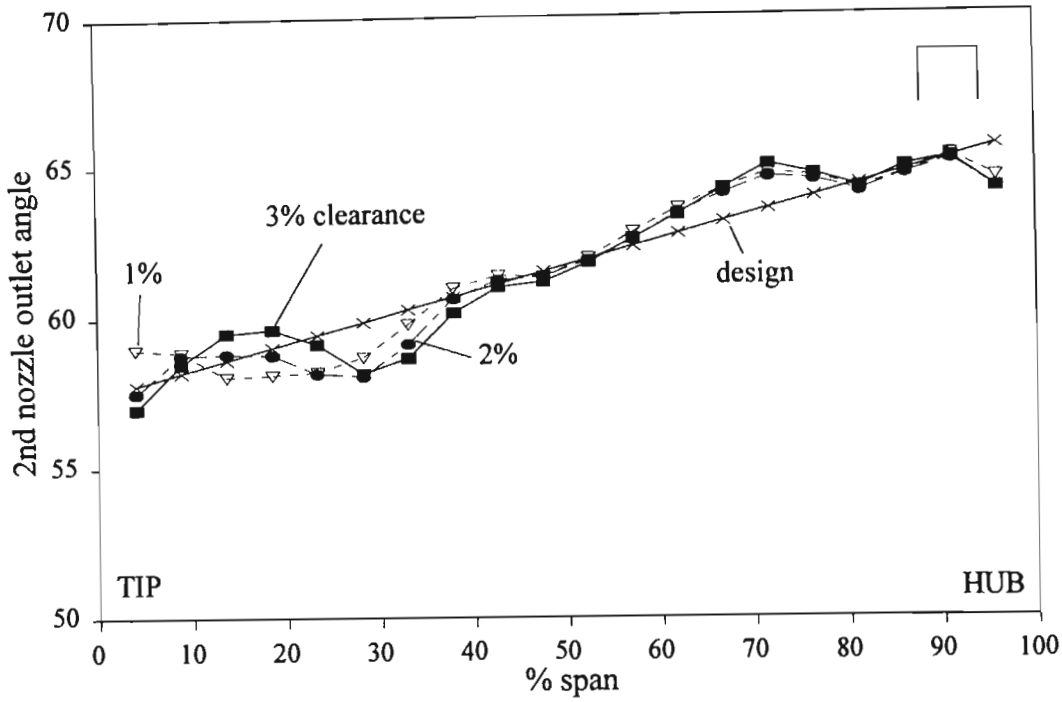

Figure 7.1 The radial variation of the tangentially averaged 2nd nozzle outlet angle for the flat tip rotor with varying tip clearance.

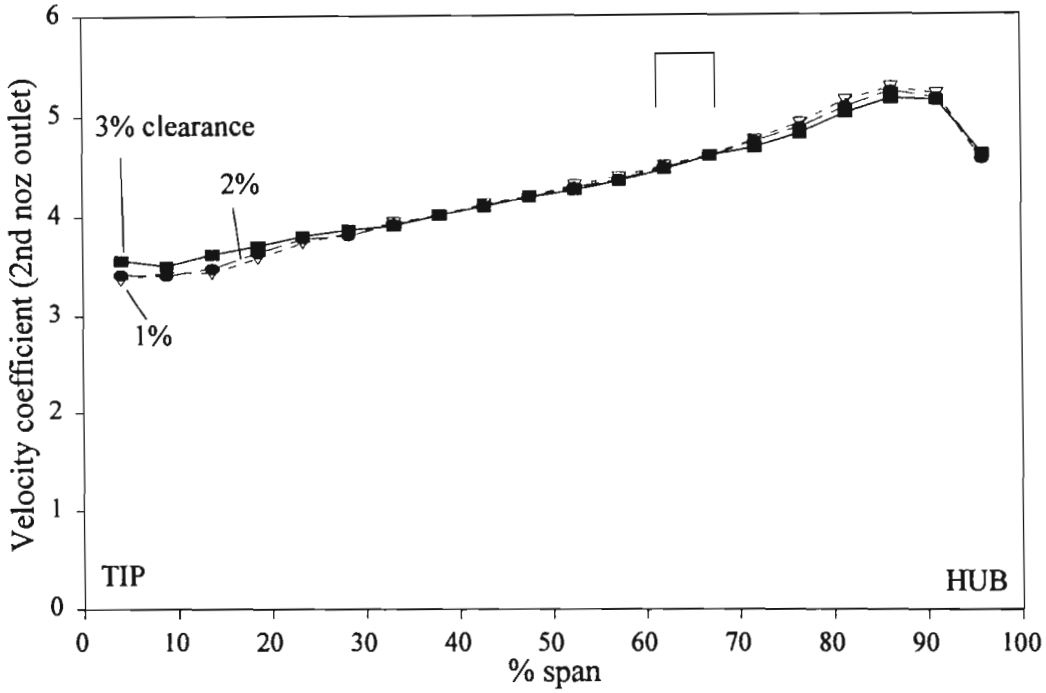

Figure 7.2 The radial variation of the tangentially averaged velocity coefficient at the 2nd nozzle outlet for the flat tip rotor with varying tip clearance.

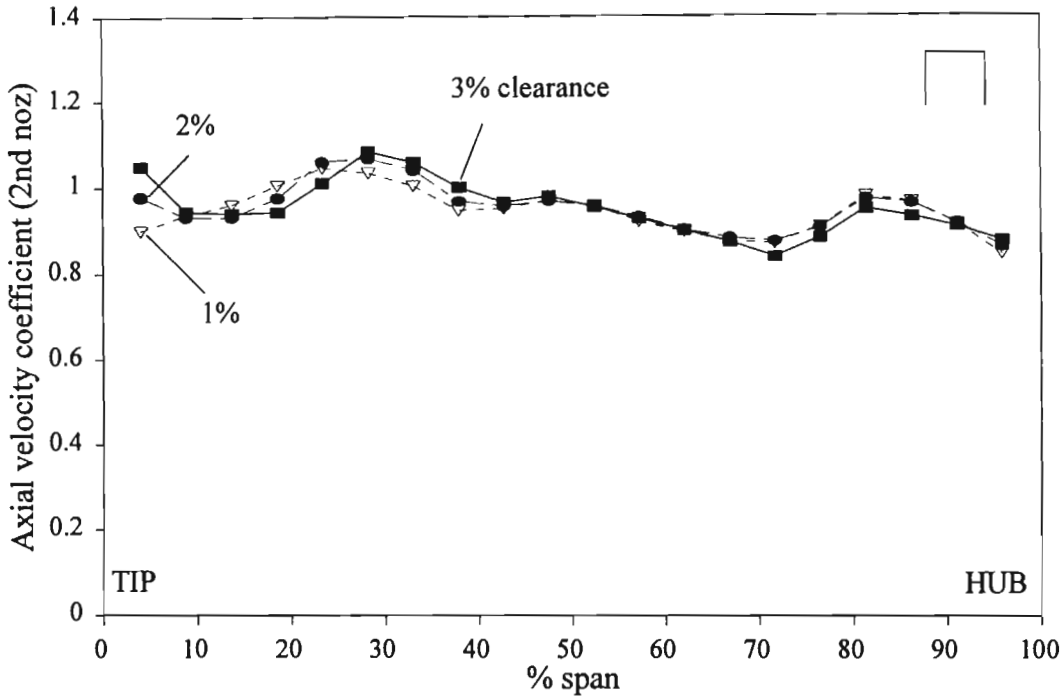

Figure 7.3 The radial variation of the tangentially averaged axial velocity coefficient at the 2nd nozzle outlet for the flat tip rotor with varying clearance.

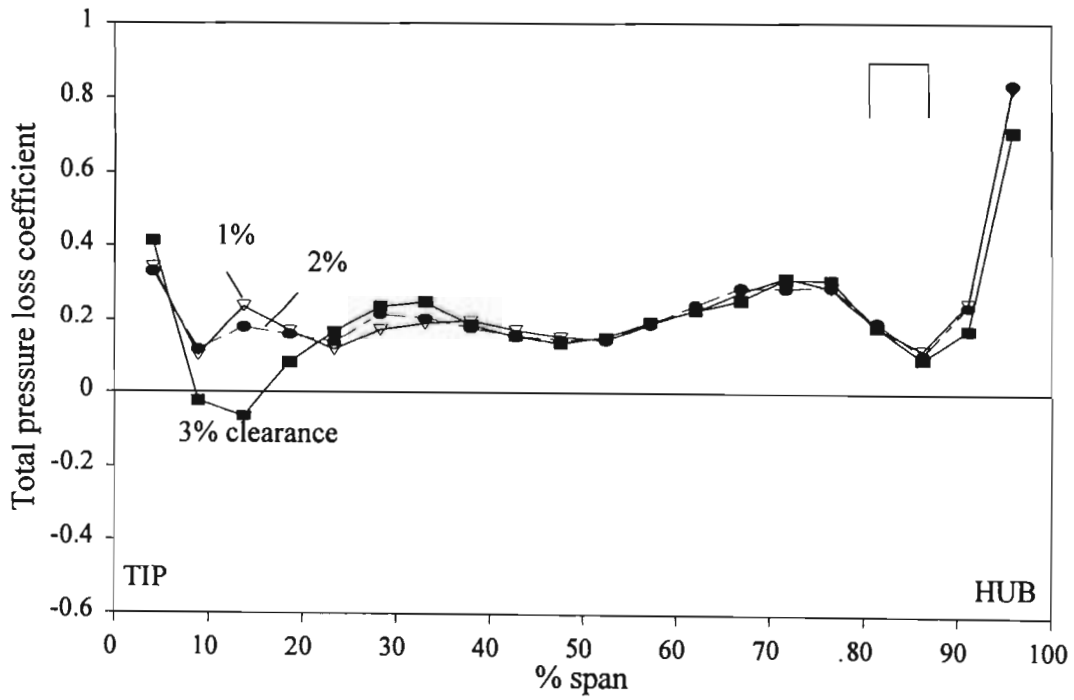

Figure 7.4 The radial variation of the tangentially averaged total pressure loss coefficient developed across the 2nd nozzle for the flat tip rotor with varying tip clearance.

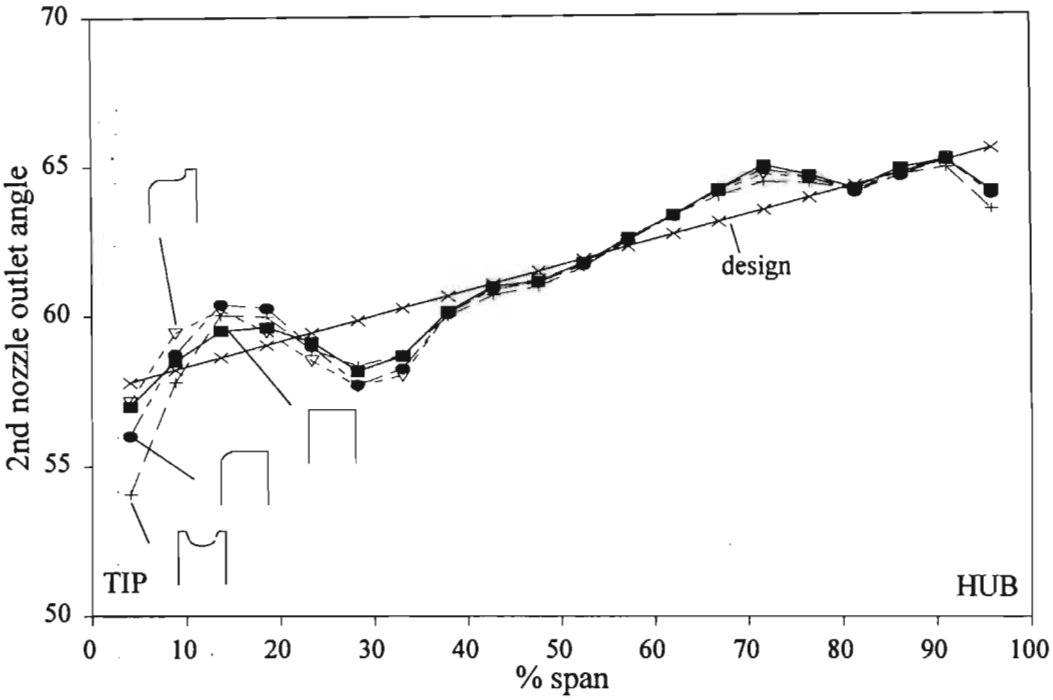

Figure 7.5 The radial variation of the tangentially averaged 2nd nozzle outlet angle for various tip shapes at 3% clearance.

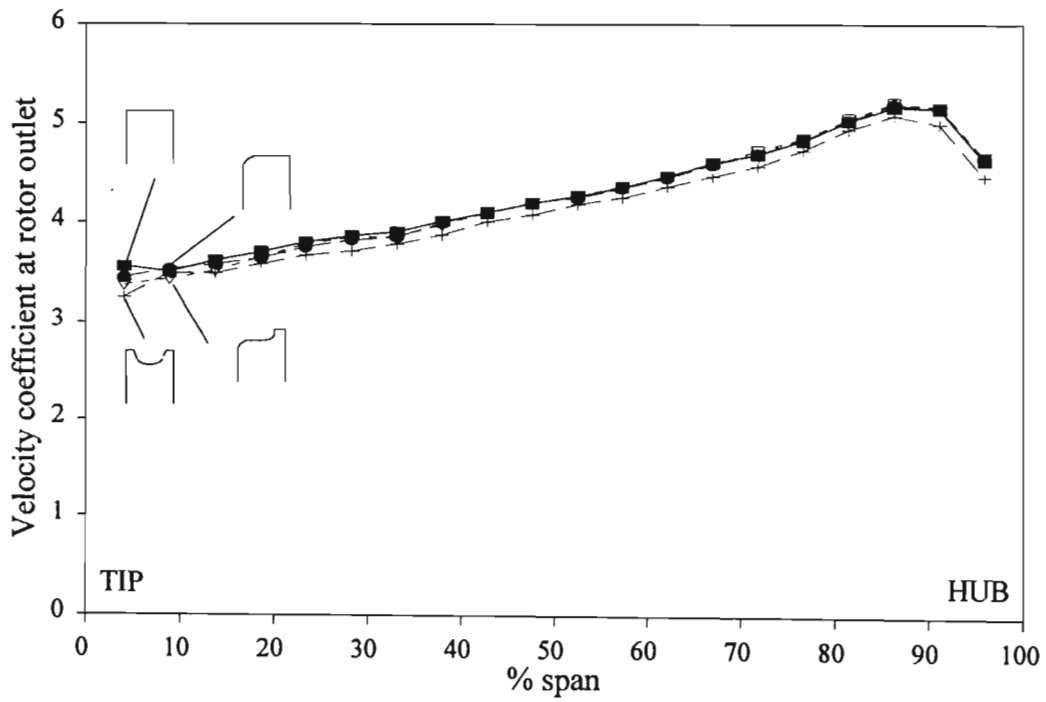

Figure 7.6 The radial variation of the tangentially averaged velocity coefficient at the 2nd nozzle outlet for various tip shapes at 3% clearance.

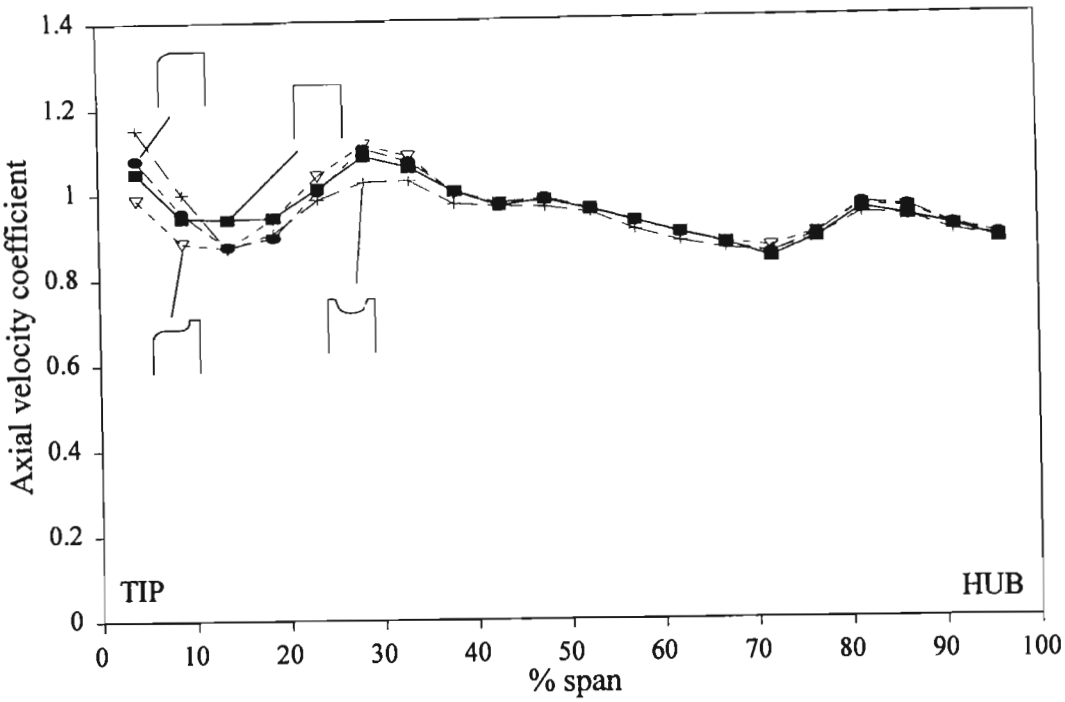

Figure 7.7 The radial variation of the tangentially averaged axial velocity coefficient at the 2nd nozzle outlet for various tip shapes at 3% clearance.

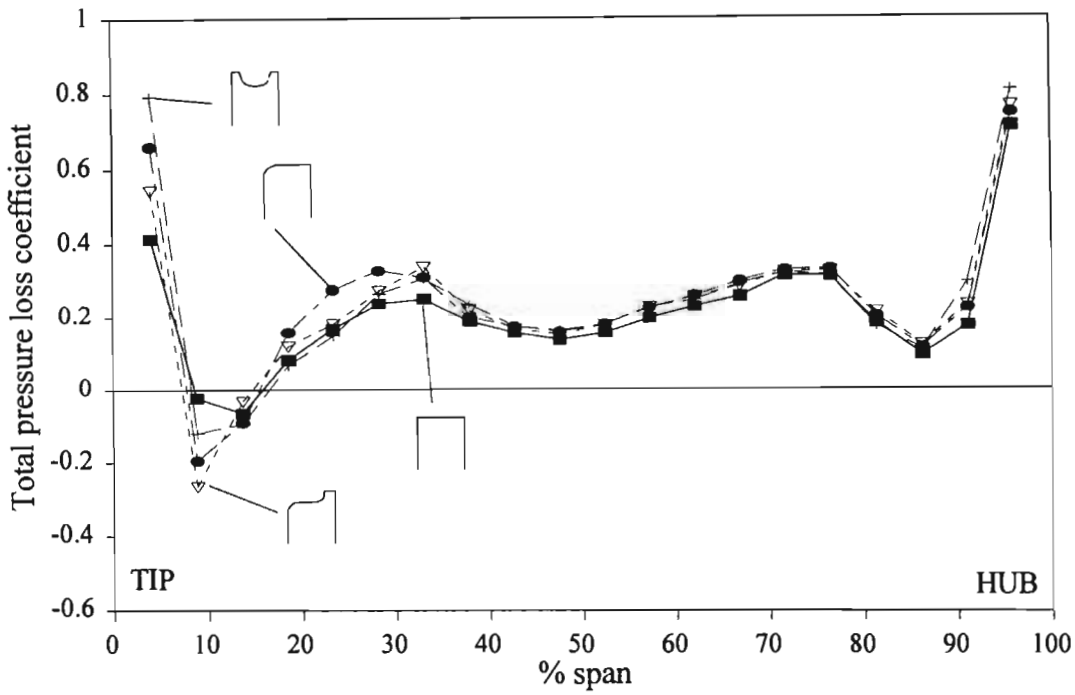

Figure 7.8 The radial variation of the tangentially averaged total pressure loss coefficient developed across the 2nd nozzle for various tip shapes at 3% clearance.

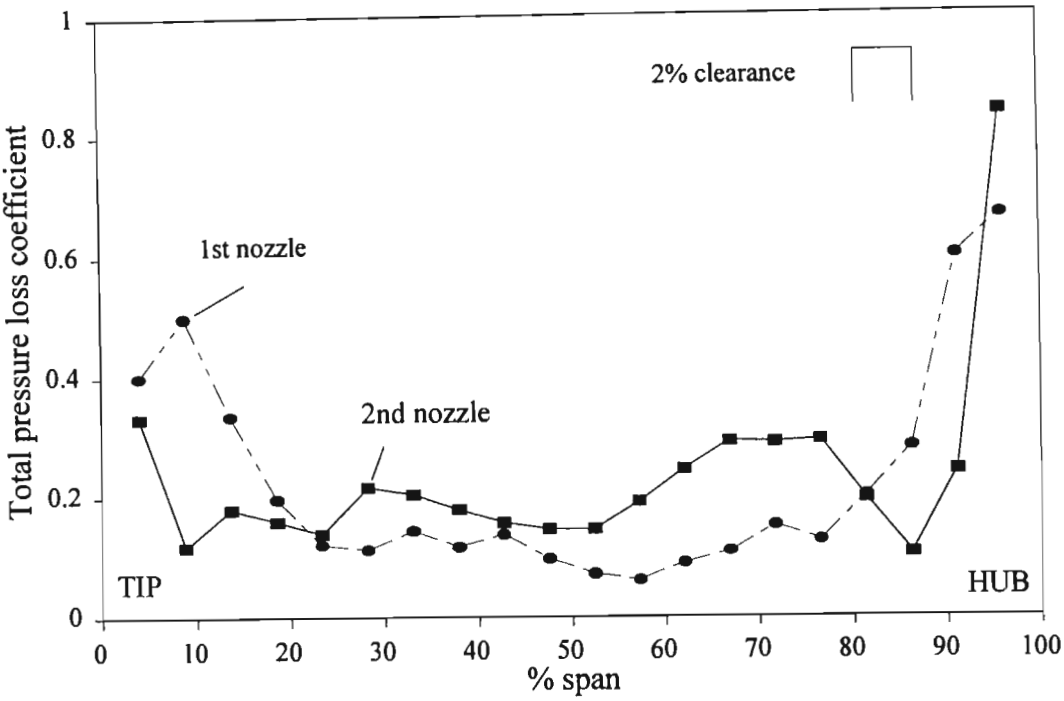

Figure 7.9 A comparison of the radial variation of the tangentially averaged total pressure loss coefficient developed across the 1st and 2nd nozzles for the flat tip rotor at 2% clearance.

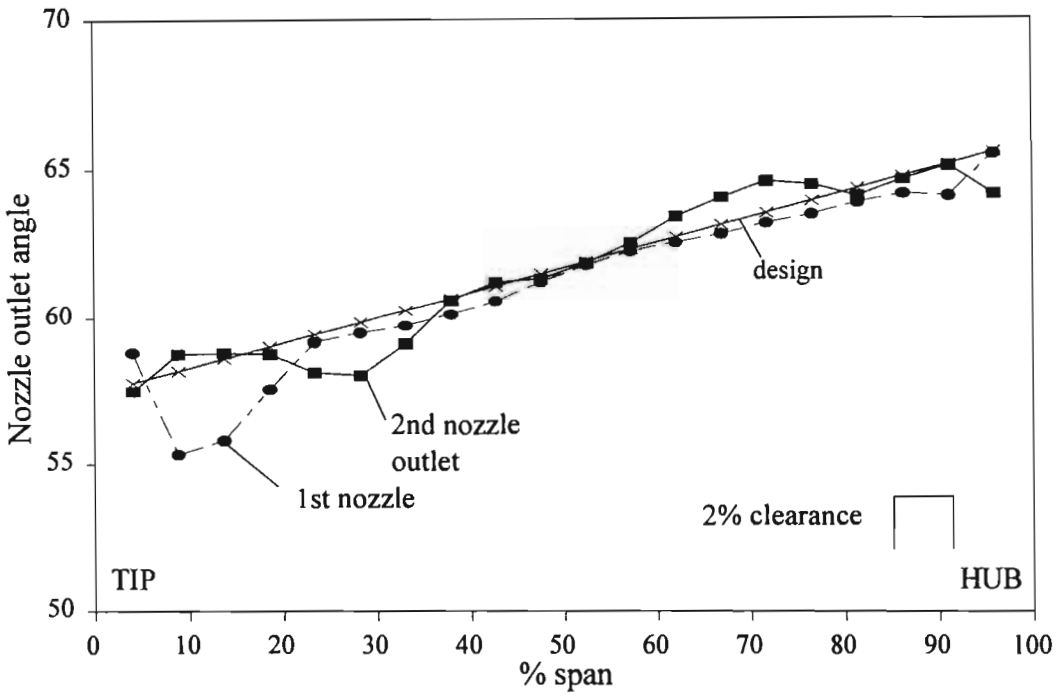

Figure 7.10 A comparison of the tangentially averaged outlet angle of the 1st and 2nd nozzles for the flat tip rotor at 2% clearance.

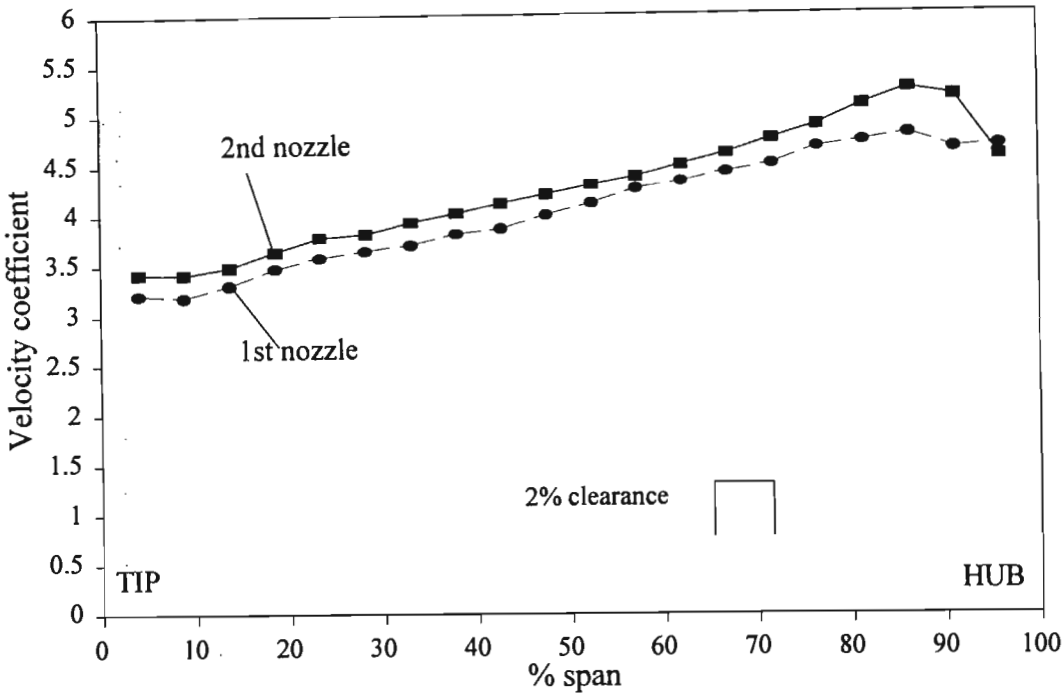

Figure 7.11 A comparison of the tangentially averaged velocity coefficient at the outlet of the 1st and 2nd nozzles for the flat tip rotor at 2% clearance.

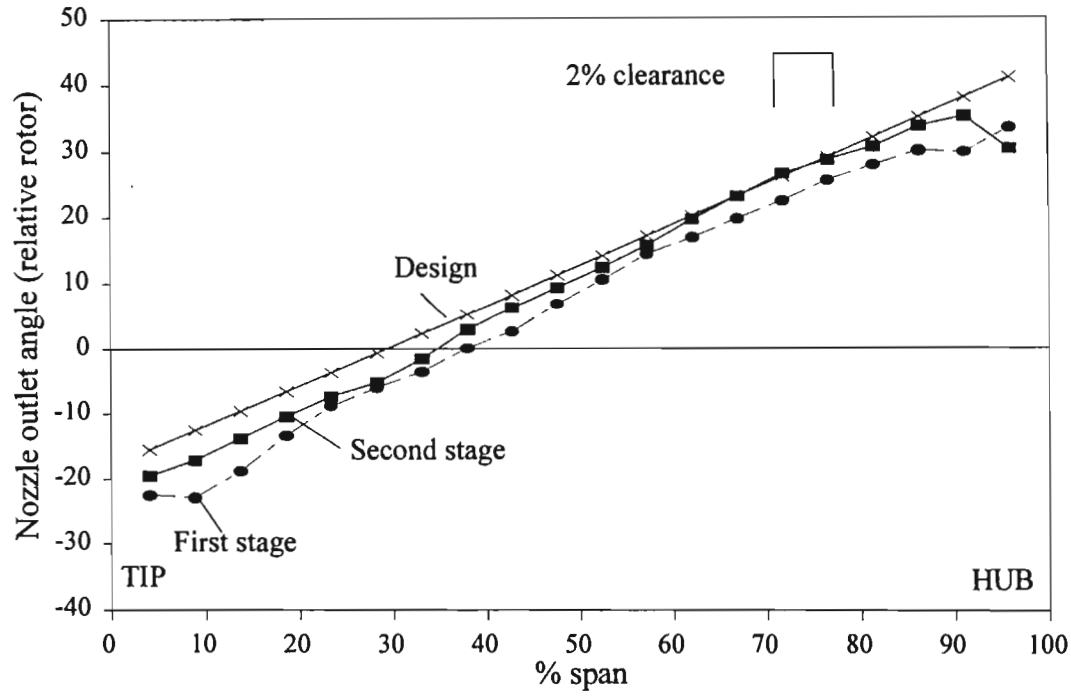

Figure 7.12 A comparison of the tangentially averaged outlet angle of the 1st and 2nd nozzles relative a subsequent rotor for the flat tip rotor at 2% clearance.

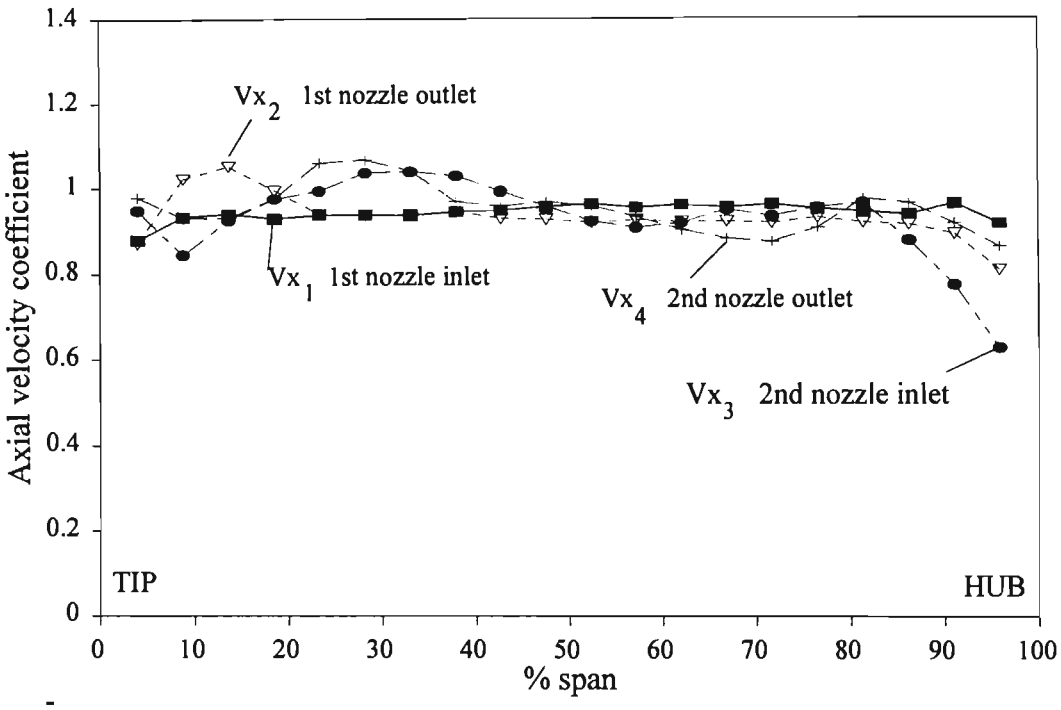

Figure 7.13 A comparison of the tangentially averaged axial velocity coefficients at the inlet and outlet of the 1st and 2nd nozzles for the flat tip rotor at 2% clearance.

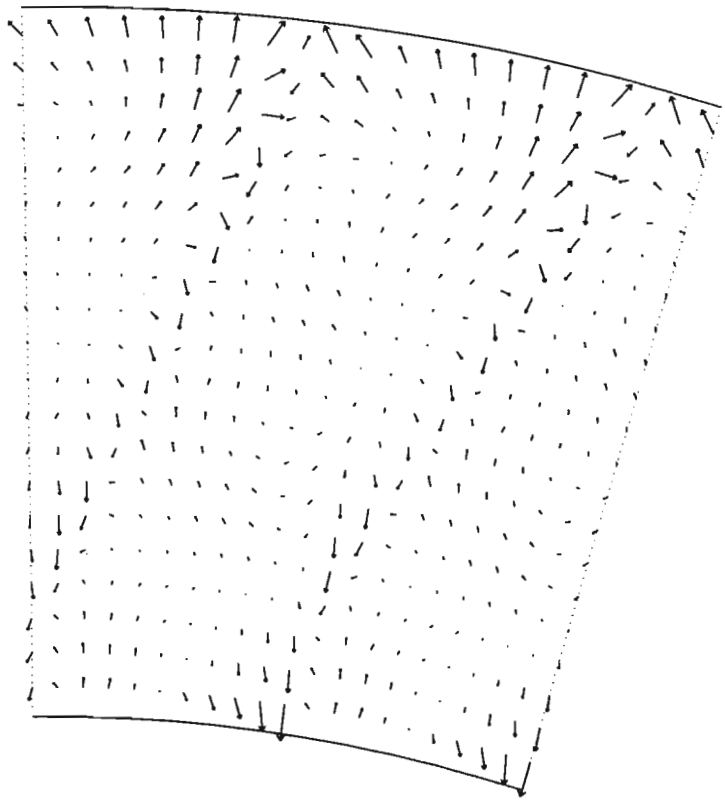

Figure 7.14 The secondary flow vectors at the outlet from the second nozzle for the flat tip rotor at 1% clearance.

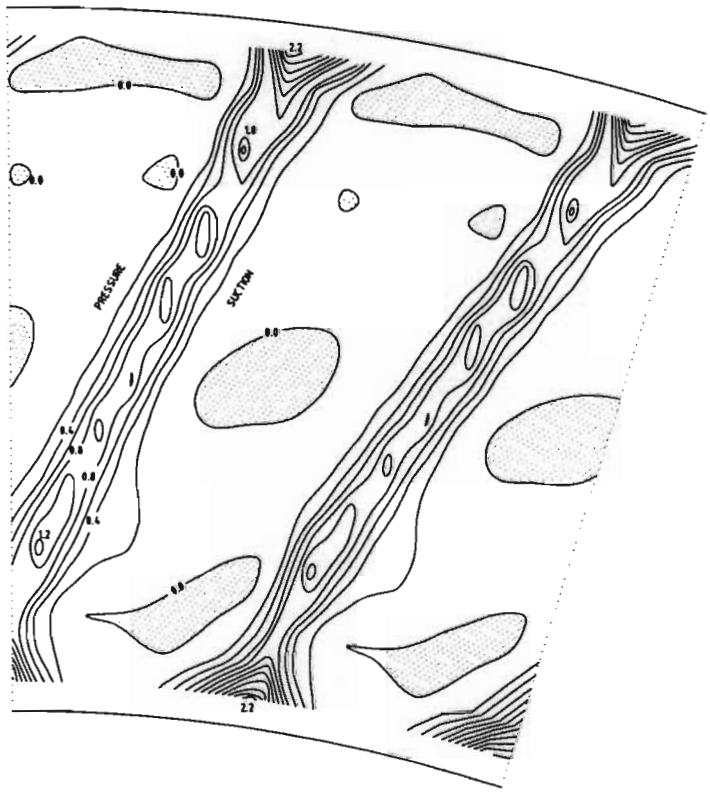

Figure 7.15 Total pressure loss contours at the outlet from the second nozzle for the flat tip rotor at 1% clearance.

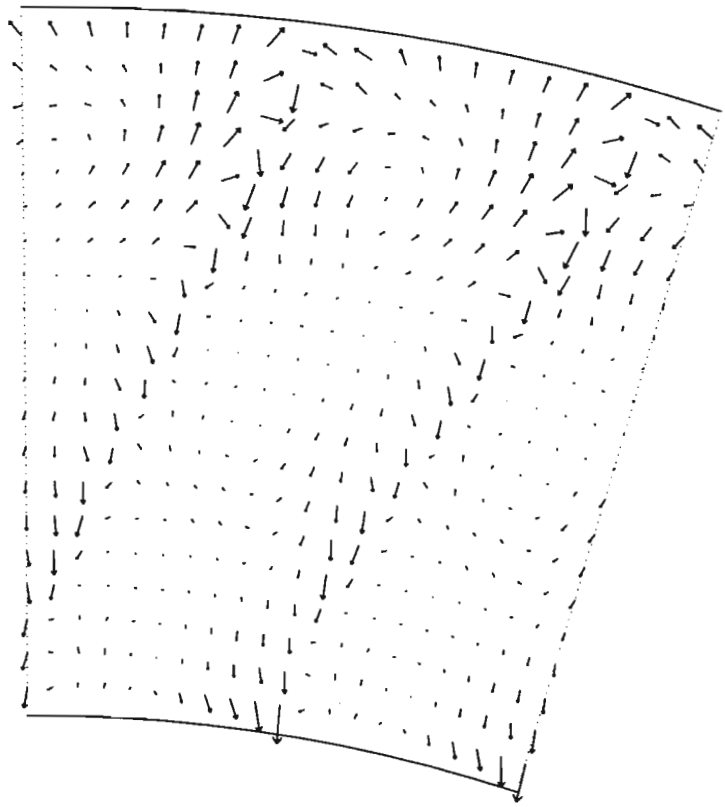

Figure 7.16 The secondary flow vectors at the outlet from the second nozzle for the flat tip rotor at 2% clearance.

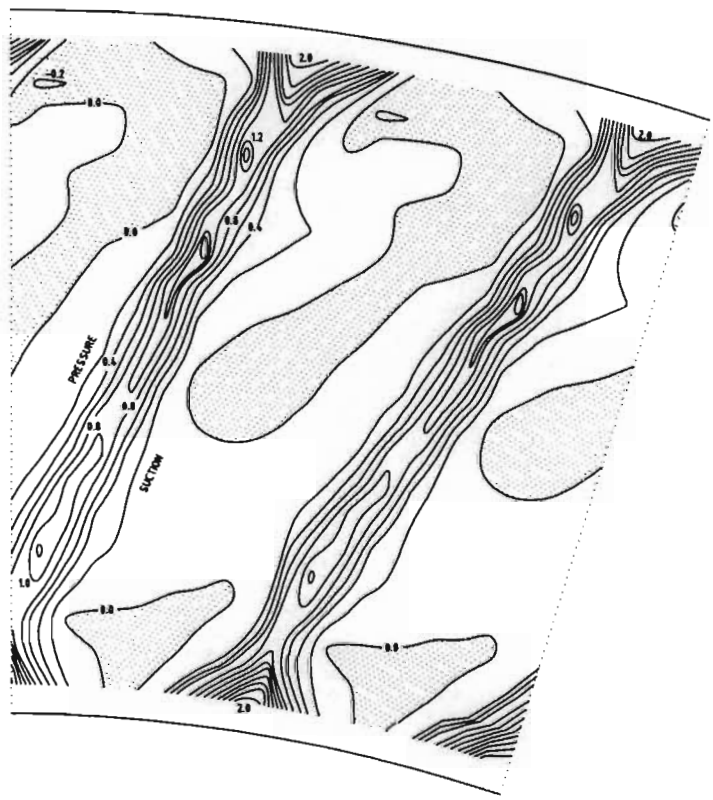

Figure 7.17 Total pressure loss contours at the outlet from the second nozzle for the flat tip rotor at 2% clearance.

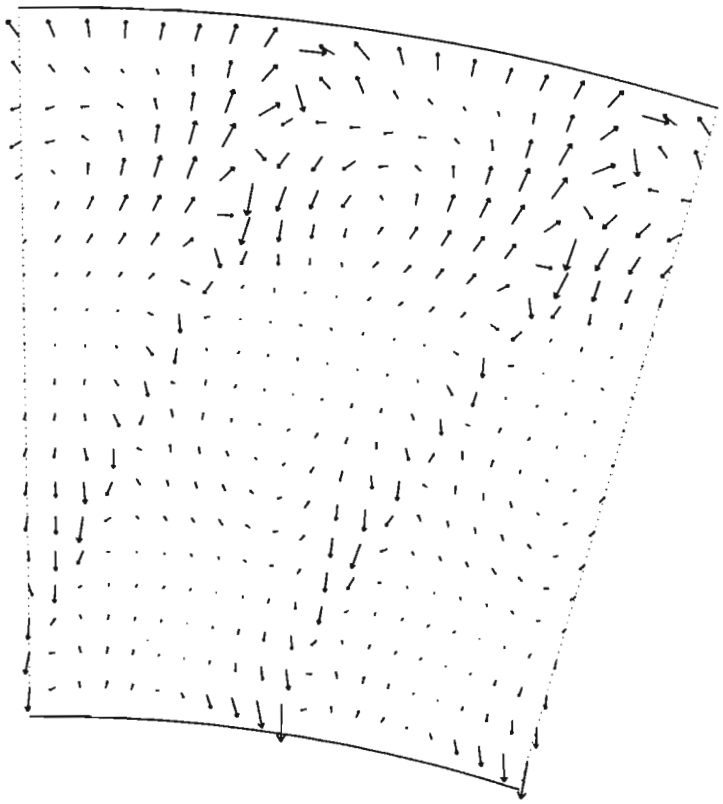

Figure 7.18 The secondary flow vectors at the outlet from the second nozzle for the flat tip rotor at 3% clearance.

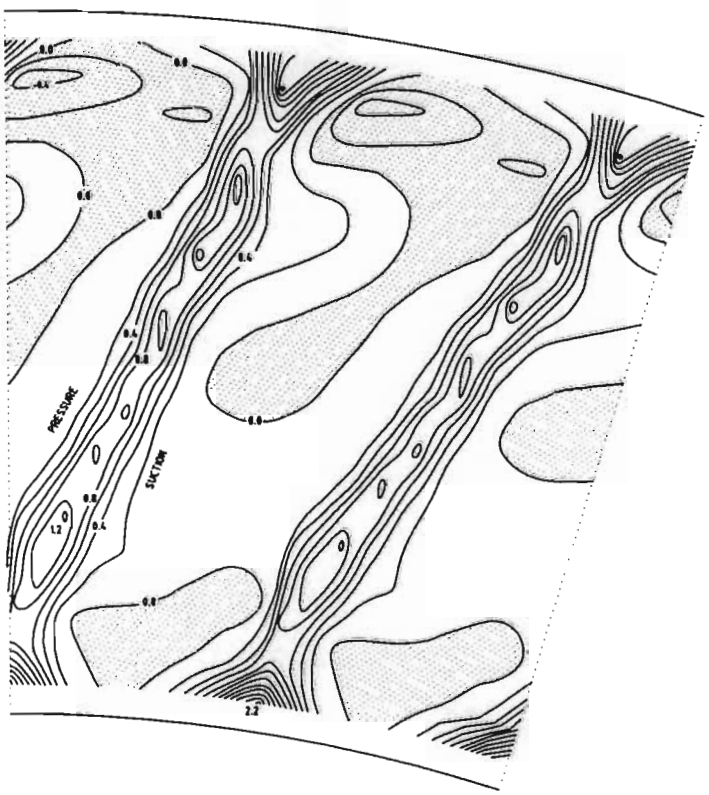

Figure 7.19 Total pressure loss contours at the outlet from the second nozzle for the flat tip rotor at 3% clearance.

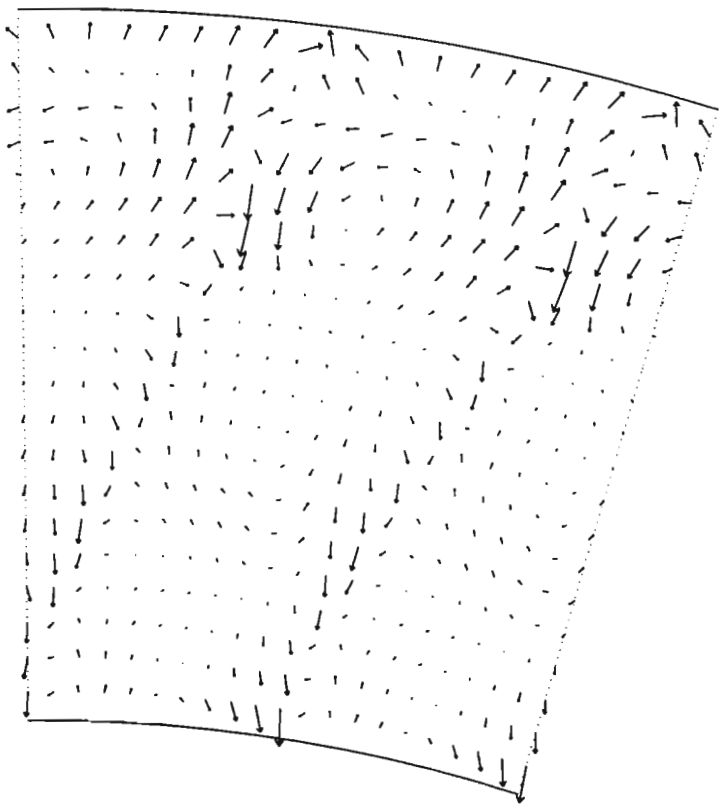

Figure 7.20 The secondary flow vectors at the outlet from the second nozzle for the radiused tip rotor at 3% clearance.

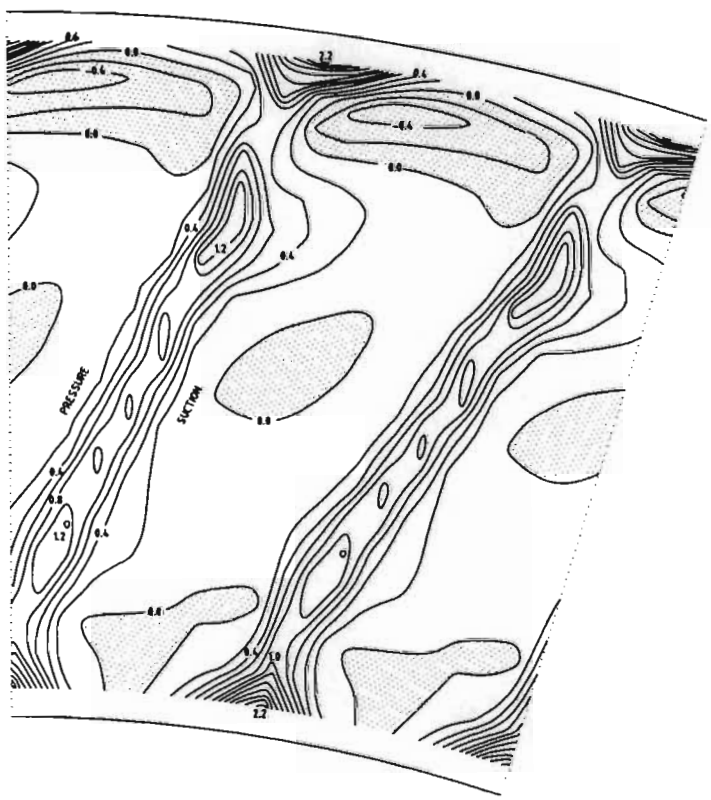

Figure 7.21 Total pressure loss contours at the outlet from the second nozzle for the radiused tip rotor at 3% clearance.

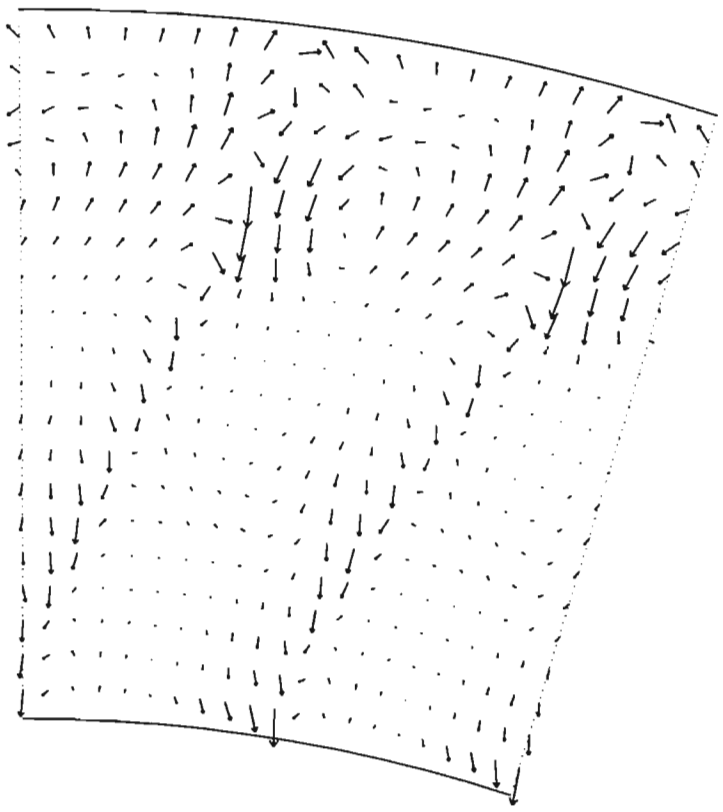

Figure 7.22 The secondary flow vectors at the outlet from the second nozzle for the squealer tip rotor at 3% clearance.

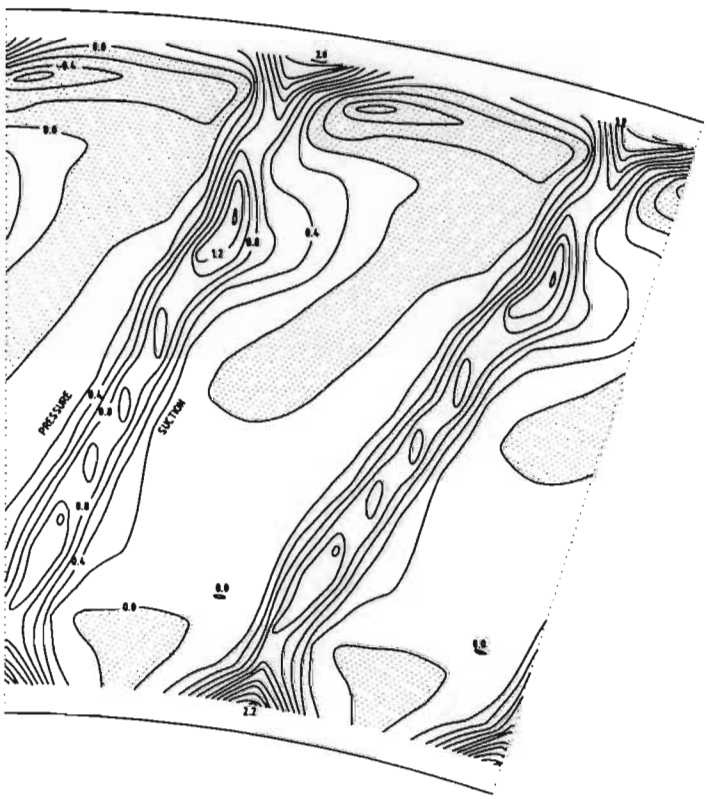

Figure 7.23 Total pressure loss contours at the outlet from the second nozzle for the squealer tip rotor at 3% clearance.

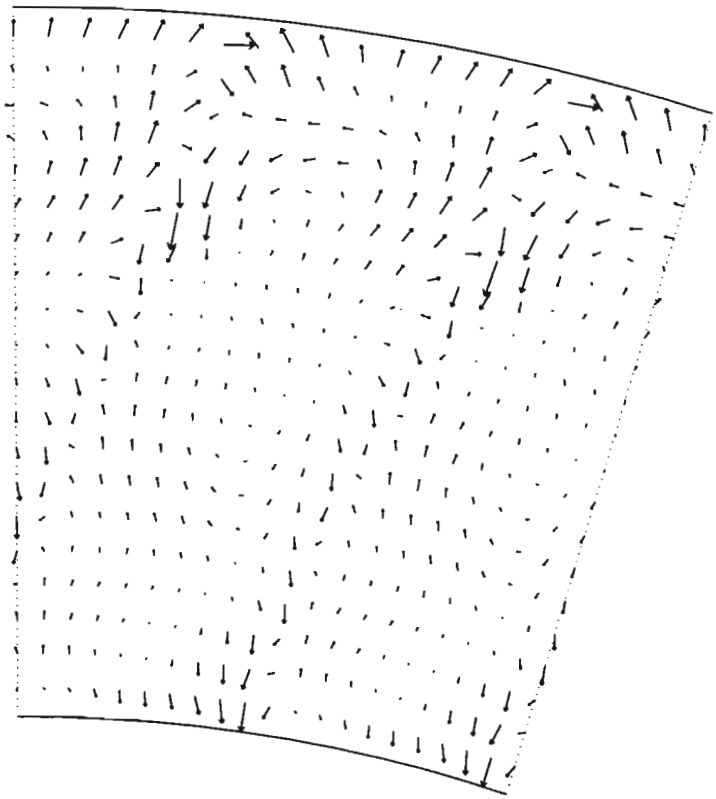

Figure 7.24 The secondary flow vectors at the outlet from the second nozzle for the double squealer tip rotor at 3% clearance.

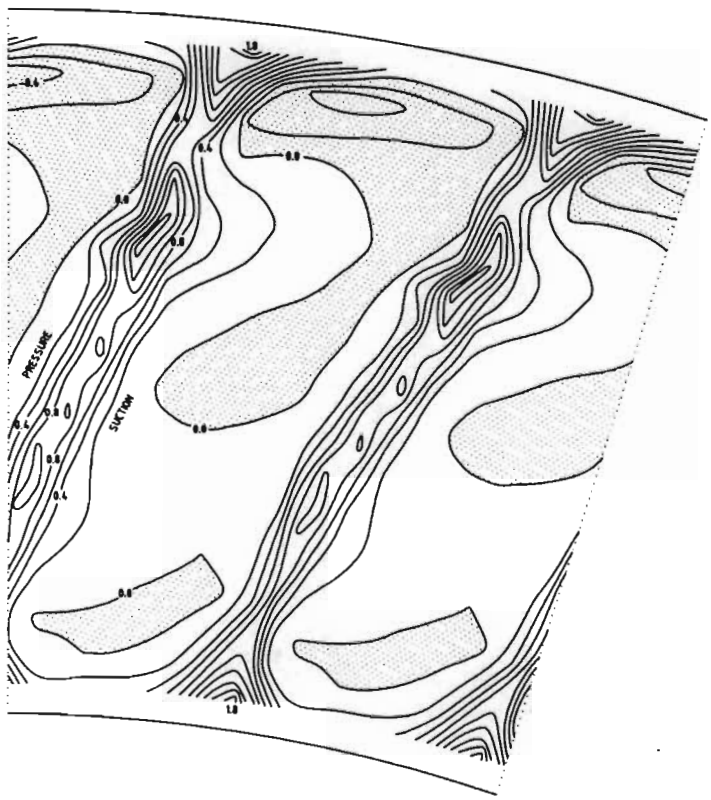

Figure 7.25 Total pressure loss contours at the outlet from the second nozzle for the double squealer tip rotor at 3% clearance.

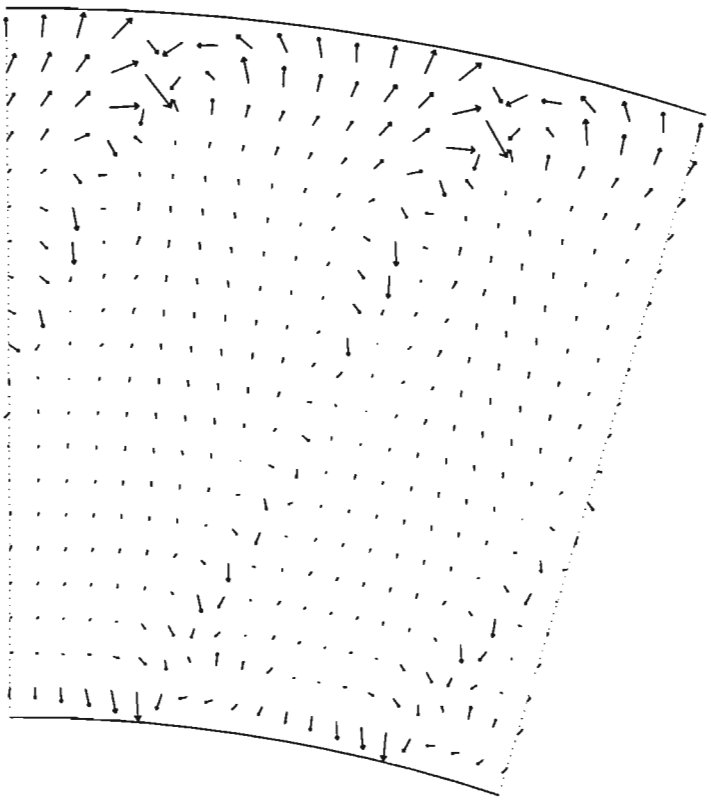

Figure 7.26 The secondary flow vectors at the outlet from the 1st nozzle.

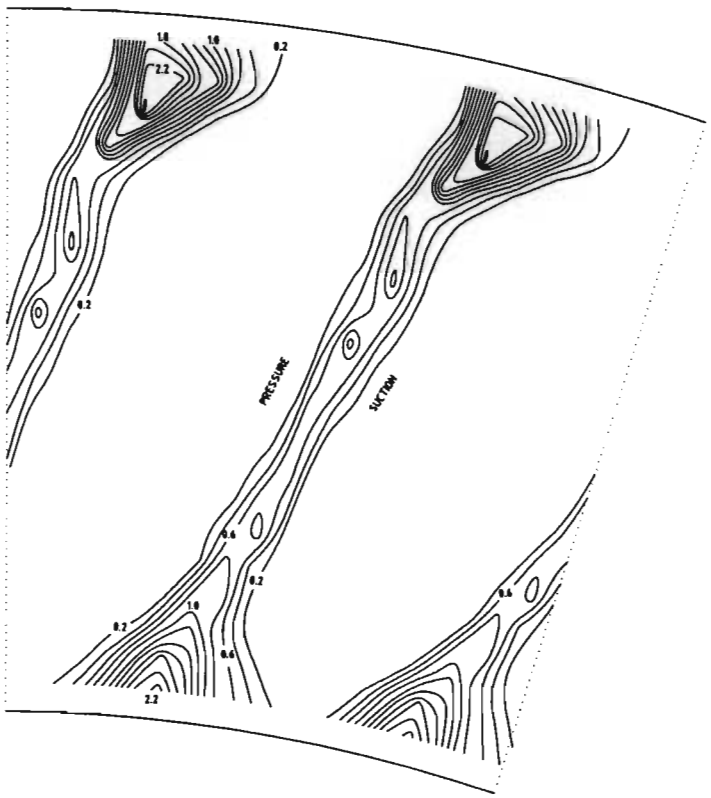

Figure 7.27 Total pressure loss contours at the outlet from the 1st nozzle.

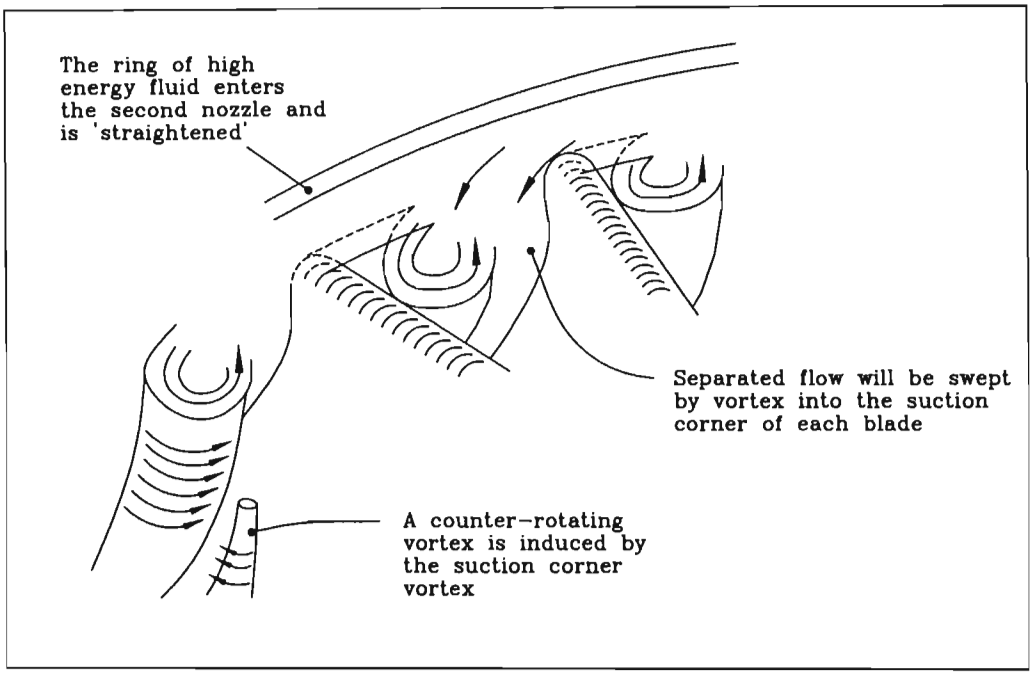

Figure 7.28 A proposed model of the mechanism by which the second nozzle 'straightens' the leakage flow leading to the observed vortex structure in the tip suction corner and the counter-rotating vortex near mid span.

CHAPTER 8

CONCLUSIONS

The previous uncertainty in the measured results was significantly improved and it is believed that the present results are a true reflection of the trends observed. The reliability of the second nozzle efficiency was expected to be better than ±0.36% and other quantities are of the order of 0.25% of the nominal values.

Considering the overall performance of the 1.5 stage turbine, the flat tip shape performed slightly better than a radiused tip, suction squealer and double squealer tip. This was found to be due to a combination of increased leakage flow deflection as well as a reduction in the leakage flow rate. The radiused tip had a slight advantage over the suction squealer due to an increased leakage flow deflection even though the leakage flow rate was seen to be moderately greater. The double squealer tip was shown to perform the worst due to a slightly higher leakage flow rate with poorer deflection and possibly greater internal gap loss.

The single stage total-to-total and total-to-static efficiencies suggest that the radiused tip may not significantly lower the machine performance compared to the flat tip. The 1.5 stage efficiency, however, showed that the extra mixing loss generated within the second nozzle will result in a slightly better performance by the flat tip. The squealer tip was seen to produce the greatest amount of mixing in the second nozzle because of a higher leakage swirl velocity confirming that, besides the leakage flow rate, the deflection of the leakage fluid must be considered in an evaluation of a tip geometry.

Due to the comparable behaviour of the radiused tip and the flat tip for both the single and 1.5 stage performance, it may be feasible to consider the former in a cooled stage given that the peak velocity on the pressure corner is reduced and the separation bubble eliminated which may decrease the heat transfer coefficient on the tip surface.

It was seen that if the leakage flow was allowed to mix out downstream of the rotor, the low entropy tip shapes may perform better than the flat tip. This was possibly due to a lower pressure loss associated with the low entropy tips and suggests that consideration of the internal gap entropy generation is important. This result is also important for the last stage of a multistage machine where additional losses will be formed by the complete mixing of the leakage flow whereas in a jet engine, slightly lower mixing may occur at the engine outlet with a low entropy tip.

The second nozzle was confirmed to operate somewhat more efficiently than the first stage nozzle, probably due to the reduction of secondary flow at the tip and hub. The high energy ring of fluid close to the endwall was seen to be 'straightened' by the nozzle blades and energised the passage flow by the radial transport of high energy fluid in a vortex structure which persists through to the outlet of the second nozzle. Within both nozzles, low momentum fluid was seen to be transported radially from tip to hub in the blade wakes due to the radial pressure gradient and regions of low and high axial velocity corresponded to regions of over and underturning respectively.

The efficiency of the second nozzle was a maximum for the lowest clearance, confirming that additional mixing losses offset the secondary flow loss reduction gains. The flow from the second nozzle showed that a hypothetical second rotor

would actually experience less inlet incidence than the first. The vortices present in the outlet flow seemingly have little effect on a second rotor and suggest that a portion of the leakage flow persisting at the second nozzle outlet may be converted to work.

The specific loss formation on the suction side of the blade wakes as reported by other researchers was found to be caused by the sweeping effect that the high velocity leakage flow has on the endwall and suction surface of the nozzle blades and the subsequent accumulation of low momentum fluid on the blade suction surface.

Tip clearance was confirmed to cause a mass flow deficit from about 25% span up to the hub which lowers the work extraction. This occurs in addition to the increased leakage flow rate that undergoes poor deflection. A minimum axial velocity was evident at approximately 10% chord and is believed to be an indication of the presence of the overturned flow in the passage vortex when viewed in the conjunction with the linear cascade results. This deficit was also seen to act as a flow blockage.

In general, the trends in the results from the turbine agreed fairly well with linear cascade work although the effect of relative motion was seen to be an important factor in determining the leakage flow rate as well as the outlet angle of the fluid near the endwall. Also, in a rotating machine, the leakage flow has relatively high kinetic energy and this will not be correctly modelled in a linear cascade which will show the leakage fluid as having a total pressure either equal to or less than that at the inlet to the cascade. Linear cascade results may be useful as an indication of the mechanism of tip clearance but fail to model some important features such as relative motion and the radial pressure gradient.

REFERENCES

Ainley D G & Mathieson G C R "An examination of the flow and pressure losses in blade rows of axial-flow turbines"Communicated by the Principal Director of Scientific Research (Air) Ministry of Supply, Reports and Memoranda No. 2891, March, 1951

Basson A H (1993) "Numerical simulation of steady three-dimensional flows in axial turbomachinery bladerows" PhD Thesis, The Pennsylvania State University, The Graduate School, Department of Aerospace Engineering, December, 1992

Biesenger T E & Gregory-Smith D G (1993) "Reduction in secondary flows and losses in a turbine cascade by upstream boundary layer blowing" ASME Paper number 93-GT-114, Presented at the International Gas Turbine and Aeroengine Congress and Exposition, Cincinatti, Ohio, May 24-27, 1993

Bindon J P (1979) "The effect of hub inlet boundary layer skewing on the endwall shear flow in an annular turbine cascade", ASME International Gas Turbine Conference, San Diego, March 1979, Paper 79-GT-13

Bindon J P (1980) "Exit plane and suction surface flows in an annular turbine cascade with a skewed inlet boundary layer" International Journal of Heat and Fluid flow, Vol 2, No2, 1980, pages 57-66

Bindon J P (1986a) "Pressure and flow field measurements of axial turbine tip clearance flow in a linear cascade" Report number CUED/A-Turbo TR 123, Whittle Laboratory, Cambridge University, 1986.

Bindon J P (1986b) "Visualisation of axial turbine tip clearance flow using a linear cascade" Report number CUED/A-Turbo TR 123, Whittle Laboratory, Cambridge University, 1986.

Bindon J P (1987a) "Pressure distributions in the tip clearance region of an unshrouded axial turbine as affecting the problem of tip burnout" ASME paper number 87-GT-230, Presented at the IGTi Conference and Exposition, Anaheim, California , May 31-June 4, 1987.

Bindon J P (1987b) "Visualisation of axial turbine tip clearance flow using a linear cascade" Published by the American Institute of Aeronautics and Astronautics, ISABE 87-7032, 1987.

Bindon J P (1987c) "The measurement of tip clearance flow structure on the end-wall and within the clearance gap of an axialturbine cascade" Proceedings of the ImechE International Conference on Turbomachinery Efficiency, Prediction and Improvement, Cambridge, September 1987, No C273/87, Pages 43-52

Bindon J P (1988) "The measurement and formation of tip clearance loss" ASME paper number 88-GT-203, Presented at the Gas Turbine and Aeroengine Congress and Exposition, Amsterdam, The Netherlands, June 5-9, 1988

Bindon J P & Morphis G (1990) "The development of axial turbine leakage loss for two profiled tip geometries using linear cascade data" ASME Paper number 90-GT-152, Presented at the Gas Turbine and Aeroengine Congress and Exposition, Brussels, Belgium, June 11-14, 1990

Bindon (1994) - Private correspondence

Boletis E & Sieverding C H (1991) "Experimental study of the three dimensional flow field in a turbine stator preceeded by a full stage" Journal of Turbomachinery, Vol 113, January 1991, pages 1-9

Booth T C, Dodge P R & Hepworth H K (1982) "Rotor-tip leakage : Part i - Basic methodology" Journal of Engineering for Power, Vol 104, January 1982, pages 154-161

Booth T C (1985) "Tip clearance effects in axial turbomachines, Von Karmen Institute for Fluid Dynamics, Lecture Series 1985-05, April 15-18, 1985

Chan J K K, Yaras M I & Sjolander S A (1994) "Interaction between inlet boundary layer, tip leakage and secondary flows in a low-speed turbine cascade" ASME paper number 94-GT-250, Presented at the International Gas turbine and Aeroengine Congress and Exposition, The hague, The Netherlands, June 13-16, 1994

Chen G, Dawes W N & Hodson H P "A numerical and experimental investigation of turbine tip gap flow" Paper number AIAA 93-2253, AIAA/SAE/ASME/ASEE 29th Joint Propulsion Conference and Exhibit, Monterey, CA, June 28-30, 1993

Denton J D (1993) "Loss Mechanisms in Turbomachines", Scholars' Paper, ASME Gas Turbine Congress, Cincinatti, May 1993

Dishart P T & Moore J "Tip leakage losses in a linear turbine cascade" ASME paper number 89-GT-56, Presented at the Gas Turbine and Aeroengine Congress and Exposition, Toronto, Ontario, Canada, 1989

Dossena V, Perdichizzi A, Ubaldi M & Zunino P (1993) "Turbulence measurements downstream of a turbine cascade at different incidence angles and pitch-chord ratios" ASME Paper number 93-GT-52, Presented at the International Gas Turbine and Aeroengine Congress and Exposition, Cincinatti, Ohio, May 24-27, 1993

Gearhart W S (1964) "Tip clearance flow in turbomachines" The Pennsylvania State University Science and Engineering Ordnance Research Lab, Technical memorandum, File number TM 506.2491-04, August 27, 1964.

Graham J A H (1986) "Investigation of a tip clearance cascade in a water analogy rig" Journal of Engineering for Gas Turbines and Power, Vol 108, January, 1986, pages 38-46

Gregory-Smith D G (1982) "Secondary flows and losses in axial flow turbines" Journal of Engineering for Power, Vol 104, October 1982, pages 819-822

Heyes F G J, Hodson H P & Dailey G M (1991) " The effect of blade tip clearance on the tip leakage flow in axial turbine cascades" ASME Paper number 91-GT-135, Presented at the IGTI Conference and Exposition, Orlando, Florida, June 3-6, 1991

Heyes F G J & Hodson H P (1992) "The measurement and prediction of the tip clearance flow in linear turbine cascades" Asme paper number 92-GT-214, Presented at the IGTI Congress and Exposition, Cologne, Germany, June 1-4, 1992

Holman J P (1985) "Experimental methods for engineers" MCGraw-Hill International Student Edition, Fourth Edition, 3rd printing, 1985

Hunter I H (1982) "Endwall boundary layer flows and losses in an axial turbine stage" journal of Engineering for Power, Vol 104, January 1982, pages 184-193

Joslyn D & Dring R (1990) "Three dimensional flow in an axial turbine", ASME Paper number 90-GT-56, Presented at the Gas Turbine and Aeroengine Congress and Exposition, Brussels, Belgium, June 11-14, 1990

Kaiser I (1992) "Tip clearance gap flow measurements in an annular cascade with a rotating endwall" Masters Thesis, University of Natal, Durban, South Africa, 1992

Kingcombe R C, Smith I M & Steeden R V (1990) ASME Paper Number 90-GT-312, Presented at the Gas Turbine and Aeroengine Congress, Brussels, Belgium, June 11-14, 1990

Mayle R E & Metzger D E (1982) "Heat transfer at the tip of an unshrouded turbine blade" Proceedings of the 7th International Heat Transfer Conference, Munich, March 1982, pages 87-92

Metzger D E & Bunker R S (1985) "Cavity heat transfer on a transverse grooved wall in a narrow channel" ASME Paper number 85-GT-57, Presented at the National Heat Transfer Conference, Denver, Colorado, August 4-7, 1985

Metzger D E & Rued K (1988) "The influence of turbine clearance gap leakage on passage velocity and heat transfer near blade tips Part i : Sink flow effects on blade pressure side" ASME Paper number 88-GT-98, Presented at the Gas Turbine and Aeroengine Congress and Exposition, Amsterdam, The Netherlands, June 5-9, 1988

Moore J & Tilton J S (1987) "Tip leakage flow in a linear turbine cascade" ASME paper number 87-GT-222, Presented at the IGTI Conference and Exposition, Anaheim, California, May 31-June 4, 1987

Moore J, Moore J G, Henry G S & Chaudry U (1989) "Flow and heat transfer in turbine tip gaps" Journal of Turbomachinery, Vol 111, July 1989, pages 301-309

Moore J & Elwood K E (1992) "Shock formation in overexpanded tip leakage flow" ASME Paper number 29-GT-1, Presented at the Interantional Gas Turbine and Aeroengine Congress and Exposition, Cologne, Germany, June 1-4, 1992

Morphis G & Bindon J P (1988) "The effects of relative motion, blade edge radius and gap size on the blade tip pressure distribution in an annular turbine cascade with clearance" ASME Paper number 88-GT-256, Presented at the Gas Turbine and Aeroengine Congress, Amsterdam, The Netherlands, June 6-9, 1988

Morphis G (1989) "The measurement of axial turbine tip clearance flow phenomena in a moving wall annular cascade and in a linear cascade" Masters Thesis, University of Natal, Durban, South Africa, 1989

Morphis G (1993) "The performance of a one and a half stage axial turbine including various tip effects" PhD thesis, University of Natal, Durban, South Africa, 1993

Morphis G & Bindon J P (1994a) "The performance of a low speed one and a half axial turbine with varying rotor tip clearance and tip gap geometry" ASME Paper number 94-GT-481, Presented at the International Gas Turbine and Aeroengine Congress and Exposition, The Hague, Netherlands, June 13-16, 1994

Morphis G & Bindon J P (1994b) "The flow in a second stage nozzle of a low speed axial turbine and its effect on tip clearance loss development" ASME Paper number 94-GT-145, Presented at the International Gas Turbine and Aeroengine Congress and Exposition, The Hague, Netherlands, June 13-16, 1994

Moustapha S H, Okapuu U & Williamson R G (1986) "Influence of rotor blade aerodynamic loading on the performance of a highly loaded turbine " ASME Paper number 86-GT-56, Contributed for presentation at the 31st Interantional Gas Turbine Conference and Exhibit. Düsseldorf, Federal Republic of Germany, June 8-12, 1986

Northern Research and Engineering Corporation (1972) "The Design and Performance Analysis of Axial Flow Turbines, Volume 1 & Volume 2" Software & Manuals, 219 Vassar Str, Cambridge, Massachusetts, 02139

Offenberg L S, Fischer J D & Vander Hoek T J (1987) "An experimental investigation of turbine case treatments" Paper Number AIAA-87-1919, AIAA/SAE/ASME/ASEE 23rd Joint Propulsion Conference, San Diego, California, June 29-July 2, 1987

Özişik M N (1987) "Heat transfer - A basic approach" McGraw-Hill International Edition, 2nd printing, 1987

Peacock R E (1983) "A review of turbomachinery tip gap effects - Part 2 : Rotating turbomachinery" International Journal of Heat and Fluid Flow, Vol 4, No 1 March 1983, pages 3-16

Rains D A (1954) "Tip clearance flows in axial flow compressors and pumps" California Institute of Technology, Hydrodynamics Laboratory Report No.5 1954

Sharma O P, Renaud E, Butler T L, Milsaps K (Jr), Dring R P & Joslyn H D (1988) "Rotor-stator interaction in multi-stage axial-flow turbines" AIAA/ASME/SAE/ASEE 24th Joint Propulsion Conference, Boston, Massachusetts, July 11-13, 1988

Sieverding C H, Van Hove W & Boletis E (1984) "Experimental study of the three dimensional flow field in an annular turbine nozzle guidevane" Journal of Engineering for Gas Turbines and Power, Vol 106, April 1984, pages 437-444

Storer J A & Cumpsty N A (1990) "Tip leakage flow in axial compressors" ASME Paper number 90-GT-127, Presented at the Gas Turbine and Aeroengine Congress and Exposition, Brussels, Belgium, June 11-14, 1990

Storer J A (1989) The interaction between Tip Clearance and the Passage Flow in an Axial Compressor Cascade", ISABE Paper No. 89-7024, Ninth International Symposium on Air Breathing Engines, Vol 1, Athens, Greece, September 1989

Sjolander S A & Amrud K K (1987) "Effects of tip clearance on blade loading in a planar cascade of turbine blades" ASME paper number 86-GT-245, Presented at the IGTI Conference and Exposition, Düsseldorf, Federal Republic of Germany, June 8-12, 1986.

Sjolander S A & Amrud K K (1987) "Effects of tip clearance on blade loading in a planar cascade of turbine blades" Journal of Turbomachinery, Vol 109, April 1987, pages 237-245

Sjolander S A & Cao D (1994) "Measurements of the flow in an idealised turbine tip gap" ASME Paper number 94-GT-74, Presented at the International Gas Turbine and Aeroengine Congress and Exposition, The Hague, Netherlands, June 13-16, 1994

Tremblay B, Sjolander S A & Moustapha S H (1990) "Off design performance of a linear cascade of turbine blades" ASME Paper number 90-GT-314, Presented at the Gas Turbine and Aeroengine Congress and Exposition, Brussels, Belgium, June 11-14, 1990

Wadia A R & Booth T C (1982) "Rotor-tip leakage : Part ii - Design optimization through viscous analysis and experiment" Journal of Engineering for Power, Vol 104, January 1982, pages 162-169

Walsh J A & Gregory-Smith D G (1987) "The effect of inlet skew on the secondary flow and losses in a turbine cascade" Proc. I Mech E, Int Conf-Turbomachinery Efficiency Prediction and Improvement, Cambridge, Septembrt 1987

Yaras M, Yingkang Z & Sjolander S A (1988) "Flow field in the tip gap of a planar cascade of turbine blades" ASME Paper number 88-GT-29, Presented at the Gas Turbine and Aeroengine Congress, Amsterdam, The Netherlands, June 5-9, 1988

Yaras M I & Sjolander S A (1989) "Losses in the tip-leakage flow of a planar cascade of turbine blades" Paper number 20, AGARD-CP-469, "Secondary flows in turbomachinery", Luxembourg, September, 1989

Yaras M I & Sjolander S A (1991a) "Effects of simulated rotation on tip leakage in a planar cascade of turbine blades, Part i : Tip Gap Flow" ASME paper number 91-GT-127, Presented at the International Gas Turbine and Aeroengine Congress and Exposition, Orlando, Floeida, June 3-6, 1991

Yaras M I & Sjolander S A (1991b) "Effects of simulated rotation on tip leakage in a planar cascade of turbine blades, Part ii : Downstream flow field and blade loading" ASME paper number 91-GT-128, Presented at the International Gas Turbine and Aeroengine Congress and Exposition, Orlando, Florida, June 3-6, 1991

APPENDIX A

1. Introduction

During follow up work based on the results of Morphis (1993) it was realised that the repeatability of the second nozzle performance was not as good as previously thought which negated any conclusions made regarding the efficiency of the second nozzle. This required an in depth investigation into the source of the poor repeatability and explored ways of minimising this variability.

2. The variation of the second nozzle efficiency

Figure A-2 illustrates the time dependent variation of various flow coefficients that were obtained from a number of traverses. It is necessary to evaluate the effect of these variations on the reliability of the second nozzle efficiency which is determined by measuring the flow at the inlet and the outlet to the nozzle in order to determine the driving pressure across the nozzle as well as the outlet velocity. With an unpredictable variation in results between traverses, the second nozzle efficiency could be a maximum or a minimum depending on the choice of traverse. Table A-1 presents the possible worst case variation of the second nozzle efficiency by considering a maximum numerator and minimum denominator to obtain a minimum efficiency and vice versa.

Table A-1 The effect of the variation of the flow coefficients on the second nozzle efficiency

	$\overline{C_{P_{00}-P_{03}}}$	$\overline{C_{P_{00}-P_{s4}}}$	$\overline{C_{V_4}}$	$\eta_{nozzle2}$
min	5.3	9.576	3.965	91.2%
mean	5.335	9.611	3.961	
max	5.37	9.646	3.966	95.0%

It is expected therefore that the second nozzle lies in the range 91.2-95.0% which gives a variation of ± 1.9%. This obviously invalidates any comparison between the effects of tip treatments since the variation in the results was seen to be less than this range.

3. The source of the variation

The variation of the work coefficient C_w seen in Figure A-1 was not expected since by definition this had been normalised to exclude atmospheric variations. It was necessary to examine the influence each transducer had on the determination of the work coefficient because it was not known which of the transducers could be responsible for the unrepeatability.

If the power developed by the rotor is considered to be proportional to the Euler work then $\dot{W} = \dot{m}(U_1V_{\theta_1} - U_2V_{\theta_2})$. It is easily shown that because V_X/U was controlled to a fixed value, both V_{θ_1} and V_{θ_2} are linear functions of V_X as is the blade speed U. The mass flow $\dot{m}$ is again proportional to V_X with the result that

$\dot{W} \propto V_X^3$. The axial velocity V_X was calculated from the reference dynamic pressure q_{ref} at the inlet to the turbine using Bernoulli's relationship ie $V_X = \sqrt{2 q_{ref}/\rho}$ which suggested that the variation was due to the measurements from which the axial velocity was calculated

4. Kline McKlintock analysis

Having established the above relationships it was seen from Figure A-1 that the probable source of the variation or uncertainty was due to the variation from the ambient pressure transducer. This was verified by the methods of Kline McKlintock as described in Holman (1984) where

$w_R = [(\frac{\partial R}{\partial x_1} w_1)^2 + (\frac{\partial R}{\partial x_2} w_2)^2 + ... + (\frac{\partial R}{\partial x_2} w_2)^2]^{1/2}$ is the uncertainty

expected in a result R that in turn is a function of a number of other independent quantities (x_i) each with an uncertainty (w_i). From Figure A-1 the uncertainty of the ambient pressure measurement was estimated as 0.8kPa and that for the

ambient temperature as 0.1°C. The uncertainty for the density was then evaluated as

$$\rho = \frac{P}{RT} = \frac{100\,300}{287 \times 300} = 1.165$$

$$\frac{\partial \rho}{\partial P} = \frac{1}{RT}, \quad w_P = 0.8\,\text{kPa}, \quad P = 100\,\text{kPa}$$

$$\frac{\partial \rho}{\partial T} = -\frac{P}{RT^2}, \quad w_T = 0.1\,^{\circ}\text{C}, \quad T = 300\,\text{K}$$

$$w_\rho = \left[\left(\frac{1}{287 \times 300}\right) \times 800)^2 + \left(\frac{100\,300}{287 \times 300^2} \times 0.1\right)^2 \right]^{1/2}$$

$$= [\ 8.633e{-}5 + 1.508e{-}7\ ]^{1/2}$$

$$= 0.0093\ (0.8\%)\ \ \text{kg/m}^3$$

Figure A-2 confirms that the uncertainty for the density is representative of the above calculation.

Proceeding in a similar manner yields the corresponding uncertainties for each graph in Figure A-2 based on the measured data. The derived values are presented in Table A-2.

Table A-2 Uncertainty values for various quantities

	V_x (m/s)	**Power (kW)**	**C_w**
Nominal value	30	4.70	4.58
Uncertainty	0.124 (0.4%)	0.016 (0.34%)	0.055 (1.2%)

These values are confirmed by the apparent uncertainty present in the results shown in Figure A-2. An investigation revealed that the cause of the uncertainty for the Kulite ambient pressure transducer was in fact due to the resolution of the

A/D card. The problem was rectified by amplifying and filtering the output from the transducer to correspond to a 0-10V voltage to match the span of the card. The improved measured results can be seen in Figure A-4. The calculated results for the improved uncertainties are presented in Table A-3 and agree quite well with the experimental values.

Table A-3 The improved uncertainty for various quantities

	V_x (m/s)	Power (kW)	C_w
Nominal value	30	4.70	4.58
Uncertainty	0.06 (0.2%)	0.006 (0.13%)	0.024 (0.5%)

The effect this improvement had on the repeatability of the second nozzle was recalculated and is presented in Table A-4.

Table A-4 The improved uncertainty for the second nozzle

	$\overline{C_{P_{00}-P_{03}}}$	$\overline{C_{P_{00}-P_{s4}}}$	$\overline{C_{V_4}}$	$\eta_{nozzle2}$
min	5.2896	9.5751	4.0316	94.08%
mean	5.2946	9.5951	4.0416	
max	5.2996	9.6051	4.0516	94.76%

The variation is thus ± 0.34% and was verified in a number of experiments, the results of which are presented in Figure A-3. Interestingly, the variation of both the static pressure coefficient and the velocity coefficient were found to have a

similar trend such that for a higher static pressure coefficient behind the nozzle, a higher velocity coefficient was also measured which tended to stabilise the calculated result according to the definition used. It is believed that the repeatability of the second nozzle efficiency was better than the above figure when an average of three or more measurements was taken and an experimental result confirmed that the average uncertainty was ± 0.17 which allowed a reasonable comparison of the effect of tip shape on the second nozzle efficiency.

Various other calculated quantities such as the single stage efficiency were obtained from a single run. These typically were repeatable to within 0.12% of the nominal value and thus the comparison of tip shape was believed to be reliable. Tip clearance was seen to have a 1%-1.5% change in efficiency per 1% clearance which was approximately a factor of 8 greater than the uncertainty.

One other time dependent variation was noticed in both Figure A-1 and Figure A-4. This concerned the significant increase in ambient temperature which then reduced the inlet air density. This effect was minimised by allowing a warm up period prior to taking measurements. The control routine was then set to maintain a constant V_X and V_X/U ratio which reduced the variation in power output and hence the variation in the work coefficient.

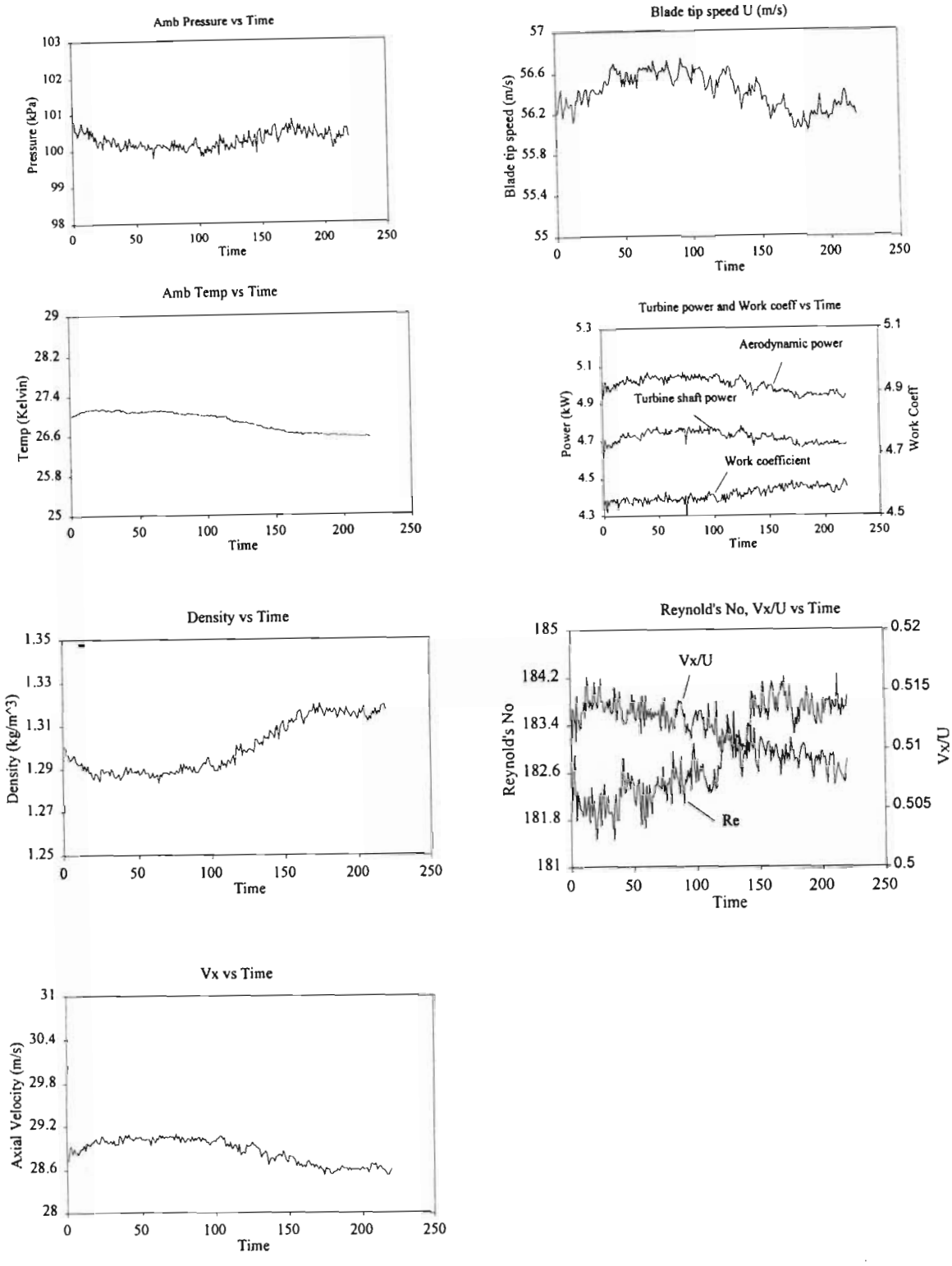

Figure A-1 The variation or uncertainty present in the instantaneous measurement of various quantities.

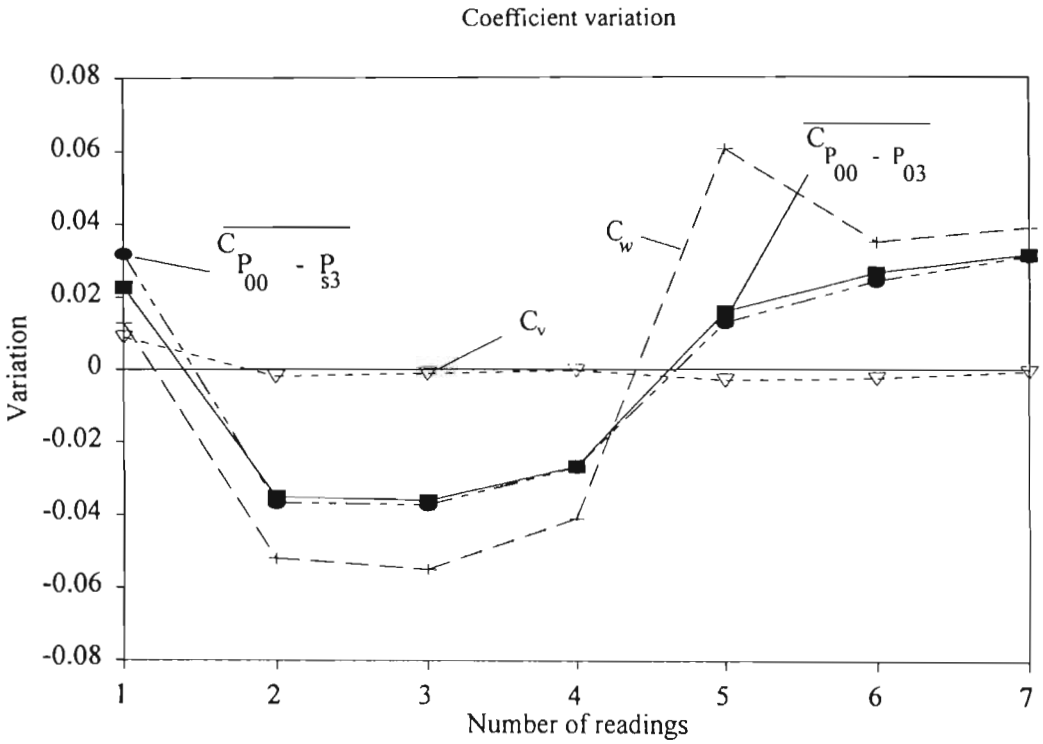

Figure A-2 The variation of various mass averaged quantities over a number of individual readings

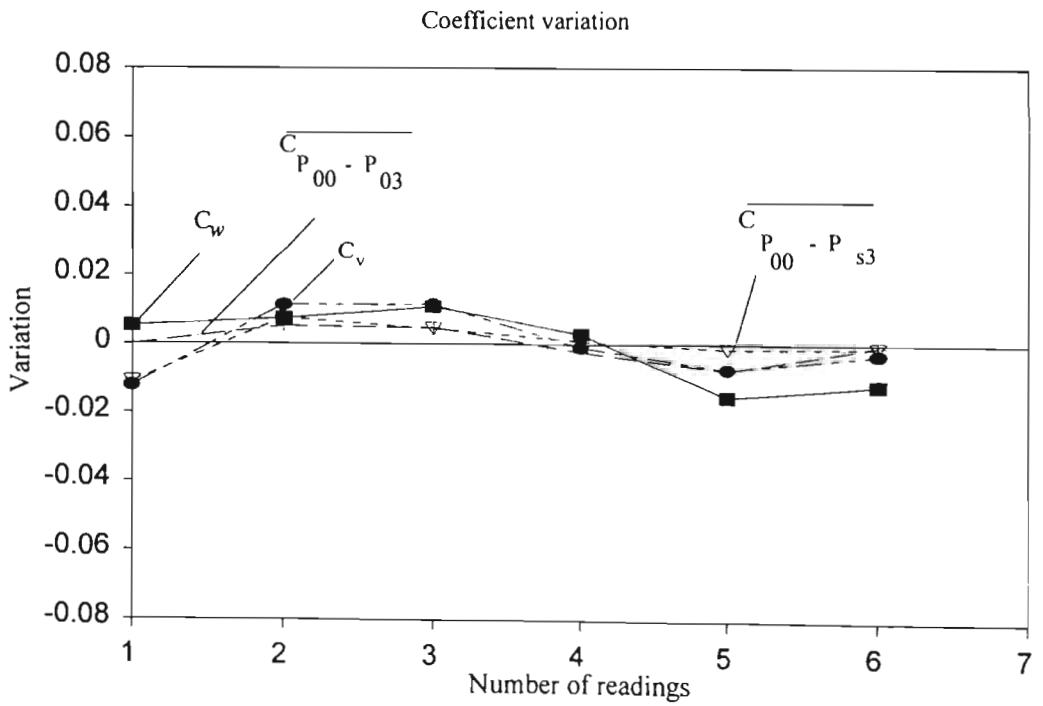

Figure A-3 The improved variation of various mass averaged quantities over a number of individual readings

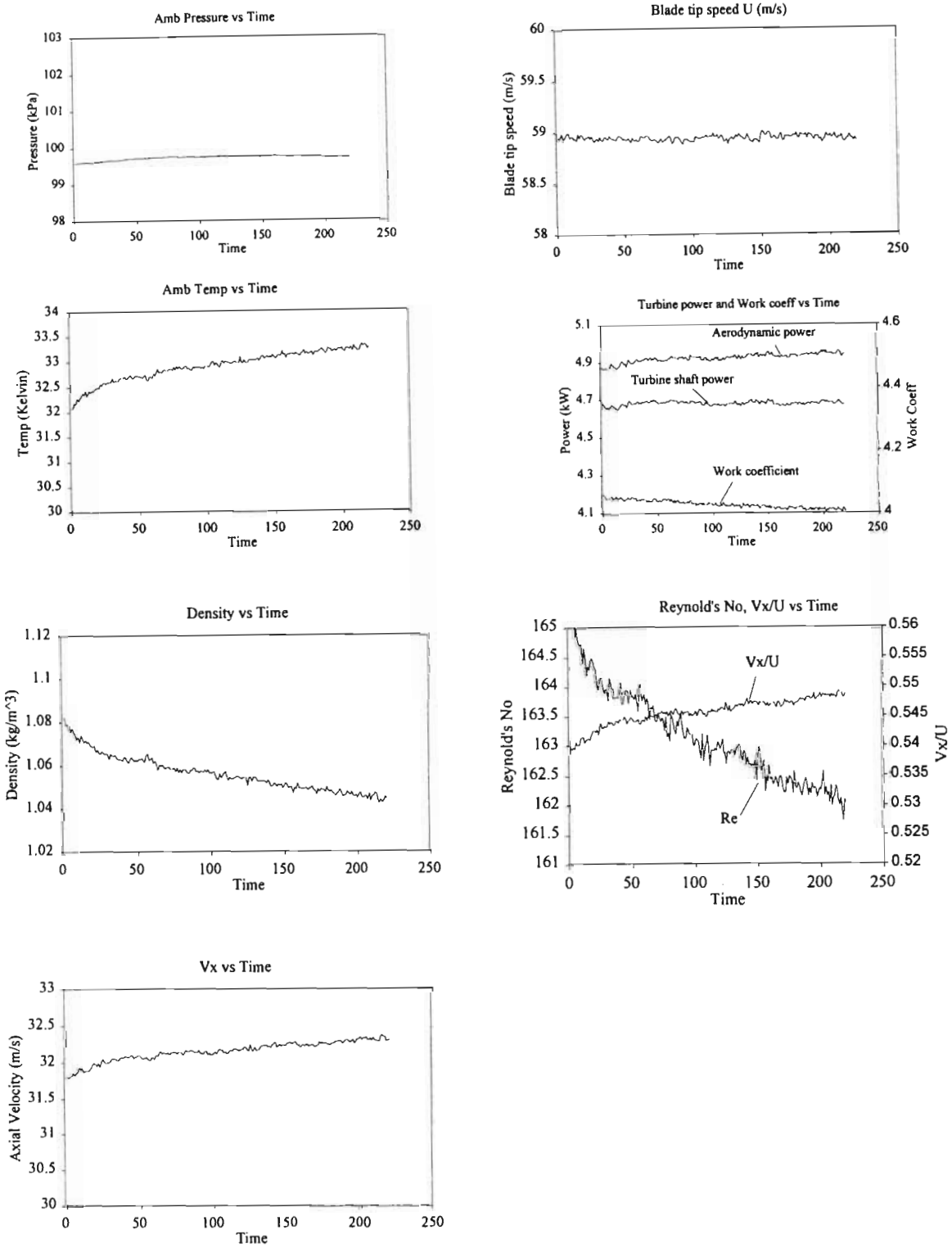

Figure A-4 The improved variation or uncertainty present in the instantaneous measurement of various quantities